JAGIELLONIAN UNIVERSITY

DOCTORAL THESIS

Theoretical and Phenomenological Cosmology: Early Universe and Gravitational Wave Physics

---

Author:
Paola Carolina MOREIRA DELGADO

Supervisors:
Dr hab. Jakub GIZBERT-STUDNICKI
Dr. Chunshan LIN

A thesis submitted in fulfillment of the requirements for the degree of Doctor of Philosophy

in the

Faculty of Physics, Astronomy and Applied Computer Science

March 26, 2024

Declaration of Authorship

I, Paola Carolina Moreira Delgado, hereby declare that this thesis entitled "Theoretical and Phenomenological Cosmology: Early Universe and Gravitational Wave Physics" is my original work submitted for the degree of Doctor of Philisophy at Jagiellonian University. All sources of information used in this thesis have been properly acknowledged and cited. Any assistance received in the preparation of this thesis has been acknowledged. The work presented in this thesis has not been submitted for any other degree or qualification. The research conducted for this thesis complies with ethical standards and guidelines. This thesis meets the requirements and regulations of Jagiellonian University for the submission of graduate theses.

Signed:

Date:

"O Universo não é uma ideia minha. A minha ideia do Universo é que é uma ideia minha."

Alberto Caeiro

JAGIELLONIAN UNIVERSITY

Abstract

Faculty of Physics, Astronomy and Applied Computer Science

Doctor of Philosophy

Theoretical and Phenomenological Cosmology: Early Universe and Gravitational Wave Physics

by Paola Carolina MOREIRA DELGADO

In English:

This thesis presents a comprehensive exploration in the realms of cosmology and gravitational wave physics, investigating various aspects and challenges within the standard ΛCDM model while also scrutinizing motivated alternative theories. Our purpose is to shed light on unresolved dilemmas within the ΛCDM framework (such as the singularity problem, the origin of cosmological perturbations, the Cosmic Microwave Background (CMB) anomalies on large scales, the dark energy and the dark matter problems) and on possibly new phenomena in the realm of gravitational wave resonance (such as the conversion of gravitational waves to photons and the gravitational wave resonance in Ultralight Dark Matter (ULDM) halos). By scrutinizing a plethora of scenarios, we aim to elucidate fundamental aspects of cosmological physics, offering new perspectives to longstanding puzzles in the field.

The first chapter presents a novel nonsingular cosmological model exhibiting a rich evolution, which encompasses a contracting phase, a bounce, a quasi-de Sitter inflationary epoch, and a subsequent radiation-dominated expansion. The bounce and the quasi-de Sitter phases appear due to quantum effects originating from the Wheeler-DeWitt equation. The model is compatible with the observed almost scale invariant scalar power spectrum, while further developments are needed to address the magnitude of the tensor-to-scalar ratio.

Chapter two investigates non-Gaussianities in bouncing models aimed at mitigating large-scale anomalies in the CMB data. While these models exhibit interesting features, they are excluded wih high significances when comparing the CMB reduced bispectrum with the Planck data. Although the bispectrum decays exponentially, the signal surpasses the noise for very large scales, leading to a large cumulative signal-to-noise ratio. This result highlights the sensitivity of the Planck data to scales beyond the pivot scale.

The third chapter investigates the implications of holographic dark energy (HDE) on single-field slow-roll inflation, demonstrating compatibility with observational constraints on both scalar and tensor power spectra.

Gravitational wave physics takes center stage in the fourth chapter, where we explore the possibility of damping gravitational waves via parametric resonance with an electromagnetic field. We elucidate the conditions under which such damping occurs and discuss potential astrophysical implications.

Lastly, the fifth chapter investigates the amplification of gravitational waves due to parametric resonance with the gravitational potentials of Ultralight Dark Matter (ULDM) halos. We explore various masses of Ultralight Axions (ULA) and halo densities, considering their implications for current gravitational wave amplification.

Throughout these chapters, we probe diverse aspects of the early Universe

and gravitational wave physics, shedding light on fundamental questions and paving the way for further exploration and refinement of theoretical and phenomenological frameworks.

In Polish:

Ta praca doktorska przedstawia wszechstronne badania w dziedzinach kosmologii i fizyki fal grawitacyjnych, badając różne aspekty i wyzwania w ramach standardowego modelu ΛCDM, a także analizując motywowane alternatywne teorie. Naszym celem jest rzucenie światła na nierozstrzygnięte dylematy w ramach modelu ΛCDM (takie jak problem singularności, pochodzenie perturbacji kosmologicznych, anomalie w mikrofalowym tle kosmicznym (CMB) na dużych skalach, problemy z ciemną energią i ciemną materią) oraz na ewentualnie nowe zjawiska w obszarze rezonansu fal grawitacyjnych (takie jak konwersja fal grawitacyjnych w fotony i rezonans fal grawitacyjnych w halo Ultralekkiej Ciemnej Materii (ULDM)). Poprzez analizę wielu scenariuszy, naszym celem jest wyjaśnienie fundamentalnych aspektów fizyki kosmologicznej, oferując nowe perspektywy dla długotrwałych zagadek w dziedzinie.

Pierwszy rozdział przedstawia nowy model kosmologiczny bez osobliwości, który wykazuje bogatą ewolucję, obejmującą fazę kurczenia, odbicie, quasi-epokę de Sittera i następującą po niej ekspansję dominującą promieniowaniem. Fazy odbicia i quasi-de Sittera pojawiają się z powodu efektów kwantowych wynikających z równania Wheelera-DeWitta. Model jest zgodny z obserwowanym prawie skończonym skalarnym spektrum mocy, podczas gdy potrzebne są dalsze prace rozwojowe, aby zająć się amplitudą stosunku tensorowo-skalarnego.

Drugi rozdział bada niewielkogausowskie w modelach odbijających mających na celu złagodzenie dużych anomali w danych CMB. Choć te modele wykazują interesujące cechy, są one wykluczone z dużą istotnością, porównując zredukowany bispektrum CMB z danymi Plancka. Chociaż bispektrum maleje wykładniczo, sygnał przewyższa szum dla bardzo dużych skal, prowadząc do dużego stosunku sygnał-szum. Ten wynik podkreśla wrażliwość danych Plancka na skale poza skalą odniesienia.

Trzeci rozdział bada implikacje holograficznej ciemnej energii (HDE) na inflację wolno-pola, demonstrując zgodność z ograniczeniami obserwacyjnymi zarówno dla skalarnych, jak i tensorowych spektrów mocy.

Fizyka fal grawitacyjnych zajmuje centralne miejsce w czwartym rozdziale, gdzie badamy możliwość tłumienia fal grawitacyjnych poprzez rezonans parametryczny z polem elektromagnetycznym. Wyjaśniamy warunki, w których takie tłumienie występuje, i omawiamy potencjalne implikacje astrofizyczne.

Na koniec, piąty rozdział bada wzrost fal grawitacyjnych z powodu rezonansu parametrycznego z potencjałami grawitacyjnymi hal Ultralekkiej Ciemnej Materii (ULDM). Badamy różne masy Ultralekkich Aksjonów (ULA) i gęstości hal, rozważając ich implikacje dla aktualnego wzrostu fal grawitacyjnych.

Przez wszystkie te rozdziały sondujemy różnorodne aspekty wczesnego Wszechświata i fizyki fal grawitacyjnych, rzucając światło na fundamentalne pytania i torując drogę dalszej eksploracji i doskonaleniu teoretycznych i fenomenologicznych ram.

Acknowledgements

I wish to express my sincere appreciation to my supervisor, Chunshan Lin, for his guidance and expertise throughout the completion of this thesis. His valuable insights have been very helpful, and I am grateful for his dedication to my academic development.

I would like to extend my appreciation to Jakub Gizbert-Studnicki for his role as the official supervisor of this thesis. Despite not having worked directly together, I am grateful for his oversight and support throughout my studies.

I extend my sincere appreciation to my collaborators, Ruth Durrer, Nelson Pinto Neto, Alexander Ganz, Robert Brandenberger, Bartjan van Tent, Piero A. P. Molinari, and Rodrigo F. Pinheiro, for their dedication, expertise, and shared enthusiasm.

My gratitude also extends to Carla R. Almeida, Shingo Akama, and George Zahariade for their insightful discussions and valuable input to papers included in this thesis.

I am thankful to the members of the committee for their willingness to review my work and participate in the defense.

I am also grateful to the members of the cosmology group, both current and past, who contribute to a respectful and friendly environment.

The support provided by the funding agency UMO2018/30/Q/ST9/00795 from the National Science Centre, Poland, is greatly appreciated.

My appreciation goes to Ewa Witkowska and Ewa Lelek for their invaluable assistance and support, which greatly facilitated the administrative aspects during my PhD.

Lastly, I want to express my heartfelt appreciation to my partner, Lucca Fazza, for his support and companionship. His encouragement and understanding have been invaluable to me, making this experience all the more fulfilling. Additionally, I extend my heartfelt gratitude to my parents, Mercês Moreira and Tadeu Delgado, for their dedication and sacrifices in providing me with a good education. Their encouragement and love are the foundation of everything I have achieved.

Contents

List of Figures

List of Tables

List of Abbreviations

BipoSH	Bipolar Spherical Harmonics
BOSS	Baryon Oscillation Spectroscopic Survey
CAMB	Code for Anisotropies in the Microwave Background
CDM	Cold Dark Matter
CLASS	Cosmic Linear Anisotropy Solving System
CMB	Cosmic Microwave Background
CMB-S4	Cosmic Microwave Background Stage 4
COBE	Cosmic Background Explorer
DES	Dark Energy Survey
FLRW	Friedman-Lemaître-Robertson-Walker
GR	General Relativity
HDE	Holographic Dark Energy
HERA	Hydrogen Epoch of Reionization Array
IR	Infrared
ΛCDM	Lambda Cold Dark Matter
LIGO	Laser Interferometer Gravitational-Wave Observatory
LQC	Loop Quantum Cosmology
MCMC	Markov Chain Monte Carlo
NANOGrav	North American Nanohertz Observatory for Gravitational Waves
PTA	Pulsar Timing Array
SNR	Signal-to-Noise Ratio
SPARC	Spitzer Photometry and Accurate Rotation Curves
ULA	Ultralight Axion
ULDM	Ultralight Dark Matter
UV	Ultraviolet
VEVs	Vacuum Expectation Values
WMAP	Wilkinson Microwave Anisotropy Probe
WKB	Wentzel-Kramers-Brillouin
dBB	de Broglie-Bohm
qdS	quasi-de Sitter

To Mercês Moreira and Tadeu Delgado.

Chapter 1

Introduction

Historically, the quest to understand the origin, evolution and structure of the Universe has been marked by paradigm-shifting observational discoveries and theoretical breakthroughs, which jointly formed the comprehensive description of the cosmos that we currently have.

One such milestone is the theory of inflation, proposed in the early 1980s [1, 2, 3, 4]. It posits that the universe underwent a period of exponential expansion in its beginning, resolving long-standing puzzles such as the horizon and flatness problems (discussed in 3.1) and predicting the almost scale invariant power spectrum of cosmological scalar perturbations [5].

Observational cosmology has also made significant strides, with pivotal discoveries shedding light on the Universe's early history and structure. The Cosmic Microwave Background (CMB) radiation, discovered in 1965 [6], serves as a relic of the hot, dense primordial Universe. Measurements of the CMB by missions such as the Cosmic Background Explorer (COBE) [7], the Wilkinson Microwave Anisotropy Probe (WMAP) [8], and the Planck satellite [9, 10, 11] have provided maps of temperature fluctuations, offering a way to infer the Universe's composition, geometry, and evolution.

More recently, the detection of gravitational waves has opened a new window onto the cosmos, allowing us to directly probe extreme phenomena, such as the mergers of black holes and neutron stars [12]. Groundbreaking experiments such as the Laser Interferometer Gravitational-Wave Observatory (LIGO) [13] and the Virgo Collaboration [14] have detected multiple gravitational wave events, while the North American Nanohertz Observatory for Gravitational Waves (NANOGrav) has recently reported the first-ever evidence of the gravitational wave background [15].

All the aforementioned milestones have played pivotal roles in advancing our understanding and solidifying the foundation of the standard cosmological model (SCM), commonly known as the Lambda Cold Dark Matter (ΛCDM) model. Remarkably, this model, characterized by merely six parameters, aligns exceptionally well with contemporary cosmological data [9, 10, 11].

Despite its achievements, the ΛCDM model still faces several challenges and tensions. One major challenge is the identification and understanding of dark matter. While its gravitational effects are evident, its nature remains unknown. Numerous experiments aim to directly detect dark matter particles, but so far, no conclusive evidence has been found [16, 17, 18].

Another significant challenge lies in the nature of dark energy, whose existence is required to explain the observed accelerated expansion of the Universe [19, 20]. Understanding the origin and properties of dark energy is arguably one of the most critical questions in cosmology, and although many proposals have been made [21, 22, 23], a conclusive explanation has not been found.

Additionally, the ΛCDM model encounters tensions when comparing observations at different cosmic scales. These include discrepancies in the measured expansion rate of the universe, the Hubble parameter, when comparing local measurements to those derived from the CMB radiation [24, 5, 25]. Another discrepancy involves the amplitude of matter fluctuations on large scales, denoted by σ_8 (the level of matter density fluctuations at a scale of 8 Mpc). Measurements of σ_8 from different cosmological observations, namely the Planck satellite and galaxy surveys data, do not agree within their respective uncertainties [26, 27]. In addition to these tensions, whose significance is relatively high (for cosmology standards), there exist the so-called anomalies. These are features observed on large scales in the CMB radiation that have a very low probability of happening within ΛCDM, but that in principle might appear due to new physics in the early Universe [28, 29].

Another extremely important concern in ΛCDM is the singularity problem, which arises when we trace back the expansion of the Universe and reach a point of infinite density known as the Big Bang singularity [30]. At this point, the equations of General Relativity (GR) break down, and they cannot provide a meaningful description of the space-time. This singularity problem implies that our current laws of physics are inadequate to describe the Universe's behavior under such extreme conditions, where quantum or modified gravity effects might become important.

In this thesis, we explore various aspects and challenges encountered within the ΛCDM model of cosmology and motivated alternative theories. We aim to scrutinize a number of scenarios that may either offer solutions to some of the dilemmas previously mentioned or provide remarkable insights into gravitational and cosmological physics. The chapters are arranged in descending order of redshift, or ascending order in time.

Firstly, in Chapters 2 and 3, we delve into the realm of bouncing cosmologies, which arise as solutions to the initial singularity problem. Our study encompasses investigations within the frameworks of both the Wheeler-DeWitt equation [31, 32] and phenomenological bounces (motivated by the scale factor of matter bounces from loop quantum cosmology [33]), probing

how these approaches may address fundamental issues within the SCM. For the Wheeler-DeWitt case, we propose a radiation-dominated bouncing model that intrinsically presents an almost de Sitter expansion, akin to inflation, without the need of any extra field or reheating [34]. For the phenomenological cases, we investigate whether the bounce is able to mitigate the CMB anomalies on large scales, as it was believed in the literature [29]. We show the scenarios that alleviate the anomalies are excluded by the Planck data due to their high non-Gaussianities [35, 36].

Secondly, in Chapter 4, we scrutinize an inflationary mechanism within the context of a modified gravity theory designed to account for the nature of dark energy, namely the holographic dark energy model [37]. We investigate its implications during a single-field inflationary phase and its compatibility with current cosmological constraints [38]. We show the scalar field that drives inflation, the so-called inflaton, dominates the dark energy components. Additionally, we compute both the scalar and tensor power spectra and obtain the modified gravity corrections to it, which decay very quickly after the first inflationary e-folds.

Thirdly, in Chapter 5, we investigate the possibility of gravitational wave conversion into photons via parametric resonance, a phenomenon situated within the realm of GR [39]. We show that a non-negligible conversion takes place in a medium with sub-luminal speed of light, which allows the resonance to occur in the so-called first resonance band.

Lastly, in Chapter 6, we explore the phenomenon of gravitational wave resonance in Ultralight Dark Matter (ULDM) halos, which arises due to the time-dependent characther of the gravitational potentials [40]. We show that non-negligible gravitational wave amplification nowadays can happen in very dense regions in the halos.

In Chapter 7, we summarize our findings and discuss the main implications of this thesis.

The notation used within each chapter is distinctly defined in order to enhance readability and facilitate comprehension of the subject matter presented therein.

Chapter 2

Radiation-Dominated Bouncing Model with Slow Contraction and Inflation

2.1 Introduction

The standard cosmological model, solidly grounded in GR theory and a variety of cosmological observations (the Cosmic Microwave Background (CMB) radiation and its anisotropies [41], the abundance of light elements [42], the features of the distribution of large scale structure and cosmological redshifts [43, 44], among others), asserts that the Universe is expanding from a very hot era dominated by radiation, when the geometry of space was highly homogeneous and isotropic, with very small deviations from this special, symmetric state. However, extrapolating the standard cosmological model back to the past using GR, one necessarily encounters a singularity, where physical quantities diverge. Hence, the model is incomplete: GR is pointing us to its own limits, requiring new physics to understand these extreme situation, which is still under debate.

Assuming that the Universe had a beginning immediately followed by a hot expanding phase implies some important new puzzles, related to initial conditions. The size of regions in causal contact in the Universe is given by the Hubble radius, $R_H \equiv |1/H| \equiv |a/\dot{a}|$, where a is the scale factor, and the overdot represents a derivative with respect to cosmic time. The Hubble radius R_H evolves with respect to the scale factor a as

$$\frac{\mathrm{d}\ln(\mathrm{R_H})}{\mathrm{d}\ln(\mathrm{a})} = 1 - \frac{\ddot{a}a}{\dot{a}^2}. \tag{2.1}$$

If the cosmic fluid has non-negative pressure in the hot era, the Friedmann equations imply $\ddot{a} < 0$, so that $\mathrm{d}\ln(\mathrm{R_H})/\mathrm{d}\ln(\mathrm{a}) > 1$. Hence, in the past of an expanding universe the size of cosmological scales we are able to see today, which evolve with the scale factor, were much larger than the Hubble radius. This implies that the basic properties of the CMB, its temperature

isotropy and its tiny anisotropies, cannot be explained by causal physics, as the scales presenting these observed properties contained hundreds of causally disconnected regions on the last scattering surface. This is called the horizon problem. Furthermore, the observed matter and dark energy density of the Universe today, ρ_0, is very close to the total energy density of a Universe with flat spatial sections, ρ_c. Using again the Friedmann equations, the ratio $\Omega(t) \equiv \rho(t)/\rho_c(t)$ evolves as

$$\frac{\mathrm{d} \mid \Omega(t) - 1 \mid}{\mathrm{d}t} = -2\frac{\ddot{a}}{\dot{a}^3}. \tag{2.2}$$

As $\dot{a} > 0$ and $\ddot{a} < 0$, if $\Omega(t)$ is close to unity today, it must have been much closer to unity at earlier times, a spectacular fine tuning of initial conditions. This is the so called flatness problem.

A simple solution to these puzzles is to evoke that at some early stage a new field dominates the Universe evolution, for which $p/\rho < -1/3$ which implies $\ddot{a} > 0$, such that $\mathrm{d}\ln(\mathrm{R_H})/\mathrm{d}\ln(\mathrm{a}) < 1$ and $\mathrm{d}\,|\Omega(t) - 1|/\mathrm{d}t < 0$. This primordial phase is called inflation [1, 2, 3, 4], usually driven by a simple scalar field, which can be investigated in the framework of standard quantum field theory in curved spacetime. It not only solves the above puzzles, but it also predicted the observed almost scale invariant marginally red-tilted spectrum of primordial cosmological scalar perturbations [45]. Inflation became an essential part of any cosmological model in which the Universe has a beginning.

However, there is an alternative simple solution to the above puzzles if one assumes that the Universe had a very long contracting decelerating phase before the present expanding era. In this case, Eq. (2.1) implies that the Hubble radius was much bigger than any cosmological scale of physical interest in the far past of the contracting phase, because a contracting universe running backwards in time implies larger scale factors. Also, as $\dot{a} < 0$, $\ddot{a} < 0$, and $\ddot{a}/\dot{a}^3 > 0$, Eq. (2.2) implies that flatness becomes an attractor in the contracting phase, rather than a repeller. Hence, the Universe looks spatially flat to us now because it has not expanded long enough in comparison with the very long contracting phase it experienced in the past.

In realistic models with a contracting phase, there must be a bounce connecting it to the present expanding phase. In GR contraction generally leads to the time reversal of the Big Bang singularity, the Big Crunch. To avoid this, bouncing models must necessarily involve new physics. In other words, bouncing models must face the cosmological singularity problem, which is not addressed by inflation. A realistic bouncing model then not only solves the above puzzles related to initial conditions, but it is also complete, i.e., free of singularities.

The new physics required for bouncing models can be classical extensions of GR [46, 47, 48, 49, 50, 51, 52, 53], or quantum gravity effects [54, 55, 56, 57, 58, 59, 60, 61, 62, 63, 64, 65]. Different models have been investigated in the

last decades, and it has been shown that many of them [66, 67, 68, 69, 70] satisfy the constraints imposed by cosmological observations on the properties of primordial cosmological perturbations, and other cosmological features, without the need of an inflationary phase. Nevertheless, bouncing models are not incompatible with inflation. Indeed, in some scenarios, bouncing models lead to the appropriate initial conditions for inflation [71].

In this chapter, we present a cosmological model where the bounce and an expanding inflationary phase are both induced by quantum effects, without any inflaton field. The quantum effects arise from a canonical quantization of gravity restricted to the mini-superspace configuration of homogeneous and isotropic geometries, with a constant perfect fluid equation of state parameter $w = p/\rho$ satisfying $-1/3 < w < 1$, leading to an effective Schrödinger equation for the cosmological wave function. As is well known, this simple quantum geometrical approach can be viewed as an approximation of a more involved quantum theory of gravity, hence we limit the maximum energy density and spacetime curvature of the effective model to be some few orders of magnitude below the Planck scale, where this simple approach can be reliable [72]. The wave function solution is interpreted using the de Broglie-Bohm quantum theory [73, 74], where a quantum scale factor evolution can be calculated.

The initial wave function is chosen to be a Gaussian moving in configuration space. The time-dependent solution is calculated, leading to a bouncing non-singular asymmetric scale factor, reaching its standard classical evolution in the asymptotic past and future of the model. Depending on the sign of the momentum of the wave function, the classical contraction can be either much slower or faster than the classical expansion, with a huge creation or annihilation of particles between these phases, respectively. In the sequel, it is noticed that, specifically for $w \approx 1/3$, the model experiences either a quantum inflationary or deflationary era during its evolution. Clearly, the physically interesting possibility is the former, on which we focused our attention.

The resulting model is a radiation-dominated universe classically and slowly contracting from an almost flat spacetime up to a quantum bounce, followed by an era of a quantum quasi-de Sitter expanding phase, which changes smoothly to the classical radiation-dominated era before nucleosynthesis (thus a transition opposite to that obtained in [75]). In order to have inflation during a sufficiently long period, the wave function from which it originates must be moving with high momentum in configuration space. During the quantum era, a large amount of radiation is quantum created. Therefore, surprisingly, we obtain a very simple radiation-dominated, non-singular cosmological model, the primordial era of which combines the three main ingredients of the primordial Universe that have been investigated so far: a slow contraction [76, 77] (although in a very different way, with possible different consequences), a bounce and inflation. The scalar power spectrum of cosmological perturbations is calculated, presenting an almost scale invariant behavior and an amplitude compatible with observations for very reasonable

parameter choices; namely, that the minimum curvature scale of the model ($1/R^{1/2}$, where R is the Ricci scalar) is around four orders of magnitude bigger than the Planck length.

Concerning the slow contraction, in the present model it happens because there is much less matter-energy in the contracting phase then in the expanding phase. In ekpyrotic models, the slow contraction arises from the fact that the matter content dominating contraction has an equation of state parameter much bigger than the equation of state parameters of the fluids dominating the expanding case. As a consequence, in ekpyrotic models anisotropies generally become irrelevant during contraction, which is not automatically the case in the present model. However, in our view, the homogeneity problem (the infinitely many fine tunings of initial conditions in order to have a homogeneous spacelike hypersurface geometry) is vastly more serious than the anisotropy issue. If some yet unknown physical mechanism or theory of initial conditions is capable to justify such an extremely fine-tuned state, then it would not be a big surprise that it could also make identical the three remaining time functions characterizing the three directions of space. Once one assumes a homogeneous and isotropic universe, it has been proved in [78] that shear perturbations coming from vacuum fluctuations in usual bouncing models will generally not overcome the background degrees of freedom, even growing as fast as $1/a^6$ in the contracting phase. This is because the shear perturbation in such models is multiplied by a very small number - the ratio between the Planck length and the Hubble radius squared - and it can be shown that if the bounce is not very deep, the shear will remain sufficiently small.

In Sections 2.1.1, 2.1.2 and 2.1.3 we review the foundations of the cosmological model considered in this chapter - the ADM formalism, the canonical quantization, a minisuperspace filled with a perfect fluid and a de Broglie-Bohm bounce. In Section 2.2 we obtain the wave function which originates the class of scale factors we will investigate. The free parameters are connected to physically meaningful cosmological quantities. A very simple expression for the scale factor and the independent free parameters of the theory is exhibited, and its properties in different phases are described in detail. It is shown that the case $w \approx 1/3$ implies an era of quantum quasi-de Sitter expansion after the bounce. In Section 2.3 we make analytic estimations of the primordial scalar perturbations originated from quantum vacuum fluctuations in the asymptotic past of the model, first for general w, then for $w \approx 1/3$, calculating their amplitude and spectral index. In Section 2.4, the numerical calculations are shown, confirming the analytical estimations: an almost scale invariant spectrum of scalar perturbations, with an amplitude compatible with observations if the minimum curvature scale of the model is around three orders of magnitude larger than the Planck length. We conclude in Section 2.5 with a discussion and the possible future developments of the model.

2.1.1 Hamiltonian Formulation of General Relativity

The Hamiltonian formulation of GR was developed by Richard Arnowitt, Stanley Deser, and Charles Misner, and became known as the ADM formalism [79]. The formulation relies on geometric quantities that characterize a foliation of spatial hypersurfaces[1] in the time direction.

Such hypersurfaces are defined through the constancy of a function f of the coordinates, i.e., $f(x^\mu) =$ constant, and their normals η_μ. By introducing the temporal coordinate $t \equiv x^0$, we can write $\eta_\mu = -N\delta^0_\mu$, where N is called the lapse function and is normalized through $g^{\mu\nu}\eta_\mu\eta_\nu = -1$. We can also define the projector $h^{\mu\nu} \equiv g^{\mu\nu} + \eta^\mu\eta^\nu$, so that its inverse matrix $h_{\mu\nu}$ is the metric tensor of the hypersurfaces. Finally, we define the so-called shift vector $N^i \equiv g^{i0}N^2$, which describes the rate of change of the displacement of x^i from one hypersurface to another. In Figure 2.1, these definitions are geometrically presented. The lapse function, the shift vector, and the metric of the hypersurfaces are then used to describe the metric of the four-dimensional spacetime in question:

$$g^{\mu\nu} = \begin{pmatrix} -\frac{1}{N^2} & \frac{N^i}{N^2} \\ \frac{N^j}{N^2} & h^{ij} - \frac{N^iN^j}{N^2} \end{pmatrix}. \tag{2.3}$$

An important quantity in the context of differential geometry when considering hypersurfaces embedded in a manifold is the extrinsic curvature. In the present considered scenario, such quantity is given by

$$K_{ij} = \frac{1}{2N}\left[\dot{h}_{ij} - \nabla_i N_j - \nabla_j N_i\right], \tag{2.4}$$

where $\nabla\mu V_\nu \equiv \partial_\mu V_\nu - \Gamma^\lambda_{\mu\nu}V_\lambda$ is the covariant derivative of the spacetime in question (derivative along tangent vectors of the manifold), and ∇_i is the three-dimensional covariant derivative. The quantity

$$\Gamma^\lambda_{\mu\nu} \equiv \frac{1}{2}g^{\lambda\rho}\left(\partial_\nu g_{\rho\mu} + \partial_\mu g_{\rho\nu} - \partial_\rho g_{\mu\nu}\right) \tag{2.5}$$

represents the Christoffel symbols, which describe the affine connection of the spacetime. The dot represents the time derivative.

The Lagrangian density of this system can be written in terms of the previously defined quantities as

$$\mathcal{L} = Nh^{\frac{1}{2}}\left(R^{(3)} + K^{ij}K_{ij} - K^2\right), \tag{2.6}$$

[1] Hypersurfaces are algebraic varieties of dimension $n-1$ embedded in an n-dimensional space. In the case of GR, the varieties encompass the 3 spatial dimensions, and time is described as the extra dimension in the $n = 4$ space.

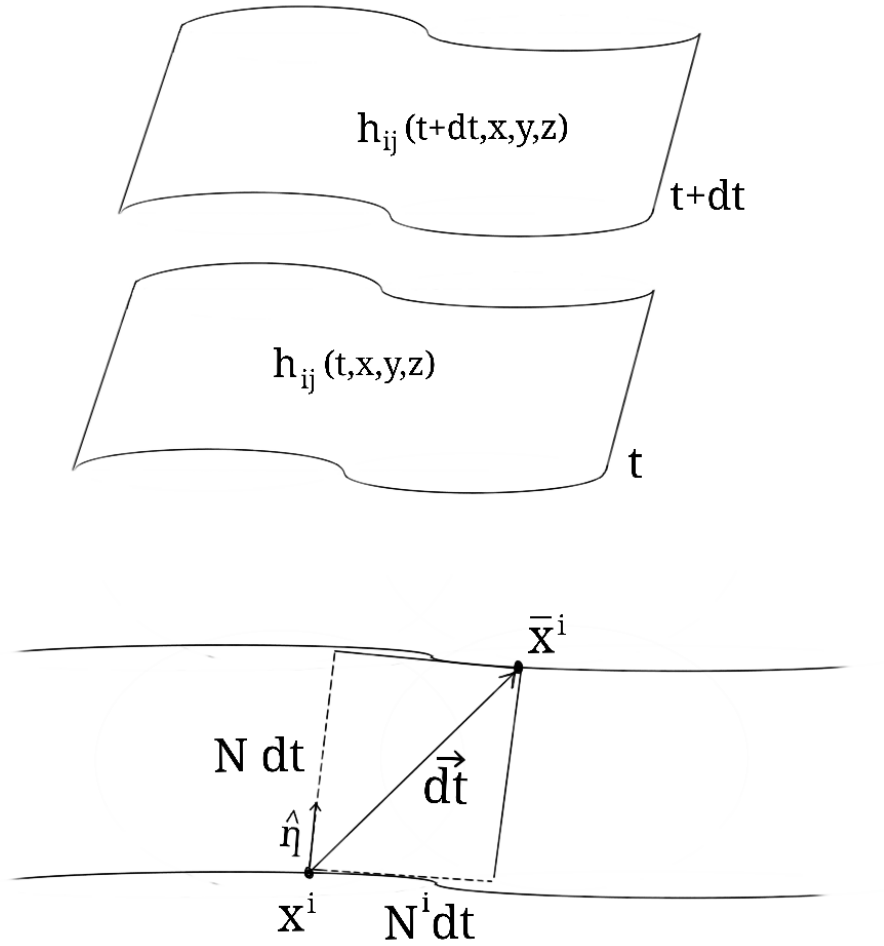

FIGURE 2.1: Two hypersurfaces separated in the time direction by an infinitesimal interval dt. The lapse function N and the shift vector N^i are geometrically represented. The normal η_μ to the surface $h_{ij}(t, x, y, z)$ is represented through its corresponding unitary $\hat{\eta}$.

where $R^{(3)}$ is the Ricci scalar of the hypersurfaces, which quantifies the curvature of the variety, $K \equiv K^i_i$, and h is the determinant of the metric of the hypersurfaces. Since this Lagrangian density does not depend on $\partial_0 N$ or $\partial_0 N^i$, the conjugate momenta of the lapse N and the shift function N^i are zero. Such non-dynamic variables must be included in the system's action as multiplicative factors of the constraints, the so-called Lagrange multipliers.

Thus, the gravitational action S can be written as

$$\begin{aligned} S &= \frac{1}{16\pi}\int \Big[\Pi^{ij}\dot{h}_{ij} + N_i 2\nabla_j \Pi^{ij} + \\ &- N\left(G_{ijkl}\Pi^{ij}\Pi^{kl} - h^{\frac{1}{2}}R^{(3)}\right)\Big] dtd^3x, \\ \Pi^{ij} &\equiv \frac{\delta\mathcal{L}}{\delta(\partial_0 h^{ij})} = -h^{\frac{1}{2}}\left(K_{ij} - h_{ij}K\right), \\ G_{ijkl} &\equiv \frac{h^{-\frac{1}{2}}}{2}\left(h_{ik}h_{jl} + h_{il}h_{jk} - h_{ij}h_{kl}\right). \end{aligned} \tag{2.7}$$

The quantities accompanied by the Lagrange multipliers N and N_i are the secondary constraints of the theory and are respectively called the super-Hamiltonian $\mathcal{H}$ and supermomentum $\mathcal{H}^j$ constraints[2]

$$\mathcal{H} \equiv G_{ijkl}\Pi^{ij}\Pi^{kl} - h^{\frac{1}{2}}R^{(3)} \approx 0, \tag{2.8}$$

$$\mathcal{H}^j \equiv -2\nabla_i \Pi^{ij} \approx 0. \tag{2.9}$$

The first one is related to the covariance of the theory under general time transformations, while the second one describes covariance under spatial coordinate transformations.

In turn, the Hamiltonian density $\mathscr{H} \equiv \Pi^{ij}\dot{h}_{ij} - \mathcal{L}$ takes the following form

$$\mathscr{H} = N\mathcal{H} + N_i\mathcal{H}^i. \tag{2.10}$$

2.1.2 Canonical Quantization and The Wheeler-DeWitt Equation

The Theory of GR is covariant under coordinate transformations. In other words, physical laws take the same form in all reference frames. Mathematically, this property leads to constraints, which reduce the degrees of freedom of the system. The quantization of constrained systems was developed by Paul Dirac [80] and provided the basis for the procedure of canonical quantization of GR.

First, we promote the canonical variables of the theory to quantum operators, so that the Poisson brackets $\{X, Y\}$ will be identified as commutators, i.e., $i\hbar\{X, Y\} \equiv [\hat{X}, \hat{Y}]$. Thus, the metric of the hypersurfaces h_{ij} becomes an operator $\hat{h}_{ij}$, which acts on wave functionals Ψ.

[2]The weak equality denoted by $\approx$ is due to the fact that the equations are satisfied only when the constraints are applied.

From the Hamiltonian density (2.10), we can write the following functional Schrödinger equation:

$$i\partial_0\Psi = \int \left(N\hat{\mathcal{H}} + N_i\hat{\mathcal{H}}^i\right)\Psi d^3x, \tag{2.11}$$

where the right-hand side of the equation represents the Hamiltonian H. The constraints of the super-Hamiltonian and the supermomentum take the following form:

$$\hat{\mathcal{H}}\Psi = 0, \tag{2.12}$$

$$\hat{\mathcal{H}}^i\Psi = 0. \tag{2.13}$$

The wave functional must, therefore, satisfy not only equation (2.11) but also constraints (2.12) and (2.13). Equation (2.12) is called the Wheeler-DeWitt equation, while (2.13) is the so-called diffeomorphism constraint.

2.1.3 Minisuperspace Filled with a Perfect Fluid

Superspace is the name given to the space of three-dimensional hypersurfaces h_{ij}, which has infinite dimension. In turn, a minisuperspace is a reduced form of superspace, obtained by reducing the degrees of freedom of the system through the use of symmetries. Such symmetries arise from the homogeneity and isotropy of the Universe.

In order to incorporate the symmetries of the system, we consider the homogeneous lapse function, that is, $N = N(t)$, and the shift vector $N^i = 0$, indicating the isotropy of spacetime[3]. Thus, the line element[4] can be written as

$$ds^2 = -N^2(t)dt + h_{ij}(x,t)dx^i dx^j. \tag{2.14}$$

The metric h_{ij}, in turn, can be restricted to

$$h_{ij}(x,t)dx^i dx^j = a^2(t)d\Omega_3^2, \tag{2.15}$$

where $d\Omega_3^2$ is the line element of a three-sphere and $a(t)$ is the so-called scale factor, which parametrizes the Universe's expansion. More generally, it is possible to restrict h_{ij} with a finite number of parameters $q^\alpha(t)$, with $\alpha = 1, ..., n$. In the present case, $q^1(t) = a(t)$ and the remaining q^α correspond to the degrees of freedom of matter. The conjugate momenta to the parameters q^α will be denoted by p_α.

[3]These conditions for the lapse function and the shift vector are used at the so-called background level, where cosmological perturbations are not yet considered.

[4]The line element can be understood as the line segment associated with an infinitesimal displacement vector in a metric space. Its terms are directly related to the metric tensor through $ds^2 = g_{\mu\nu}dx^\mu dx^\nu$.

Thus, the quantities used in the Hamiltonian formulation of GR can be written in terms of $N(t)$ and $a(t)$. The action of the theory, including the matter Lagrangian density $\mathcal{L}_{\rm M}$ in terms of fields ϕ^A, then takes the form

$$\begin{aligned} S &= \int N h^{\frac{1}{2}} \left(R^{(3)} + K^{ij}K_{ij} - K^2 \right) dt d^3x + \\ &+ \int \mathcal{L}_{\rm M} \left(\phi^A, h_{ij}, N_i, N \right) N h^{\frac{1}{2}} dt d^3x \\ &= \int_0^1 dt N \left[\frac{1}{2N^2} f_{\alpha\beta}(q) \dot{q}^\alpha \dot{q}^\beta - U(q) \right], \end{aligned} \tag{2.16}$$

where $f_{\alpha\beta}(q)$ is G_{ijkl} defined in (2.7) reduced to minisuperspace and $U(q)$ is a function of q that can be understood as a potential. The integration limits 0 and 1 are obtained by appropriately adjusting the lapse function and time. Note that the action (2.16) corresponds to the description of a relativistic particle in a curved spacetime, containing both kinetic and potential contributions. Thus, the challenging task of solving the Wheeler-DeWitt equation (2.12) and the diffeomorphism constraint (2.13) in superspace is simplified to the problem of a particle in minisuperspace. For consistency, the equations of motion that can be obtained from this action should correspond to the Einstein equations, which describe GR in the classical regime.

The corresponding Hamiltonian $H = p_\alpha \dot{q}^\alpha - L$ is given by

$$H = N \left[\frac{1}{2} f^{\alpha\beta} p_\alpha p_\beta + U(q) \right], \tag{2.17}$$

from which we obtain the constraint of the super-Hamiltonian

$$\frac{1}{2} f^{\alpha\beta} p_\alpha p_\beta + U(q) \approx 0. \tag{2.18}$$

Traditionally, minisuperspace models have been understood as an approximation to extract information from the Universe as a whole. However, there is no confirmation that this approach leads to a faithful and complete representation of the theory. An alternative is to interpret the quantization of minisuperspace as the quantization of the smallest representative unit of spacetime, an approach known as the single-patch approach [81]. In this chapter, we adopt the more traditional approach, in which the Universe is represented by a minisuperspace.

Considering the line element of a homogeneous and isotropic Universe, also known as the Friedmann-Lemaître-Robertson-Walker (FLRW) line element (in spherical coordinates r, θ, Φ and with spatial curvature $k = -1, 0, +1$)

$$\begin{aligned} ds^2 &= -N^2 dt^2 + a^2 \left(\frac{dr^2}{1 - kr^2} + r^2 d\theta^2 + \right. \\ &+ \left. r^2 \sin^2\theta d\Phi^2 \right), \end{aligned} \tag{2.19}$$

we obtain the Lagrangian density (2.6) in the ADM formalism

$$\mathcal{L} = \frac{\ddot{a}a^2}{N} - \frac{\dot{a}\dot{N}a^2}{N^2} + \frac{\dot{a}^2 a}{N} + kNa, \tag{2.20}$$

$$= -\frac{a\dot{a}^2}{N} + kaN \tag{2.21}$$

having used integration by parts in the last equality.

The system's Hamiltonian, in turn, is given by

$$\mathscr{H} = N\left(-\frac{P_a^2}{4a} - ka\right), \tag{2.22}$$

where $P_a = -2a\dot{a}/N$ is the canonically conjugate momentum to the scale factor a.

Now let's consider that minisuperspace is filled with a perfect fluid described by the following matter Lagrangian

$$\mathcal{L}_M = \sqrt{-g}\left(\frac{1}{2}g^{\mu\nu}\partial_\mu\phi\partial_\nu\phi\right)^n, \tag{2.23}$$

where n is an integer and ϕ is a scalar field related to the four-velocity of the fluid

$$U_\mu = \frac{\partial_\mu\phi}{\sqrt{g^{\mu\nu}\partial_\mu\phi\partial_\nu\phi}}. \tag{2.24}$$

The parameter of the equation of state of the fluid can be obtained through the definition of the momentum-energy tensor[5]

$$T_{\mu\nu} = \frac{2}{\sqrt{-g}}\frac{\partial\mathcal{L}_M}{\partial g^{\mu\nu}} \tag{2.25}$$

and is given by

$$\omega = \frac{1}{2n-1}. \tag{2.26}$$

The system's Hamiltonian is then written as

$$\mathscr{H}_M = \frac{1}{\omega(\sqrt{2}n)^{1+\omega}}N\frac{p_\phi^{1+\omega}}{a^{3\omega}}, \tag{2.27}$$

[5]For a perfect fluid, the momentum-energy tensor can be written as $T_{\mu\nu} = (\rho + P)U_\mu U_\nu - Pg_{\mu\nu}$, where ρ is the energy density and P is the pressure. On the other hand, the parameter of the equation of state is given by $\omega = P/\rho$. Combining such expressions with definition (2.25), we obtain ω in terms of n.

where p_ϕ represents the canonically conjugate momentum to ϕ. By considering the following coordinate transformation

$$T = \frac{\omega(\sqrt{2}n)^{1+\omega}}{1+\omega}\frac{\phi}{p_\phi^{1+\omega}},\ P_T = \frac{1}{\omega}\left(\frac{p_\phi}{\sqrt{2}n}\right)^{1+\omega}, \tag{2.28}$$

we obtain

$$\mathscr{H}_M = N\frac{P_T}{a^{3\omega}}. \tag{2.29}$$

An alternative derivation of this result is obtained in [82].

Considering the Hamiltonians obtained for the gravitational part (2.22) and for the matter part (2.29), we arrive at the description of a homogeneous and isotropic minisuperspace, with spatial curvature $k = 0$ and filled with a perfect fluid:

$$\mathscr{H}_{\text{total}} = N\left(-\frac{P_a^2}{4a} + \frac{P_T}{a^{3\omega}}\right). \tag{2.30}$$

2.1.4 De Broglie-Bohm Quantum Cosmology

In this section, we will address the quantization of the Universe according to the De Broglie-Bohm interpretation, which has a deterministic nature, with the probabilistic properties of Quantum Mechanics being merely statistical. Such interpretation makes use of the so-called hidden variables, which determine the development of the quantum system. The predictions of the theory agree with the traditional Copenhagen interpretation, as long as the Schrödinger equation is maintained. In this section, the quantities necessary to perform the quantization will be briefly introduced. A more comprehensive approach to the interpretation can be found in [83].

First, we will apply Dirac quantization to the Hamiltonian (2.30) by promoting it to a quantum operator and by using equation (2.12). By choosing an operator ordering[6], we obtain

$$i\frac{\partial}{\partial T}\Psi = \frac{a^{\frac{3\omega-1}{2}}}{4}\frac{\partial}{\partial a}\left[a^{\frac{3\omega-1}{2}}\frac{\partial}{\partial a}\right]\Psi, \tag{2.31}$$

which represents the Wheeler-DeWitt equation. The variable T, related to the perfect fluid, can be understood as time.

In the De Broglie-Bohm interpretation, we write the wave function as $\Psi = R\exp[iS]$, where R is the amplitude and S is the phase of the wave.

[6]The need to choose an ordering is related to Heisenberg's uncertainty principle, according to which two complementary operators cannot be measured simultaneously. Mathematically, this fact is described by the non-commutativity of such operators. In equation (2.31), the scale factor a and its conjugate momentum $\partial/\partial a$ do not commute, making the choice of ordering necessary.

Defining $\rho \equiv a^{\frac{3\omega-1}{2}}|\Psi|^2$, we obtain that (2.31) results in two equations:

$$\frac{\partial S}{\partial T} - \frac{a^{3\omega-1}}{4}\left(\frac{\partial S}{\partial a}\right)^2 + \\ + \frac{a^{\frac{3\omega-1}{2}}}{4R}\frac{\partial}{\partial a}\left[a^{\frac{3\omega-1}{2}}\frac{\partial R}{\partial a}\right] = 0, \tag{2.32}$$

$$\frac{\partial \rho}{\partial T} - \frac{\partial}{\partial a}\left[\frac{a^{3\omega-1}}{2}\frac{\partial S}{\partial a}\rho\right] = 0. \tag{2.33}$$

Moreover, the configuration space has a deterministic nature, being described by the so-called guidance equation

$$\dot{a} = -\frac{a^{3\omega-1}}{2}\frac{\partial S}{\partial a}. \tag{2.34}$$

Note that equation (2.32) takes the form of a Hamilton-Jacobi equation within the scope of Quantum Mechanics, with $Q = -\frac{a^{\frac{3\omega-1}{2}}}{4R}\frac{\partial}{\partial a}\left[a^{\frac{3\omega-1}{2}}\frac{\partial R}{\partial a}\right]$ being a quantum potential character. This potential is responsible for altering the trajectory of the scale factor a, replacing the initial singularity of the Universe with a finite scale factor. In turn, equation (2.33) takes the form of a continuity equation for ρ.

Equation (2.31) can be written in a simpler form considering the following coordinate transformation

$$\chi = \frac{2}{3(1-\omega)}a^{\frac{3(1-\omega)}{2}}, \tag{2.35}$$

which results in

$$i\frac{\partial \Psi}{\partial T} = \frac{1}{4}\frac{\partial^2 \Psi}{\partial \chi^2}. \tag{2.36}$$

The same transformation modifies (2.34) to

$$\frac{d\chi}{dT} = -\frac{1}{2}\frac{\partial S}{\partial \chi}. \tag{2.37}$$

In the context of Quantum Cosmology, Ψ is called the wave function of the Universe, which must satisfy (2.36). In order to solve this equation for Ψ, we need a boundary condition. An interesting choice is given by

$$\left(\Psi^*\frac{\partial \Psi}{\partial \chi} - \Psi\frac{\partial \Psi^*}{\partial \chi}\right)\Bigg|_{\chi=0} = 0, \tag{2.38}$$

where Ψ^* represents the conjugate of Ψ, since it leads to unitary solutions of the wave function[7].

[7]We call unitary the wave functions whose temporal evolution is represented by a unitary operator, which is closely related to measurement probabilities.

For the initial wave function, as an example, we can choose

$$\Psi_0 = \left(\frac{8}{\pi\sigma^2}\right)^{\frac{1}{4}} \exp\left(-\frac{\chi^2}{\sigma^2}\right), \tag{2.39}$$

since the boundary condition (2.38) is satisfied. The expression of the wave function for any time T is then given by

$$\Psi(\chi, T) = \int_0^\infty G(\chi, \chi_0, T)\Psi_0(\chi_0, T)d\chi_0, \tag{2.40}$$

where $G(\chi, \chi_0, T)$ is the propagator related to the Wheeler-DeWitt equation (2.36). Note that the latter is similar to the Schrödinger equation, except for the sign of the kinetic energy. Thus, the propagator is given by

$$\begin{aligned} G(\chi, \chi_0, T) &= \sqrt{-\frac{i}{\pi T}}\left\{\exp\left[-i\frac{(\chi-\chi_0)^2}{T}\right] + \right. \\ &+ \left. \exp\left[-i\frac{(\chi+\chi_0)^2}{T}\right]\right\}, \end{aligned} \tag{2.41}$$

where, in order to ensure the unitarity of the evolution, we sum one propagator for χ_0 and another for $-\chi_0$. By applying (2.41) to (2.40), we obtain

$$\begin{aligned} \Psi(\chi, T) &= \left[\frac{8\sigma^2}{\pi(\sigma^4+T^2)}\right]^{\frac{1}{4}} \exp\left[-\frac{\sigma^2\chi^2}{\sigma^4+T^2}\right] \times \\ \times &\left[-i\left(\frac{T\chi^2}{\sigma^4+T^2} + \frac{1}{2}\arctan\frac{\sigma^2}{T} - \frac{\pi}{4}\right)\right], \end{aligned} \tag{2.42}$$

which can be decomposed into the form $\Psi = R\exp[iS]$.

Solving the guidance equation (2.37), we obtain

$$\chi = \chi_b\left[1 + \left(\frac{T}{\sigma^2}\right)^2\right]^{\frac{1}{2}}, \tag{2.43}$$

which is related to the scale factor a by the transformation (2.35), resulting in

$$a = a_b\left[1 + \left(\frac{T}{\sigma^2}\right)^2\right]^{\frac{1}{3(1-\omega)}}. \tag{2.44}$$

The parameters χ_b and a_b represent the values of χ and a when the Universe has its smallest size. Figure 2.2 presents the scale factor (2.44) as a function of time T, where we can identify a contraction regime of the Universe for $T < 0$ and an expansion regime for $T > 0$. The meeting of these phases at $T = 0$ occurs in the quantum realm, where the potential Q identified in (2.32) plays a fundamental role. Thus, the classical singularity is replaced by a

minimum scale factor a_b. Note that this bounce is symmetric, meaning that the contracting phase mirrors the expansion. In the next section we obtain an asymmetric bounce, which has interesting cosmological implications.

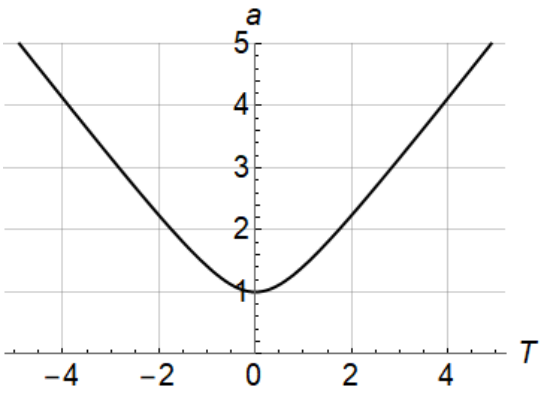

FIGURE 2.2: Resolution of the initial singularity through a bounce model obtained in De Broglie-Bohm Quantum Cosmology. In this figure, $a_b = \sigma = 1$ and $\omega = 1/3$, representing a perfect fluid of radiation.

2.2 Background Evolution

Let us start by recalling the main results of the previous sections, which will now be applied to a different boucing solution (generated by a different anzats of the initial wave function).

We consider a homogeneous and isotropic Universe filled with a perfect fluid governed by a barotropic equation of state of the form $p = w\rho$, with constant w. The Einstein-Hilbert action may be written using the ADM variables [79], considering a foliation of spacetime into space-like hypersurfaces. As we have seen in Section 2.1.1, neglecting boundary terms, the corresponding FLRW action reads

$$\begin{aligned} S &= \frac{1}{6}\int \mathrm{d}^4x\sqrt{h}N\left[K_{ij}K^{ij} - \left(h^{ij}K_{ij}\right)^2 + {}^{(3)}R\right] \\ &= \int N\mathrm{d}t\left(-\frac{a\dot{a}^2}{N^2} + ak\right) . \end{aligned} \tag{2.45}$$

The quantities N, h_{ij}, K_{ij}, ${}^{(3)}R$, a, and k are the lapse function, induced metric of the spacelike hypersurfaces, extrinsic curvature of the spacetime foliation, the Ricci scalar of the spacelike hypersurfaces, the scale factor, and the constant curvature of the homogeneous and isotropic spacelike hypersurfaces, respectively. An overdot corresponds to a derivative with respect to coordinate time t.

In the case of spatially flat hypersurfaces, which we consider from now on, the Hamiltonian is given by (2.30). The dynamical variables are the scale factor a, its conjugate momentum P_a, the perfect fluid variable T, related to the velocity field of the fluid, and its conjugate momentum P_T, related to the classically conserved total number of particles of the fluid. The latter appears linearly in the Hamiltonian, which leads to a natural interpretation of T as a time variable. This is one of the proposed solutions to the problem of time in quantum cosmology, where the degree of freedom corresponding to the perfect fluid plays the role of a time variable. This approach has been used both in canonical quantum gravity [84, 85] and in modified gravity [86]. The cosmic time τ is related to T through Hamilton's equations by $\mathrm{d}\tau \equiv N\mathrm{d}t = a^{3w}\mathrm{d}T$. Note that for dust ($w = 0$) T is cosmic time, while in the case of a radiation fluid ($w = 1/3$) T corresponds to conformal time η.

In order to perform the canonical quantization of the system, one must specify an operator ordering, which in this case is such that we obtain a covariant Laplacian under redefinitions of the scale factor a [87, 88]. With this choice, the Wheeler-DeWitt equation $\hat{\mathcal{H}}_0\Psi = 0$, where Ψ denotes the minisuperspace wave function, reads

$$\mathrm{i}\frac{\partial}{\partial T}\Psi(\chi, T) = \frac{1}{4}\frac{\partial^2}{\partial \chi^2}\Psi(\chi, T)\,, \tag{2.46}$$

where

$$\chi \equiv \frac{2}{3(1-w)}a^{3(1-w)/2}\,. \tag{2.47}$$

The concrete solutions for the scale factor are obtained by proposing an *ansatz* for the initial wave function, which must be propagated to lead to the wave function at any time T.

Let us turn our attention to the conceptual implications of this quantization procedure for a system that is the universe as a whole. The standard Copenhagen interpretation demands an external classical domain in order to collapse the wave function, as a result of a measurement process performed on the system. This external domain is by definition absent in a cosmological setting. One of the alternative interpretations of quantum mechanics that allows for consistent cosmological scenarios is the de Broglie-Bohm (dBB) Quantum Theory [73, 74], which we shall adopt from now on. This approach consists of a deterministic interpretation of quantum mechanics in which the particles or field amplitudes describe trajectories in configuration space which are objectively real, regardless of a measurement process. These trajectories satisfy judiciously chosen guidance equations, in which the initial particle positions or field configurations are not known - only a probability distribution thereof -, thus constituting the hidden variables of the theory. If this probability distribution is given by the Born rule, then all probabilistic predictions of quantum theory are recovered. The compatibility of this interpretation with quantum cosmology is a result of the so called effective collapse, which

describes the occupation of one of the branches of the wave function in a measurement process by the point particle in configuration space, depending on its initial particle positions or field configurations. Since this effective collapse does not require an external observer, the dBB theory can be applied to the universe as whole. Moreover, the "particle trajectory", which in this case is related to the evolution of the scale factor, is part of an objective reality. The resulting cosmological models might be able to avoid the initial singularity problem, replacing it with a bounce, which is preceded by a contracting phase and followed by the usual expansion of the universe [89, 90, 91].

2.2.1 Asymmetric Bounce

In reference [91] it is shown that, within the dBB interpretation, an initial state of the form

$$\Psi_0(\chi) = \left(\frac{8}{\pi\sigma^2}\right)^{\frac{1}{4}} \exp\left(-\frac{\chi^2}{\sigma^2} + \mathrm{i}p\chi\right) , \tag{2.48}$$

with $p, \sigma \in \mathbb{R}$, can be evolved by the propagator

$$G^{NU}(\chi, \chi_0, T) = \sqrt{-\frac{\mathrm{i}}{\pi T}} \exp\left[-\frac{\mathrm{i}(\chi - \chi_0)^2}{T}\right] , \tag{2.49}$$

yielding the following solution for all times

$$\begin{aligned} \Psi(\chi, T) =& R_\Psi(\chi, T) \exp\left[\mathrm{i}S_\Psi(\chi, T)\right] , \\ R_\Psi(\chi, T) \equiv& \left[\frac{8\sigma^2}{\pi(\sigma^4 + T^2)}\right]^{1/4} \times \\ & \times \exp\left[-\frac{\sigma^2}{\sigma^4 + T^2}\left(\chi + \frac{pT}{2}\right)^2\right] , \\ S_\Psi(\chi, T) \equiv& p\left(\chi + \frac{pT}{4}\right) - \frac{T}{\sigma^4 + T^2}\left(\chi + \frac{pT}{2}\right)^2 + \\ & + \frac{1}{2}\arctan\left(\frac{T}{\sigma^2}\right) . \end{aligned} \tag{2.50}$$

The quantum parameters σ and p are related to the initial width (with a standard deviation $\sigma/\sqrt{2}$) and momentum of the Gaussian in configuration space, respectively. The associated Bohmian trajectories for the variable χ, which can be translated to the trajectories of the scale factor a through definition (2.47), are a solution to the Bohmian guidance equation

$$\frac{\mathrm{d}\chi}{\mathrm{d}T} = -\frac{1}{2}\frac{\partial S_\Psi}{\partial \chi}\bigg|_{\chi(T)} = \frac{T}{\sigma^4 + T^2}\chi - \frac{p\sigma^4}{2(\sigma^4 + T^2)} , \tag{2.51}$$

which can be integrated to give

$$\chi(T) = \chi_b \left[1 + \left(\frac{T}{\sigma^2} \right)^2 + \left(\frac{p}{2\chi_b} \right)^2 \left(\sigma^4 + T^2 \right) \right]^{\frac{1}{2}} - \frac{pT}{2} , \tag{2.52}$$

where χ_b is the value of the variable χ at the bounce, occurring at $T_b = p\sigma^4/(2\chi_b)$.

Defining

$$\bar{T} \equiv \frac{T}{\sigma^2} , \quad x_b \equiv \frac{a_0}{a_b} , \quad y \equiv -\frac{p\sigma^2}{2\chi_b} , \tag{2.53}$$

we can rewrite (2.52) in the simple form

$$\chi(\bar{T}) = \chi_b \left(y\bar{T} + \sqrt{1+y^2}\sqrt{1+\bar{T}^2} \right) .$$

As a result, the scale factor reads

$$a(\bar{T}) = a_b \left(y\bar{T} + \sqrt{1+y^2}\sqrt{1+\bar{T}^2} \right)^{\frac{2}{3(1-w)}} , \tag{2.54}$$

where a_b is the scale factor at the bounce, and $\bar{T}_b = -y$ corresponds to the time at which the bounce occurs. When $|T| \gg \sigma^2$, or $|\bar{T}| \gg 1$, we have $a(\bar{T}) \propto |\bar{T}|^{\frac{2}{3(1-w)}}$ which, translated to cosmic time, corresponds to a classical single-fluid Friedmann evolution $a(\tau) \propto |\tau|^{\frac{2}{3(1+w)}}$.

Looking at Eq. (2.54), we can see that the time asymmetry of the model comes from the linear term in $\bar{T}$, with the property $a(-y, \bar{T}) = a(y, -\bar{T})$. Hence, changing $y \to -y$ is equivalent to time-reversing the original solution. From now on we will choose $y > 0$ (or $p < 0$), the case $y < 0$ being straightforwardly obtained by time reversing the conclusions.

The Hubble function is given by $H \equiv \dot{a}/(Na) = a^{-3(1+w)/2} \, (\mathrm{d}\chi/\mathrm{d}T)$. Its expression squared reads

$$H^2(\bar{T}) = \frac{4}{9(1-w)^2} \frac{a_b^{3(1-w)}}{\sigma^4 a^{3(1+w)}(\bar{T})} F(\bar{T}) , \tag{2.55}$$

where

$$F(\bar{T}) = \left(y + \sqrt{1+y^2} \frac{\bar{T}}{\sqrt{1+\bar{T}^2}} \right)^2 . \tag{2.56}$$

In the asymptotic limits we get

$$\lim_{\bar{T} \to \pm\infty} F(\bar{T}) =: F_\pm = \left(y \pm \sqrt{1+y^2} \right)^2 , \tag{2.57}$$

which is a constant. Thus, we get

$$H_{\pm}^2(\bar{T}) \propto \frac{F_{\pm}}{a_{\pm}^{3(1+w)}(\bar{T})} \propto \rho_{\pm}(\bar{T})\,, \tag{2.58}$$

which are the asymptotic classical Friedmann equations at both limits, as expected (the subscripts $\pm$ refer to the asymptotic future and past, respectively).

Fixing the same scale factor at both asymptotic classical phases, we have

$$H_{\pm}^2(a) \propto \frac{F_{\pm}}{a^{3(1+w)}} \propto \rho_{\pm}(a)\,, \tag{2.59}$$

showing that the model is not symmetric. In fact, the conserved quantities $F_{\pm}$, which can be understood as the total number of particles inside a volume cell for a given scale factor in both asymptotic phases, are different, see Eq. (2.57), with creation of particles from the asymptotic past to the asymptotic future:

$$\frac{\rho_+(a)a^{3(1+w)}}{\rho_-(a)a^{3(1+w)}} = \frac{F_+}{F_-} = \frac{\left(y+\sqrt{1+y^2}\right)^2}{\left(y-\sqrt{1+y^2}\right)^2} > 1\,. \tag{2.60}$$

For $y \gg 1$, this growth can be huge: from (2.59) and (2.60), evaluating at the same scale factor, we have that the respective ratio of the energy densities at the asymptotic future and past is given by

$$\frac{\rho_+(a)a^{3(1+w)}}{\rho_-(a)a^{3(1+w)}} = \frac{\rho_+(a)}{\rho_-(a)} = \frac{H_+^2(a)}{H_-^2(a)} \approx 16y^4 \gg 1\,, \tag{2.61}$$

implying both a large creation of particles, and a very slow asymptotic contraction when compared to the asymptotic expansion rate for the same a, $H_+ \gg |H_-|$. The ratio of Hubble radii $R_{\pm}$ then reads

$$\frac{R_-(a)}{R_+(a)} = \frac{H_+(a)}{|H_-(a)|} \approx 4y^2 \gg 1\,. \tag{2.62}$$

The classical scale factor in both asymptotic limits simplifies to

$$a_{\text{expansion}} \approx a_b\left[(2y)\bar{T}\right]^{\frac{2}{3(1-w)}}\,, \tag{2.63}$$

$$a_{\text{contraction}} \approx a_b\left[|\bar{T}|/(2y)\right]^{\frac{2}{3(1-w)}}\,. \tag{2.64}$$

Comparing $H_+^2(\bar{T})$ with the late time Friedmann equation $H^2/H_0^2 = \Omega_{w,0}x^{3(1+w)}$, where $x \equiv a_0/a$ and $\Omega_{w,0}$ is the ratio between the fluid energy density and the critical density when $H = H_0$, we can relate $\Omega_{w,0}$ and the Hubble radius today $R_{H_0} \equiv 1/H_0$ to the free parameters of the model:

$$\sigma^2 a_b^{3w} = \frac{2R_{H_0}\left(y+\sqrt{1+y^2}\right)}{3(1-w)x_b^{3(1+w)/2}\sqrt{\Omega_{w,0}}}, \tag{2.65}$$

which will be very useful in the next section.

2.2.2 Quasi de Sitter Phase

A noteworthy feature in the scenario with $y \gg 1$ arises from the fact that for $\bar{T} < 0$, $|\bar{T}| \gg 1$ and $y \gg 1$ the scale factor (2.54) reads

$$a(\bar{T}) \approx a_b \left(\frac{|\bar{T}|}{2y} + \frac{y}{2|\bar{T}|}\right)^{\frac{2}{3(1-w)}} . \tag{2.66}$$

The classical contraction is recovered when the first term in (2.66) dominates, i.e. when $|\bar{T}| \gg y$. In this case, $a \propto |\eta|^{\frac{2}{1+3w}}$, as $|\eta| \propto |\bar{T}|^{\frac{1+3w}{3(1-w)}}$. On the other hand, when $|\bar{T}| \ll y$, which happens after the bounce, the second term in (2.66) dominates and, since in this case $|\eta| \propto |\bar{T}|^{\frac{5-9w}{3(1-w)}}$, we have

$$a(\eta) \propto |\eta|^{-\frac{2}{5-9w}} . \tag{2.67}$$

Hence, an intermediate phase between the bounce and the classical expansion arises naturally, corresponding to a quantum accelerated expansion when $1/3 \leqslant w < 5/9$[8]. If $w = 1/3$, i.e. in a radiation-dominated universe, this phase is in fact a de Sitter expansion, where $a(\eta) \propto \eta^{-1}$. Moreover, since (2.67) comes from an approximation, the quantum accelerated expansion is indeed a quasi-de Sitter (qdS) phase. Accordingly, we find the Hubble parameter around this stage to be almost - but not exactly - constant. The corresponding scale factor is depicted in Figure 2.3, where a comparison between the quantum accelerated phase and the de Sitter scale factor is exhibited.

Since $y \gg 1$, this quantum accelerated expansion might last for a long time, around $-y \ll \bar{T} \ll -1$. Afterwards, when $\bar{T} \gg 1$, the classical decelerated expansion of the standard cosmological model takes place. In other words, the scenario determined by the condition $y \gg 1$ and $w \approx 1/3$ encompasses a bounce regulated by quantum effects, followed by a large period of accelerated quantum expansion, which gracefully exits into the usual classical regime. Therefore, this scenario is analogous to inflation without an inflaton and without the usual reheating phase, as it is smoothly followed by the classical decelerated expansion dominated by radiation. As discussed after Eq. (2.61), there is a huge creation of photons during the quantum phase.

[8]Note that for $w < 1/3$, which includes the matter bounce scenario, one gets an intermediate phantom accelerated expansion. This is an interesting possibility, which might be explored in future investigations.

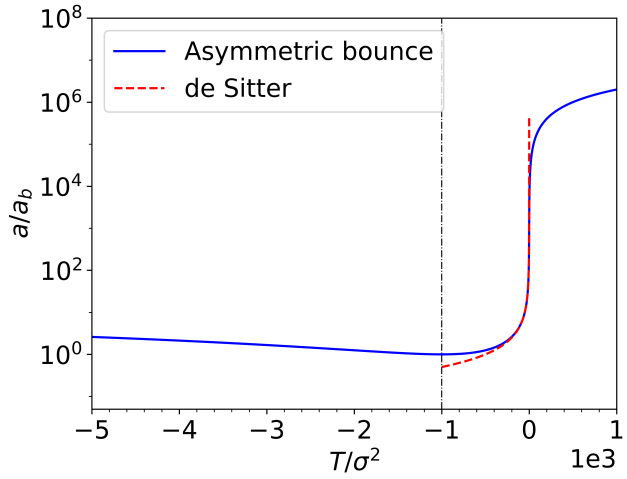

FIGURE 2.3: Evolution of the scale factor a in the scenario with a subtle contraction, compared to the de Sitter evolution $a \propto \eta^{-1}$. We use $y = 10^3$ and $w = 1/3$, corresponding to a radiation fluid. The vertical line indicates the bounce time $\bar{T}_b = -y$.

The effective energy density of this inflationary period can be obtained by expanding the Hubble parameter for large y and then large $\bar{T}$. The dominant constant term, present only in this phase, is found to be equal to $\Omega_{\rm qdS} = (x_b/y)^4 \Omega_{w,0}$. We shall later express this in a more suggestive way.

The scale factor (2.54) contains three parameters: two from the initial Gaussian wave function (σ, p), and one as an integration constant (a_b or, equivalently, x_b) of the guidance equation (2.51). They are tied together by the late time Hubble parameter expansion, see Eq. (2.65), leaving the set $\{y, x_b\}$ as free parameters. A physically important parameter is the minimum curvature scale l_c of the model, which cannot be very close to the Planck scale, where the above quantization scheme is not reliable. It is given by

$$l_c \equiv \frac{1}{\sqrt{\max[R(\bar{T})]}}\,, \tag{2.68}$$

where $R(\bar{T}) = 6\left(\ddot{a}/a + H^2\right)$ is the Ricci scalar computed from the background trajectory (here an overdot denotes a cosmic time derivative). It reads

$$\begin{aligned} R =& \frac{4\alpha^{-2\left(\frac{1+w}{1-w}\right)}}{(1-w)\left(\sigma^2 a_b^{3w}\right)^2} \times \\ & \times \left[\frac{\sqrt{1+y^2}}{(1+\bar{T}^2)^{3/2}}\alpha + \frac{1-3w}{3(1-w)}\left(\frac{\mathrm{d}\alpha}{\mathrm{d}\bar{T}}\right)^2\right], \end{aligned} \tag{2.69}$$

where $\alpha \equiv y\bar{T} + \sqrt{1+y^2}\sqrt{1+\bar{T}^2}$.

In the case of interest, i.e. $w = 1/3$, which leads to the qdS expansion, and large asymmetry ($y \gg 1$), the maximum curvature happens when [91]

$$\bar{T}_{\max} = -\sqrt{\left(\sqrt{1+y^2}-1\right)/2} \approx -\sqrt{y/2}\,. \tag{2.70}$$

Hence, from Eqs. (2.65) and (2.69), the minimum curvature scale in terms of the previous parameters and cosmological observables reads

$$l_c \equiv \frac{y^2}{x_b^2\sqrt{12\Omega_{r,0}}} R_{H_0}\,, \tag{2.71}$$

where $\Omega_{r,0} \approx 9 \times 10^{-5}$ is the density parameter of radiation today. The curvature scale is bounded from below so as not to be too close to the Planck scale, $l_P \approx 10^{-61} R_{H_0}$, at an energy scale of about 10^{19} GeV. Both the minisuperspace approximation and the Wheeler-DeWitt quantization cease to be valid or meaningful close to this boundary, requiring a full, yet unknown, theory of quantum gravity[9]. On the other hand, the model must recover its standard FLRW evolution much before nucleosynthesis, in order not to spoil its good agreement with observations, thus leading to an upper bound for l_c.

Using Eqs. (2.54) and (2.55) for $w = 1/3$, we can estimate the Hubble parameter in the classical limit around nucleosynthesis:

$$H \approx \frac{1}{\sigma^2 a_b (2y\bar{T}^2)} = \frac{1}{8\sqrt{3} l_c \bar{T}^2}\,, \tag{2.72}$$

This approximation is good from $\bar{T} \approx 10$ onward, where the relative error with respect to classic evolution is about 0.5%. From the characteristic energy density at the dawn of the nucleosynthesis era, $\varepsilon_{\text{nucleo}} \approx 10^{16}\,\text{g}\,\text{cm}^{-3}$, and using the Friedmann equation $H^2 = H_0^2 \Omega(\bar{T})$ we get

$$H^2/H_0^2 > \Omega_{\text{nucleo}} \rightarrow \frac{l_c}{R_{H_0}} < \frac{1}{8\sqrt{3}(10)^2\sqrt{\Omega_{\text{nucleo}}}}\,. \tag{2.73}$$

Thus, demanding that the transition of the quantum background to the classical behavior must take place much before nucleosynthesis, and does not reach the Planck scale by three orders of magnitude, we find the constraint

$$10^3 < \frac{l_c}{l_P} \ll 10^{35}\,. \tag{2.74}$$

Having introduced l_c, the effective qdS energy density may be rewritten

[9] The Wheeler-DeWitt equation is considered valid at least as an approximation to a more fundamental theory of quantum gravity [72]. For this reason, the most conservative approach is to take some orders of magnitude of distance from the Planck scale, where the fundamental theory would be required.

as $\Omega_{\rm qdS} = (R_{H_0}/l_c)^2/12$, which in turn gives an effective primordial cosmological constant directly related to the minimum curvature scale,

$$\Lambda_{\rm qdS} \equiv \frac{1}{4l_c^2}\,, \tag{2.75}$$

being responsible for driving the almost exponential expansion. Note this can also be obtained by comparing $a \approx y/(2|\bar{T}|)$ with the de Sitter scale factor $a = (H|\eta|)^{-1}$, with $H = \sqrt{\Lambda/3}$.

Furthermore, an initial estimate of the e−folds of this model can be made through

$$\mathcal{N} = \ln\left(\frac{a_f}{a_i}\right) \approx \ln\left[\frac{a(0)}{a(-y)}\right] \approx \ln y\,, \tag{2.76}$$

where we considered the beginning of the inflationary period to be the bounce and its end to be at $\bar{T} = 0$ [10].

To accommodate for e.g. $\mathcal{N} > 60$ we should require

$$y > 1.14 \times 10^{26}\,. \tag{2.77}$$

2.3 Cosmological Perturbations: Analytical Results

The variable generally used to describe the evolution of scalar perturbations on a homogeneous and isotropic spacetime with a single perfect fluid is the gauge invariant curvature perturbation ζ, which is a combination of fluid and (scalar) metric linear perturbations [92]. The appropriate variable to be quantized is the Mukhanov-Sasaki variable, which in the perfect fluid case is related to the curvature perturbation ζ in momentum space through $v_k \equiv a\zeta_k$. It satisfies the equation of motion

$$v_k'' + \left(c_s^2 k^2 - \frac{a''}{a}\right) v_k = 0\,, \tag{2.78}$$

where a prime denotes derivative with respect to conformal time.

In the sections below, we will present the analytical results for arbitrary w, and then particularize to $w = 1/3$.

[10] Since there is a very slow contraction, the initial time for a_i is very close to the start of the qdS phase; similarly, the transition to the classical expansion occurs around $\bar{T} \sim \mathcal{O}(1)$, and does not change the estimate significantly.

2.3.1 Arbitrary Perfect Fluid

Let us begin by analyzing the limiting cases of (2.78) and matching them at the crossing $c_s^2 k^2 \approx a''/a$ [11]. When $c_s^2 k^2 \gg a''/a$, the solution is given by

$$v_k \approx C_1(k) \mathrm{e}^{\mathrm{i}c_s k\eta} + C_2(k) \mathrm{e}^{-\mathrm{i}c_s k\eta} \,, \tag{2.79}$$

while for $c_s^2 k^2 \ll a''/a$ the solution can be approximated as

$$v_k \approx A_1(k) a + A_2(k) a \int \frac{\mathrm{d}\eta}{a^2} + \mathcal{O}(k^2) \,. \tag{2.80}$$

For the perturbation modes that cross the potential $V \equiv a''/a$ during the contracting phase, the $A_2(k)$ term - which grows when a decreases - dominates in the decelerated expansion.

On the other hand, for modes that cross the potential during the quantum accelerated expansion after the bounce, it is $A_1(k)$ that dominates in the decelerated expansion.

In order to find $A_1(k)$ and $A_2(k)$, we match both approximate solutions at the crossing $c_s^2 k^2 \cong V$. Since for $\bar{T} \to -\infty$, $a''/a \to 0$, we can choose the initial condition as the normalized adiabatic vacuum $v_k \approx \exp(-\mathrm{i}c_s k\eta)/\sqrt{2c_s k}$. Far from the bounce into the remote past, $\bar{T} \ll -y$, we can approximate the potential a''/a using the first term in (2.66), yielding

$$V \propto \left(\frac{1}{|\bar{T}|}\right)^{\frac{2(1+3w)}{3(1-w)}} \,. \tag{2.81}$$

This phase corresponds to a classical contraction with $a(\eta) \approx |\eta|^{\frac{2}{1+3w}}$, $|\eta| \propto |\bar{T}|^{\frac{1+3w}{3(1-w)}}$. Since the term that dominates the potential is proportional to $|\eta|^{-2}$, we have the horizon crossing at conformal time η_c when $c_s^2 k^2 \approx \eta_c^{-2}$. From the approximation (2.80) we then have

$$v_k = A_1(k) \eta^{\frac{2}{1+3w}} + c_1 A_2(k) \eta^{\frac{-1+3w}{1+3w}} \,, \tag{2.82}$$

[11] Note that the classical FLRW Ricci scalar may be written as $R = 6a''/a^3$ (for the case of exact radiation it vanishes identically). Moreover, for the (classical) pure de Sitter or perfect fluid cases, $R \propto H^2$. The physical curvature scale $R^{-1/2}$ may be written as $a\ell$, where $\ell \propto \sqrt{a/a''}$ is the comoving curvature scale. Therefore, apart from a factor of order unity, the potential crossing condition $c_s^2 k^2 = a''/a$ can also be understood as the time when the physical scale a/k becomes equal to the curvature scale, sometimes called Hubble crossing.

where c_1 is a constant of order unity. Matching the adiabatic vacuum and (2.82) at $\eta_c \approx k^{-1}$ for both v_k and ${v_k}'$ we find

$$A_1(k) \propto k^{\frac{3(1-w)}{2(1+3w)}}\,, \tag{2.83}$$

$$A_2(k) \propto k^{-\frac{3(1-w)}{2(1+3w)}}\,. \tag{2.84}$$

As $A_2(k)$ dominates for modes that cross the potential during the decelerated contraction, the scalar power spectrum reads [90]

$$P_\zeta(k) \propto k^3 |A_2(k)|^2 \propto k^{\frac{12w}{1+3w}}\,. \tag{2.85}$$

The almost scale invariant behavior, compatible with observations, is then obtained for $w \approx 0$. This corresponds to the result in [90] for the quantum symmetric bounce, to which the present asymmetric case reduces as $y \to 0$ [12].

Let us now investigate the quantum accelerated phase, considering the potential obtained from the second term in (2.66). For $-y \ll \bar{T} \ll -1$, we have (2.67), and the potential is approximately

$$V \propto \left(\frac{1}{|\bar{T}|}\right)^{\frac{2(5-9w)}{3(1-w)}} \propto |\eta|^{-2}\,. \tag{2.86}$$

Consequently, $\eta_c \approx k^{-1}$ also for this phase. Using (2.80) we find

$$v_k \approx A_1(k)\eta^{-\frac{2}{5-9w}} + c_2 A_2(k)\eta^{\frac{7-9w}{5-9w}}\,. \tag{2.87}$$

Matching both v_k and ${v_k}'$ with the adiabatic vacuum at $\eta_c \approx k^{-1}$, we find

$$A_1(k) \propto k^{-\frac{9(1-w)}{2(5-9w)}}\,, \tag{2.88}$$

$$A_2(k) \propto k^{\frac{9(1-w)}{2(5-9w)}}\,. \tag{2.89}$$

The quantum accelerated expansion is dominated by $A_1(k)$ and, therefore, the scalar power spectrum has the following $k-$dependence:

$$P_\zeta(k) \propto k^3 |A_1(k)|^2 \propto k^{\frac{6(1-3w)}{5-9w}}\,. \tag{2.90}$$

Note that almost scale invariance is attained for $w \approx 1/3$, as expected

[12] It is worth noting that the main $|\eta|^{-2}$ contribution to the potential in the contracting phase vanishes for $w = 1/3$. One finds that the next contribution corresponds to a $|\eta|^{-\frac{8}{1+3w}}$ behavior, thus leading to $V|_{w=1/3} \propto |\eta|^{-4}$. This is typical of an evolution which is almost, but not exactly, classically dominated by radiation. Proceeding in the same way as before, the dominant term $A_2(k)$ goes as $k^{-1/2}$, leading to a blue tilted power spectrum $P_{\zeta,1/3}(k) \propto k^2$, which coincides with (2.85) evaluated for radiation.

from the qdS behavior for this choice of fluid. Thus, if the background is dominated by a radiation fluid and the cosmological scales that we observe today cross the potential during the quantum accelerated expanding phase, then their power spectrum will be almost scale invariant. In this case, the accelerated period is a qdS expansion akin to inflation, with the advantage of happening naturally within the model, without an inflaton. The inclusion of other subdominant matter fields, so as to maintain the quasi-de Sitter behavior, does not change substantially the duration of the inflationary period nor the number of e-folds, which are corrected by $\mathcal{O}(\epsilon)$ for $w = 1/3 + \epsilon, |\epsilon| \ll 1$. Such inclusion will be investigated in future works. Let us then focus our attention to the radiation fluid, $w = 1/3$.

2.3.2 The Case of Radiation

In this case, the scale factor has the simple form

$$a(\bar{\eta}) = a_b \left(y\bar{\eta} + \sqrt{1+y^2}\sqrt{1+\bar{\eta}^2} \right) , \tag{2.91}$$

and the bounce happens when $\bar{\eta} = -y$. Recall that for $w = 1/3$ the time $\bar{T}$ is a dimensionless conformal time, which we have named $\bar{\eta}$. Equation (2.78) reads

$$v_k'' + \left(\bar{k}^2 - \frac{a''}{a} \right) v_k = 0 , \tag{2.92}$$

where the primes now denotes derivatives with respect to $\bar{\eta}$, $\bar{k} \equiv \sigma^2 c_s k$, and

$$V \equiv \frac{a''}{a} = \frac{\sqrt{1+y^2}\left(1+\bar{\eta}^2\right)^{-3/2}}{y\bar{\eta} + \sqrt{1+y^2}\sqrt{1+\bar{\eta}^2}} . \tag{2.93}$$

We will assume from now on that $y \gg 1$.

Let us make a brief qualitative summary of the history of the background and perturbations. The periods (1-3) in what follows are for $\bar{\eta} < 0$, the period (4) is the transition from $\bar{\eta}$ negative to $\bar{\eta}$ positive, and period (5) for $\bar{\eta} > 0$.

1) For $-\bar{\eta} \gg y$:

In the far past of the model, the universe is contracting from $\bar{\eta} \to -\infty$ as $a \approx -a_b\bar{\eta}/(2y)$, a classical contraction dominated by radiation. The potential $V \equiv a''/a$, also called the effective Hubble parameter, goes as $2y^2/\bar{\eta}^4$. Note that V is not zero because a is not exactly $-a_b\bar{\eta}/(2y)$. This is typical of an evolution which is almost, but not exactly, classically dominated by radiation.

As we have seen in the previous section, the wavenumbers that cross the

effective Hubble parameter at this epoch will not be scale invariant, with an associated power spectrum scaling as $\bar{k}^2$, so we must guarantee that they are very small (very large scales, much bigger than the Hubble radius today).

2) For $-\bar{\eta} \approx y$:

In this phase the quantum effects become important, they realize the bounce and launch the universe in a quantum expanding phase.

3) For $1 \ll -\bar{\eta} < y$:

The universe enters in a expanding phase with $a \approx -a_b y/(2\bar{\eta})$, which is typical of a de Sitter expansion. It is a quantum effect (note that the background fluid is always radiation)[13]. The potential $V \equiv a''/a$ goes as $2/\bar{\eta}^2$.

The wavenumbers that cross the effective Hubble parameter at this epoch will be almost scale invariant because they cross the potential in a qdS phase, as in inflation[14]. Hence, we have a bounce naturally followed by an inflationary phase. The cosmological large scales observed in the Planck satellite should cross the effective Hubble parameter in this epoch.

4) For $-\mathcal{O}(1) < \bar{\eta} < \mathcal{O}(1)$:

In this phase the maximum of the potential, or of the effective Hubble parameter, is reached. With $y \gg 1$, it happens for $\bar{\eta} = -\sqrt{2}/4$, and the maximum value of the effective Hubble parameter is $V = 32/27 \approx 1.18$. Wavenumbers larger than this value will never cross the effective Hubble parameter, hence they behave typically as the ultraviolet limit of the Minkowski vacuum. This means that there is a cutoff for the perturbation modes, beyond which no crossing occurs. The comoving wavenumbers which are bigger than the maximum effective Hubble parameter, $\bar{k}^2 > V_{\rm max} = 1.18$, never feel the evolution of the universe. Therefore, $\bar{k}_{\rm max} = \sqrt{1.18} = 1.09$ is our cutoff scale. The physical scales of these wavenumbers will be evaluated below.

5) For $\bar{\eta} \gg 1$:

In this era we have $a \approx a_b(2y\bar{\eta})$, and the potential is such that $V \propto 1/\bar{\eta}^4$. The classical radiation-dominated expanding phase is recovered. Therefore,

[13]The quantum gravity effects remain important until the so-called quantum potential of the de Broglie-Bohm theory becomes negligible in the Hamilton-Jacobi equation [91]. In the present case, this happens after the end of the accelerated expansion, since it is the quantum potential that drives any behavior of the scale factor other than the classical $a \approx a_b(2y\bar{\eta})$. Note that this is a direct consequence of the fact that the classical limit depends on the form of the wave function, as discussed in [93].

[14]Note that for $w = 1/3$ exactly the spectral index is not sufficiently red-tilted, see Fig. 2.7 below. Only for $w = 1/3 + \epsilon$, $\epsilon \approx 3.83 \times 10^{-3}$, one can get $n_s \approx 0.96$. In the Conclusion we will return to a discussion about this point.

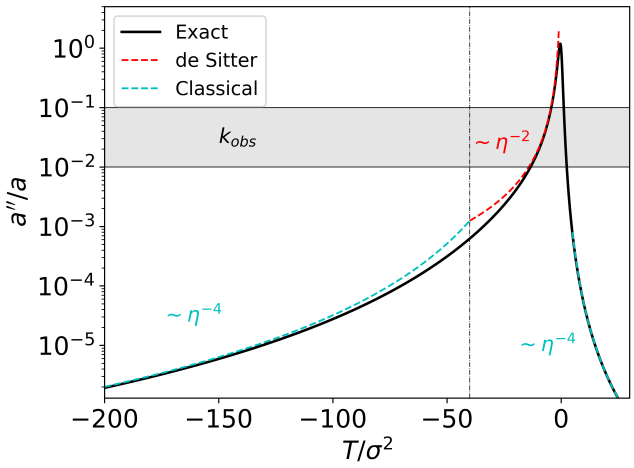

FIGURE 2.4: Perturbation potential a''/a for the radiation case and its limiting regimes for $y = 40$: in green, V during the classical contraction and expansion; in red, V during the qdS phase. The vertical line represents the bounce, while the shaded area depicts the range of observable co-moving wave-numbers k, which constrains the parameters of the model.

we have a natural graceful exit from inflation to the standard model radiation-dominated era.

Figure 2.4 shows the potential V given in Eq. (2.93) for a representative value of y, highlighting its approximate regimes discussed above. The crossing condition $\bar{k} = \sqrt{V}$ for a given comoving wavenumber within the observable range is set to take place in the accelerated phase. As mentioned above, one can see the maximum value of the potential for $y \gg 1$ is given by

$$V(\bar{\eta}_{\max}) \approx \frac{32}{27} \approx 1.18 \Rightarrow \bar{k}_{\max} \approx 1.09\,, \tag{2.94}$$

at $\bar{\eta}_{\max} \approx -\frac{\sqrt{2}}{4}$. Finally, we point again that the time parameter in Fig. 2.4 and subsequent ones is, for $w = 1/3$, $T/\sigma^2 = \eta/\sigma^2 = \bar{\eta}$.

Relations Between the Free Parameters and Physical Scales

Let us define

$$k_H \equiv kR_{H_0}/a_0 = R_{H_0}/\lambda_{\text{physical},0}\,,$$

which is the ratio of the Hubble radius today to the physical wavelength of the mode k today. Hence, the large cosmological wavelengths observed in the CMB are in the approximate range $1 < k_H < 10^3$ [94], which corresponds approximately to 10 Mpc $< \lambda_{\text{physical},0} <$ 10 Gpc today.

The relationship between k_H and $\bar{k}$ reads

$$k_H = \frac{R_{H_0}}{c_s(\sigma^2 a_b)x_b}\bar{k}\,. \tag{2.95}$$

Using Eqs. (2.65) and (2.71) for $w = 1/3$ and $y \gg 1$ we get

$$k_H = \sqrt{\frac{R_{H_0}}{l_c}}\left(\frac{\Omega_{r,0}}{12}\right)^{1/4}\frac{\bar{k}}{2c_s} \equiv C\bar{k}\,. \tag{2.96}$$

Note that C is a very large constant, so that the cosmological wavenumbers are associated with very small $\bar{k}$. We impose that these cosmological wavenumbers cross the effective Hubble parameter in the quantum inflationary phase, namely, when $1 \ll -\bar{\eta} < y$, yielding $\bar{k}_{\rm cross} = 1/|\bar{\eta}_{\rm cross}|$, which makes $\bar{\eta}_{\rm cross}$ very big. This is another reason to take $y \gg 1$, as this crossing must happen when $-\bar{\eta} < y$.

Knowing that $R_{H_0}/l_P \approx 10^{61}$, and from the range for l_c given in Eq. (2.74), we get

$$10^{15} \ll C < 10^{28}\,, \tag{2.97}$$

and $y > C$.

These huge values of y may be frightening, but in fact they are good because the effective Hubble parameter (the potential) becomes very closely independent of y in this regime,

$$V \approx \frac{1}{(1+\bar{\eta}^2)^{3/2}(\bar{\eta}+\sqrt{1+\bar{\eta}^2})}\,. \tag{2.98}$$

This approximation is excellent for any $\bar{\eta} > -y$, but it is not good otherwise. However, as we are interested in wavenumbers that cross the effective Hubble parameter only when the quantum inflationary expansion is under way - which takes place after the bounce - we can say that, for a period satisfying $-\bar{\eta} < y$, these modes satisfy $\bar{k}^2 \gg V$. Hence, we can pose vacuum initial conditions there, and all the numerical calculations are made when Eq. (2.98) is an excellent approximation.

Analytical Estimates of the Power Spectrum

The curvature perturbation ζ_k satisfies the general equation in arbitrary time:

$$\ddot{\zeta}_k + \frac{\dot{m}}{m}\dot{\zeta}_k + \nu^2\zeta_k = 0\,, \tag{2.99}$$

where m and ν are the generalized time-dependent mass and frequency. All GR linear scalar perturbations with one field as the source term can be put in this form. The generalized Mukhanov-Sasaki variable is $v_k = \sqrt{m}\,\zeta_k$, and satisfies,

$$\ddot{v}_k + \left(\nu^2 - \frac{\ddot{\sqrt{m}}}{\sqrt{m}}\right) v_k = 0\,, \tag{2.100}$$

For perfect fluids, m and ν can be read from the GR action as (see equations (92-94) of [95]),

$$m = \frac{(\rho + p)a^3}{Nc_s^2 H^2}\,, \quad \nu = \frac{Nkc_s}{a}\,, \tag{2.101}$$

where N is the lapse function and $p = w\rho$.

The vacuum (or WKB) initial condition for ζ_k can be set in the epoch when $\nu^2 \gg \ddot{\sqrt{m}}/\sqrt{m}$, yielding $|v_k^{\rm WKB}| = 1/\sqrt{2\nu}$. In our case, this phase includes the period of classical evolution, where we can use the Friedmann equation in the contracting branch of the evolution. We therefore obtain that

$$|\zeta_k^{\rm WKB}| = \frac{|v_k^{\rm WKB}|}{\sqrt{m}} = \frac{1}{\sqrt{2m\nu}} = \frac{l_P}{a}\sqrt{\frac{4\pi c_s}{3(1+w)k}}\,, \tag{2.102}$$

where in our convention $G = l_P^2$.

On the other hand, we will work with the equation with dimensionless variables and parameters,

$$v''_{k,(2)} + \left(\bar{k}^2 - \frac{A''}{A}\right) v_{k,(2)} = 0\,, \tag{2.103}$$

where we take

$$A \equiv y\bar{\eta} + \sqrt{1+y^2}\sqrt{1+\bar{\eta}^2}\,,$$

as a_b disappears from Eq. (2.103), and

$$\zeta_{k,(2)} = v_{k,(2)}/A\,.$$

The WKB curvature perturbation $\zeta_{k,(2)}^{\rm WKB}$ arising from Eq. (2.103) reads

$$|\zeta_{k,(2)}^{\rm WKB}| = |v_{k,(2)}^{\rm WKB}/A| = 1/\left(A\sqrt{2\bar{k}}\right)\,.$$

Then, we can express the dimensional curvature perturbation in terms of the dimensionless one through

$$|\zeta_k^{\mathrm{WKB}}| = \frac{Al_P}{a}\sqrt{\frac{8\pi c_s \bar{k}}{3(1+w)k}}|\zeta_{k,(2)}^{\mathrm{WKB}}|\,. \tag{2.104}$$

This relation of proportionality must be valid always, hence we can write the physical power spectrum for the dimensional curvature perturbation ζ_k in terms of the power spectrum for the dimensionless curvature perturbation $\zeta_{k,(2)}$ calculated from Eq. (2.103):

$$P_\zeta = \frac{k^3}{2\pi^2}|\zeta_k|^2 = \frac{y^2}{36\pi c_s(1+w)}\frac{l_P^2}{l_c^2}\bar{k}^3|\zeta_{k,(2)}|^2\,. \tag{2.105}$$

Let us evaluate semi-analytically $|\zeta_{k,(2)}|$. First of all, in the de Sitter expansion, the vacuum initial condition we have set is the well known Bunch-Davies vacuum associated with this spacetime,

$$v_{k,(2)} = \frac{\mathrm{e}^{-\mathrm{i}\bar{k}\bar{\eta}}}{\sqrt{2\bar{k}}}\left(1 - \frac{\mathrm{i}}{\bar{k}\bar{\eta}}\right)\,. \tag{2.106}$$

This solution is valid whenever the de Sitter expansion is taking place, even when $\bar{k}\bar{\eta} \ll 1$, where the super-Hubble expansion [87] is also valid:

$$\begin{aligned}\zeta_{k,(2)} \;=\; & A_1(\bar{k})\left[1 - \int\frac{\mathrm{d}\bar{\eta}}{A^2}\int \mathrm{d}\bar{\eta}_2 A^2\bar{k}^2 + \mathcal{O}(\bar{k}^4) + \ldots\right] + \\ & A_2(\bar{k})\left[\int\frac{\mathrm{d}\bar{\eta}}{A^2} + \mathcal{O}(\bar{k}^2) + \ldots\right]\,.\end{aligned} \tag{2.107}$$

Comparing Eq. (2.106) for $\bar{k}\bar{\eta} \ll 1$ with Eq. (2.107), knowing that $\zeta_{k,(2)} = v_{k,(2)}/A$, we can evaluate the amplitude of the dominant constant mode $A_1(\bar{k})$, yielding

$$P_\zeta = \frac{k^3}{2\pi^2}|\zeta_k|^2 = \frac{1}{16\pi c_s}\frac{l_P^2}{l_c^2}\left(1 + \bar{k}^2\bar{\eta}^2 + \ldots\right)\,, \tag{2.108}$$

where we substituted $w = 1/3$.

Hence, we get the amplitude of the power spectrum and its spectral index, which is 0 assuming the ideal case $w = 1/3$.

Note that in the numerical calculation of $v_{k,(2)}$, the result can only depend on $\bar{k}$ and $\bar{\eta}$, nothing more. The appearance of y^2 in Eq. (2.105) was canceled because $|\zeta_{k,(2)}|^2 = |v_{k,(2)}/A|^2 = |v_{k,(2)}2\bar{\eta}/y|^2$. Again, the presence of a very large y does not pose any problem to the model, it in fact helps the calculations.

2.4 Cosmological Perturbations: Numerical Results

The analytical results obtained in Section 2.3 can be confirmed by means of a numerical analysis, which is detailed in what follows.

In order to perform the numerical integration, the initial condition can be given as the adiabatic vacuum at very negative $\bar{\eta}$. However, in order to speed up the computation, we obtain corrections to the adiabatic vacuum and set the initial condition at not so large $|\bar{\eta}|$. This adiabatic expansion is made by firstly expanding the potential a''/a, equation (2.98), for $-y \ll \bar{\eta}$,

$$V_{\rm qdS} \equiv \frac{1}{(1+\bar{\eta}^2)^{3/2}(\bar{\eta}+\sqrt{1+\bar{\eta}^2})} \approx \frac{2}{\bar{\eta}^2} - \frac{5}{2\bar{\eta}^4} + \mathcal{O}\left(\bar{\eta}^{-6}\right) , \qquad (2.109)$$

where the second approximation is valid for $|\bar{\eta}| \gg 1$. Following the procedure described in [96], we obtain the initial condition

$$v_{k0}^{\rm qdS} = \frac{\mathrm{e}^{-\mathrm{i}\bar{k}\bar{\eta}_i}}{\sqrt{2\bar{k}}}\left[1 - \frac{\mathrm{i}}{\bar{k}\bar{\eta}_i} + \frac{5\mathrm{i}\bar{k}^2}{12}\frac{1}{(\bar{k}\bar{\eta}_i)^3} + \mathcal{O}\left(\bar{\eta}_i^{-4}\right)\right] . \qquad (2.110)$$

The first correction to the adiabatic vacuum is just the de Sitter term, see Eq. (2.106), as expected. We then solve equation (2.103) with the potential (2.109) and the above initial condition at a negative time $|\bar{\eta}_i| \ll y$ set before the crossing $\bar{k}^2 = V_{\rm qdS}(\bar{\eta}_c)$.

The computational time is significantly reduced by using action-angle variables [97], which we denote by θ, I, ψ and J. In terms of these variables, the equation of motion (2.92) reads

$$\begin{aligned}
\theta' &= \bar{k} - \frac{1}{\bar{k}}\frac{A''}{A}\sin^2\theta\,, \\
(\ln I)' &= \frac{1}{\bar{k}}\frac{A''}{A}\sin\left(2\theta\right), \\
\psi' &= \bar{k} - \frac{1}{\bar{k}}\frac{A''}{A}\sin^2\psi\,, \\
(\ln J)' &= \frac{1}{\bar{k}}\frac{A''}{A}\sin\left(2\psi\right), \qquad (2.111)
\end{aligned}$$

while the initial condition (2.110) becomes

$$\begin{aligned}
\tan\theta_i &= \frac{\bar{k}q_1}{{q_1}'}\,, \quad I_i = \frac{\bar{k}q_1^2}{2} + \frac{{q_1}'^2}{2\bar{k}}\,, \\
\tan\psi_i &= \frac{\bar{k}q_2}{{q_2}'}\,, \quad J_i = \frac{\bar{k}q_2^2}{2} + \frac{{q_2}'^2}{2\bar{k}}\,, \qquad (2.112)
\end{aligned}$$

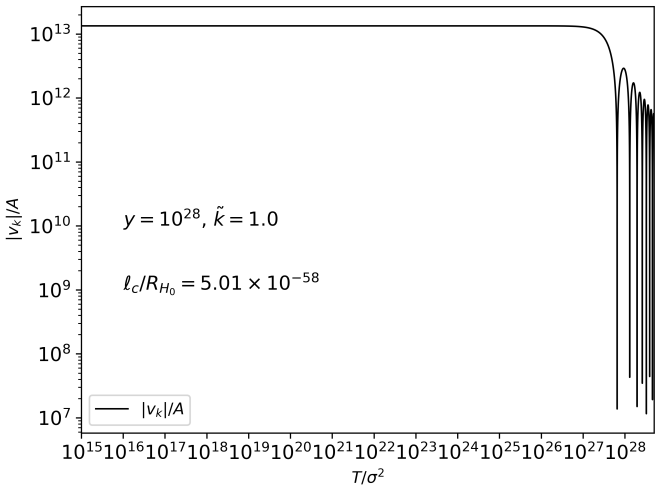

FIGURE 2.5: Modulus of the curvature perturbation mode $\zeta_k \equiv v_k/A$ for $w = 1/3$, showing the horizon reentry.

where

$$q_1 \equiv -2\Im\left[v_{k0}^{\mathrm{qdS}}\right] , \quad q_2 \equiv 2\Re\left[v_{k0}^{\mathrm{qdS}}\right] . \tag{2.113}$$

The usual Mukhanov-Sasaki variable and its derivative are then recovered as

$$\begin{aligned} v_{k,(2)} &= \frac{1}{\mathrm{i}\sqrt{2\bar{k}}}\left(\sqrt{I}\sin\theta + \mathrm{i}\sqrt{J}\sin\psi\right) , \\ {v_{k,(2)}}' &= \frac{1}{\mathrm{i}}\sqrt{\frac{\bar{k}}{2}}\left(\sqrt{I}\cos\theta + \mathrm{i}\sqrt{J}\cos\psi\right) . \end{aligned} \tag{2.114}$$

Since the qdS potential does not depend on y, the crossing condition leads to the usual relation $\bar{k}\bar{\eta} \approx 1$ (which corresponds precisely to $c_s k\eta \approx 1$), provided that the modes cross the potential not too close to $\bar{\eta} \approx -1$. This is the case for the frequencies (2.96) satisfying (2.97). The initial time for the integration must then be in the range $-10^{28} < \bar{\eta}_i < -10^{15}$. Since this must happen after the bounce and within the qdS period, it follows that $y > -\bar{\eta}_i$.

Figure 2.5 shows the results of the numerical integration for the curvature perturbation $\zeta_k = v_{k,(2)}/a$, where one can identify the frozen regime and the oscillations after horizon reentry (for a mode with $k_H = 1.0$). The initial time of integration was set at $\bar{\eta}_i = -10^{15}$, as the initial condition (2.110) remains appropriate even after the crossing time for this case, $\bar{\eta}_c \approx -3 \times 10^{27}$. The real and imaginary parts of $v_{k,(2)}$ (their absolute value), as well as $|v_{k,(2)}|$, are displayed in Figure 2.6. The initial adiabatic oscillations $\mathrm{e}^{-\mathrm{i}\bar{k}\bar{\eta}}$ change, after crossing the horizon, to a growing mode proportional to the scale factor, being dominated by the imaginary part.

Now let us use the numerical results for $\zeta_{k,(2)}$ to calculate the scalar power spectrum given in Eq. (2.105) expressed in terms of $k_H = R_{H_0}/\lambda_{\text{physical},0}$ for $w = c_s^2 = 1/3$,

$$P_\zeta = \sqrt{\frac{2}{3}} \frac{y^2}{\pi (3\Omega_{r,0})^{3/4}} \left(\frac{l_P}{R_{H_0}}\right)^2 \sqrt{\frac{R_{H_0}}{l_c}}\, k_H^3 \frac{|v_{k,(2)}|^2}{A^2}\,. \tag{2.115}$$

Our analytical estimates can be read in Eq. (2.108) for $w = c_s^2 = 1/3$,

$$P_\zeta\Big|_{\bar{k}|\bar{\eta}|<1} \approx \frac{\sqrt{3}}{16\pi} \left(\frac{l_P}{l_c}\right)^2 \times \left[1 + \mathcal{O}\left(\bar{k}\bar{\eta}\right)^2 + \ldots\right], \tag{2.116}$$

which of course corresponds to (2.115) evaluated with the dominant term in (2.110) at horizon crossing. We computed the scalar power spectrum numerically from the perturbation amplitude on super-horizon scales by means of expression (2.115), which is shown in Figure 2.7. Note that the dependence on l_c^{-2} given in Eq. (2.116) is confirmed. We also went beyond the observational range, and deviations from scale invariance only occur close to the cutoff scale (2.120). The scalar amplitude compatible with the CMB observations $A_s = 2.3424 \times 10^{-9}$, where $P_\zeta = A_s (k/k_*)^{n_s - 1}$, leads to the numerical value $l_c/R_{H_0} = 5.01 \times 10^{-58}$, which in turn translates to

$$\frac{l_c}{l_P} = 2.868 \times 10^3 h^{-1}\,. \tag{2.117}$$

As discussed in Section 2.2, this is a very reasonable value (see Eq. (2.74)), taking the usual CMB/Supernovae values $0.67 < h < 0.74$.

From this value of the minimum curvature scale we obtain through the energy density provided by (2.75) the characteristic energy scale in the qdS phase

$$H^* = \sqrt{\frac{\Lambda_{\text{qdS}}}{3}} \approx 10^{14}\,\text{GeV}\,, \tag{2.118}$$

which is similar to that of usual inflationary models.

It was also noticed that the power spectrum does not depend on y for $y \gg 1$. However, since $y > C$ and from Eq. (2.97) , we obtain that

$$y \gtrsim 10^{27}\,, \tag{2.119}$$

which is in remarkable agreement with the inflationary e-folds lower bound (2.77) (note that y can be even larger, the only effect being pushing the start of the qdS phase farther into the past and increasing the number of e-folds). The observational constraints are thus contained in the allowed parameter space of this model. From these values of asymmetry y and minimum curvature scale l_c one finds through Eqs. (2.71), (2.65), (2.53) the values of a_b and the

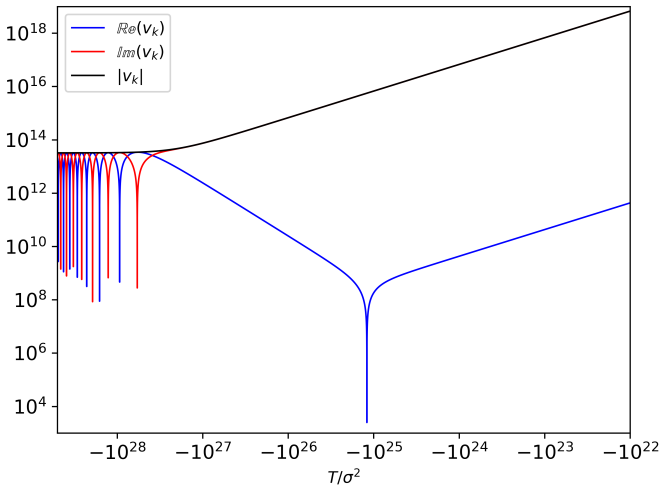

FIGURE 2.6: Absolute value of the Mukhanov-Sasaki variable $|v_{k,(2)}|$ related to the scalar perturbations, as well as its real and imaginary parts, for $y = 5 \times 10^{29}$, $l_c/l_P = 2.868 \times 10^3 h^{-1}$ and $k_H = 1.0$.

original Gaussian parameters. The values (2.117), (2.119) therefore lead to $a_b \approx 10^{-57} a_0$ and a very wide Gaussian traveling in configuration space (χ, T). This is in accordance with a model which naturally transits from the very small scales around the bounce to the large scales arising from inflation.

We observe that, as expected for the case $w = 1/3$, the power spectrum is very nearly scale invariant, with a deviation from $n_s = 1$ in the fifth decimal place (this makes the normalization by the pivot scale k_* of little effect to the amplitude of A_s).

The cutoff scale (2.94) may now be evaluated quantitatively. From $\bar{k}^2_{\max} = V(\bar{\eta}_{\max})$ we find

$$k_{H\max} \approx 1.6 \times 10^{27} \;\rightarrow\; k_{\max} \approx 5.3 \times 10^{20} h\,\mathrm{Mpc}^{-1}\,, \tag{2.120}$$

being well beyond the modern observational limits. Any perturbation mode above this value will never cross the horizon, remaining "sub-Hubble" throughout the entire evolution of the universe. For $h \simeq 0.67$ they correspond to $\lambda_{\text{physical},0} \approx 0.54$ m, which at the time of perturbation generation would be below the Planck scale.

In summary, the numerical results are consistent with previous analytical estimates and the amplitude of almost scale invariant scalar perturbations are in agreement with current observational constraints, indeed mimicking inflation. The fact that a qdS phase can be achieved due to quantum effects, both at the background and perturbation levels, is remarkable.

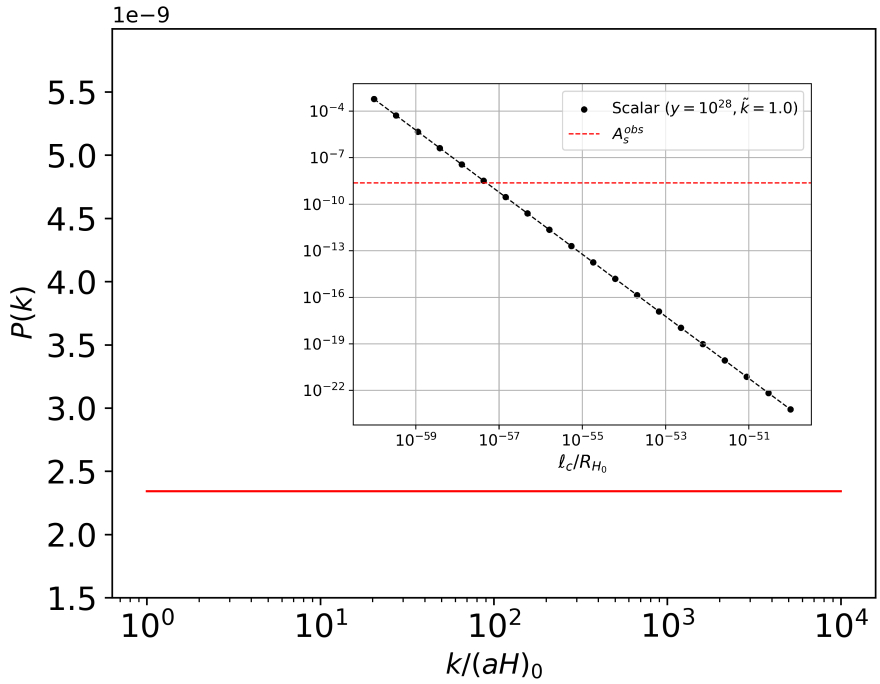

FIGURE 2.7: Scalar power spectrum obtained numerically for $w = 1/3$, $l_c/l_P = 4.22 \times 10^3$ and initial conditions (2.113) at initial time $\bar{\eta}_i = -10^{10}$. In addition, the scalar power spectrum as a function of l_c, with the observed scalar amplitude in red.

2.5 Conclusions and Discussion

In this chapter we presented a very simple nonsingular cosmological model which contains a classical slowly contracting phase, a bounce, a quasi-de Sitter inflationary phase, and finally reaches the usual classical radiation-dominated expanding phase before nucleosynthesis. The unique matter component is a radiation fluid. The bounce and the inflationary phase result from quantum effects arising from a Gaussian wave function solution of the Wheeler-DeWitt equation, which reduces to a Schrödinger equation in this case, traveling with high momentum in configuration space. During the quantum phase, there is a huge creation of photons, so that the contracting phase corresponds to an almost empty universe.

All this rich phenomenology is described by the astonishingly simple analytical scale factor given in Eq. (2.91) evolving in conformal time:

$$a(\bar{\eta}) = a_b \left(y\bar{\eta} + \sqrt{1+y^2}\sqrt{1+\bar{\eta}^2} \right) , \tag{2.121}$$

Independently of its origin, Eq. (2.121) is a new, so far unknown, scale factor evolution which is amazingly interesting in itself, and it is really worth looking for other theoretical contexts where it can be obtained. For instance, the

classical contracting phase happens with a very tiny number of photons in a given cell with physical volume $V_{\rm phys} = a^3 V_{\rm com}$, where $V_{\rm com}$ is the comoving volume of the cell,

$$\frac{N_-(a)}{N_+(a)} \approx \frac{1}{16y^4} < 10^{-109}\,, \tag{2.122}$$

where $N_\pm(a)$ is the total number of photons in the same cell with a given a at the classical expanding (contracting) phase, respectively. In order to obtain Eq. (2.122), we used Eqs. (2.61) and (2.119). Taking the cell to have the volume of our universe today, which contains around 10^{90} photons, the same volume in the classical contracting phase would have 10^{-19} photons or less, so it was practically empty[15]. Hence, one may think that the scale factor (2.121) might have been originated from some quantum gravity instability of a primordial Minkowski spacetime, leading to a tiny number of massless particles, which is substantially increased at the bounce and inflationary quantum phases afterwards.

Note that the generalization of Eq. (2.121) to any $w = p/\rho = $ const. is also very simple, see Eq. (2.54), where $\mathrm{d}\bar{T} = a^{1-3w}\mathrm{d}\bar{\eta}$, allowing many different scenarios and possibilities. For instance, in the case of the matter bounce scenario, $w \approx 0$, there is a phantom-like expanding phase after the bounce without any phantom, the consequences of which might be interesting to be investigated.

Taking the background as given by Eq. (2.121) for $y \gg 1$, we found out that the scalar cosmological perturbations are almost scale invariant and with the right amplitude for the scales observed in the Planck satellite [94]. The value of y for which these observed scales acquire their observed properties should satisfy the inequality $y \gtrsim 10^{27}$, which coincides with a number of e-folds $\mathcal{N}$ during inflation given by $\mathcal{N} > 60$, see (2.77). Furthermore, the observed value of the amplitude of scalar perturbations by Planck imposes that the minimum curvature scale of the background model l_c should be

$$\frac{l_c}{l_P} = 2.868 \times 10^3 h^{-1}\,, \tag{2.123}$$

where l_P is the Planck length, which is consistent with the quantum approach we are using: it is not of the order of the Planck length, where a yet unknown full theory of quantum gravity should be used inescapably, but it still corresponds to energy scales far bigger than that of nucleosynthesis, where quantum cosmological effects may begin to be important. It was also obtained that the energy scale of the quantum inflationary phase is about $E_{\rm qi} \approx 10^{14}\,$GeV, see Eq. (2.118).

[15]Note that the scale factor corresponding to today's Hubble radius yields a much bigger Hubble radius in the classical contracting phase, see Eq. (2.62), compatible with the fact that spacetime in this era is close to Minkowski spacetime.

Concluding, this astonishingly simple non-singular cosmological model yields many observed features of the standard cosmological model, and it naturally contains three key ingredients of the primordial universe which have been investigated so far: a very slow contraction (although with a different origin than that of the usual ekpyrotic scenarios - see Eq. (18), showing that the slow contraction in the present model arises from the fact that the contracting phase is almost empty, while in the ekpyrotic models it arises from the fact that the field dominating contraction has a huge equation of state parameter), a bounce, and a inflationary phase, reaching the standard classical radiation-dominated phase before nucleosynthesis. All these different phases are continuously connected within the simple expression given in Eq. (2.121).

Of course, this very simple model is an important first step, but it is not the final word, and it must be supplemented by new ingredients. For instance, and perhaps most importantly, it does not lead to a red-tilted spectral index, unless we take $w = 1/3 + \epsilon$ with $0 < \epsilon \ll 1$ in order to give $n_s \approx 0.9649$ [94] (see the analytic result (2.90)), nor to primordial gravitational waves with the right amplitude. In order to understand this last point, take the tensor metric perturbations $w_{ij} = \zeta^h e_{ij}$, where e_{ij} is the transverse-traceless polarization 3-tensor [98]. It can be shown that the perturbation mode $v_k^h = a\zeta_k^h$ satisfies equation (2.78) with $c_s = 1$. After calculations similar to those employed in the scalar case, we find that the tensor power spectrum P_h will also be scale invariant for modes that cross the horizon during the qdS phase, but with the tensor-to-scalar ratio given by

$$r \equiv \frac{A_t}{A_s} \simeq \frac{32}{\sqrt{3}} \approx 18.48\,. \tag{2.124}$$

where $P_h = A_t(k/k_*)^{n_t}$, with k_* a selected pivot scale.

Complete numerical computations are in full agreement with the analytical predictions given in (2.124), to a percentage error of around 10^{-6}. This clearly violates the observational constraint $r < 0.063$ [94]. Loop Quantum Cosmology (LQC) matter bounce models (e.g. the bounces in Chapter 3) suffer with the same difficulty to reproduce a correct tensor-to-scalar ratio upper bound [99]. Note that this specific issue is not present in a fluid matter bounce model, as shown in [90] for a symmetric bounce.

One way out usually implemented to solve these types of problems is to evoke the presence of a curvaton field (maybe associated to dark matter, which is here absent) [100, 101, 102, 103], which does not affect the background evolution, but whose presence can increase the amplitude of scalar perturbations with respect to tensor perturbations. Also, one can induce a red-tilt in the spectrum index of scalar perturbations by considering an effective global equation of state parameter $w = 1/3 + \epsilon$, as mentioned above, where the small deviation is due to the presence of the curvaton field.

Chapter 3

The CMB Bispectrum from Bouncing Cosmologies and Planck Constraints

3.1 Introduction

As discussed in Chapter 2, inflation is a simple idea which not only solves some important puzzles arising in Big Bang Cosmology [104], but which has also predicted from weak assumptions the red tilted, almost scale invariant spectrum of scalar cosmological perturbations [105], afterwards confirmed by detailed observations of the Cosmic Microwave Background (CMB) [94]. However, inflationary models generally make use of a scalar field called inflaton, which is not observed in Nature (except in the case of Higgs inflation [106]). They also do not address the initial singularity of the standard cosmological model [30], turning the resulting scenario incomplete in this sense.

Bouncing models without singularities emerged in the last decades as possibilities to complete the standard cosmological model [107, 108, 109, 89, 88, 87, 110, 111, 112, 113]. In fact, such models do not contain the puzzles inherent to the Big Bang Cosmology [90, 87], and some of them can also lead to almost scale invariant spectra of scalar cosmological perturbations, although only in some specific cases. Some bouncing models have a unique bounce, usually with a matter dominated contraction in order to yield the correct spectrum of perturbations [114, 115, 103], and others are cyclic, with a very slow contracting phase [76]. Usually, bouncing models do not require an inflationary phase [90], but they are not incompatible with inflation, with many scenarios containing both phases [116]. In many cases, the bounce itself helps in yielding initial conditions for inflation. However, contrary to inflation, where the physical requirements on the inflaton field Lagrangian are standard, the bounce itself requires some new physics. It can come either from non-minimal couplings [107], semi-classical corrections leading to nonlinear curvature terms in the gravitational action and/or an effective energy-momentum tensor of matter violating the null energy condition [108],

or quantum corrections arising from quantum gravity approaches applied to Cosmology [89, 116, 117, 118].

The next step in this investigation is to find observable "fingerprints", which indicate the existence of a previous contracting phase and a bounce. In [29], in the context of bouncing models with inflation, it was shown that non-Gaussianities originating from the contracting era before inflation [119] can substantially alleviate the large scale anomalies detected in the CMB [120]. The model contains a canonical scalar field with potential $V(\varphi)$, and the scale factor around the bounce is generically parametrized as

$$a(t) = a_b(1 + bt^2)^n, \tag{3.1}$$

where t is cosmic time, the bounce happens at $t = 0$, a_b is the scale factor at the bounce, and b is a constant parametrizing the Ricci scalar at the bounce, $R_b = 12nb$. The parameter n controls the way the model enters and leaves the bouncing phase and starts classical expansion. For $n \approx 1/6$, the scalar field energy density just after the bounce is concentrated in the kinetic term (this is the case of Loop Quantum Cosmology (LQC) models [64]), and inflation starts later, while for larger values of n the scalar field potential is already relevant at the bounce, and inflation starts earlier. Hence, the features of this class of bouncing models are controlled by the bounce Ricci scalar R_b, and by n.

The initial quantum state for the perturbations is chosen to be the adiabatic (Minkowski) vacuum in the far past of the contracting phase. Therefore quantum state of cosmological perturbations at the onset of inflation deviates from the Bunch-Davies vacuum. In terms of the modes one can write as

$$v_k(\eta) = \alpha_k v_k^{\rm BD}(\eta) + \beta_k v_k^{*\rm BD}(\eta), \tag{3.2}$$

where η is conformal time, implying that the ratio between the primordial dimensionless power spectrum $\mathcal{P}_{\mathcal{R}}(k)$ and the pure Bunch-Davies primordial dimensionless power spectrum $\mathcal{P}_{\mathcal{R}}^{\rm BD}(k)$ reads

$$\frac{\mathcal{P}_{\mathcal{R}}(k)}{\mathcal{P}_{\mathcal{R}}^{\rm BD}(k)} = \mid \alpha_k + \beta_k \mid^2 . \tag{3.3}$$

This class of models has two fundamental scales: the bounce scale given by the comoving wave number $k_b \equiv a_b\sqrt{R_b/6}$, and the (comoving) inflation scale $k_i \equiv 2\pi a_i\sqrt{R_i/6}$, where a_i and R_i are the scale factor and Ricci scalar at the beginning of inflation, respectively. As the energy scale of the bounce is larger than the energy scale of inflation, $k_i < k_b$. One has three different regimes for the power spectrum: $k > k_b$, $k_i < k < k_b$, and $k < k_i$ (corresponding to length scales smaller than the bounce length scale, bigger than the bounce length scale but smaller than the inflation length scale, and bigger than the inflation length scale, respectively). Scales smaller than the bounce scale do not feel the bounce, hence they will not deviate from inflationary (Bunch-Davies)

results. However, the two other scales are affected by the bounce, leading to different physical effects. Indeed, it is shown in [29] that non-Gaussianities arise, correlating super-horizon modes with infrared scales, enhancing the probability of the appearance of CMB anomalies at large scales. If the duration of inflation is very long, such effects are suppressed, yielding the constraint $n < 1/4$ for these effects to be significant. The scales which contribute most to the non-Gaussianity are in the range $k_i < k < k_b$, which is larger for a bounce closer to the Plank scale. Hence, models with bounce phases occurring at length scales larger than the Planck length need a larger $f_{\rm nl}$ parameter to yield the desired effects, some of them require $f_{\rm nl}$ of order 10^4. As the non-Gaussian correlations obtained in [29] are restricted mostly to super-horizon modes, the authors suggest that these large values of $f_{\rm nl}$ should not be directly observed. However, the CMB bispectrum of these models is not calculated, and it is not clear under which conditions the model satisfies the Planck constraints on it [121].

The aim of this chapter is to fill this gap. In Sections 3.1.1 and 3.1.2 we introduce the large-scale anomalies and briefly explain how the bounce cosmologies considered are able to mitigate them. In Sections 3.2.1 and 3.2.2 we calculate the bispectrum for the two representative models mostly studied in [29]: the LQC case $n = 1/6$ [64], and the $n = 0.21$ case, which best mitigates the CMB anomalies according to [29]. For these two cases, we consider the minimum and maximum values of $f_{\rm nl}$ allowed (3326 and 8518 for $n = 1/6$, and 959 and 4372 for $n = 0.21$). In Section 3.2.3 we compute the cosmic variance related to the CMB bispectrum measurement. The Signal-to-Noise Ratio (SNR) of the bispectrum is computed in Section 3.2.4 in order to decide whether it can be measured in a CMB experiment which is cosmic variance limited at low multipoles, $\ell < 30$, like the Planck experiment [122]. We find that the cumulative SNR for a cosmic variance limited CMB experiment with 70% sky coverage becomes larger than 10 for all models that are able to mitigate the large-scale anomalies in the CMB. In Section 3.2.5 we explain why the Limber approximation could not be used to compute the bispectrum. The comparison with the actual Planck data is given in Section 3.3, excluding all of the scenarios that mitigate the CMB anomalies with high significances. In Section 3.4 we present the main conclusions.

3.1.1 The CMB Anomalies on Large Scales

One of the most debated problems of standard cosmology are the large-scale anomalies of the CMB data, namely the power suppression, the dipolar asymmetry and the parity asymmetry [123, 120, 121]. Even though these anomalies have a statistical significance around 2 to 3σ and may be accepted as coincidences, they could be less anomalous in scenarios that introduce new physics, e.g. a model with significant non-Gaussianity on very large scales (this is exactly what the bouncing models investigated in [29] predict). In the

present section, let us review the anomalies and how they are quantified in the Planck data.

Let us start recalling that a temperature fluctuation $\delta T(\hat{n})$ in a direction $\hat{n}$ in the sky can be decomposed in spherical harmonics as

$$\delta T(\hat{n}) \equiv \frac{T(\hat{n}) - \bar{T}}{\bar{T}} = \sum_{\ell m} a_{\ell m} Y_{\ell m}(\hat{n}), \tag{3.4}$$

where $\bar{T} = 2.275 \pm 0.002$K is the mean temperature, $Y_{\ell m}$ are the spherical harmonics and $a_{\ell m}$ are the coefficients of the decomposition.

From a cosmological model, e.g. ΛCDM, we can only predict the statistics of CMB quantities. Therefore, we are interested in the correlators of the coefficients $a_{\ell m}$, which tell us how much a number of points in the sky are correlated with each other. The largest correlator is the one related to two points in the sky, i.e. the two-point correlation function

$$\left\langle a_{\ell m} a^*_{\ell' m'} \right\rangle = C_\ell \delta_{\ell \ell'} \delta_{m m'}, \tag{3.5}$$

where C_ℓ is the so-called angular power spectrum. The deltas, as well as the independence of C_ℓ on m, are related to the cosmological principle (homogeneity and isotropy) predicted by ΛCDM. The even-point correlators (especially the two-point, as it is the largest) are the only ones that matter for a Gaussian distribution. On the other hand, if non-Gaussianity is present, one is also interested in the three-point correlator, which is related to the bispectrum [124].

Note that such statistical properties cannot be obtained as it is usually done for other physical systems. In the case of CMB, we only have one single realization of the temperature map. In practice, we average over many directions in the sky and assume this corresponds to averaging over "many Universes". On large scales, however, our ensemble is still very limited, leading to an intrinsic uncecrtainty to our measurements, which is known as cosmic variance.

This statistical character of a model's prediction implies that we need a statistical way to quantify departures from the theory. For this purpose, we use the so-called p-values, which represent the probability that, given ΛCDM, a given event can happen. More details can be found in [125], where one can have a good understanding from Figure 1.

The CMB anomalies on large scales are features that have a very low probability of happening assuming ΛCDM. The associated p-values are smaller or equal to 1%. As mentioned above, this corresponds to statistical significances of 2 to 3σ, which are not extremely high. But since the features appear in different surveys [8, 11, 7] and can be mittigated by introducing new physics, they have been receiving attention in the community.

Power Suppression

The power suppression anomaly refers to the lack of two-point correlators in angular scales larger than 60. It has been observed by COBE [7], WMAP [8] and Planck [11]. The estimator used to quantify this anomaly is given by

$$S_{1/2} = \int_{-1}^{1/2} C(\theta)^2 d(cos\theta). \tag{3.6}$$

While the Planck data indicate $S_{1/2} = 1209.2\mu\text{K}^4$ [126], ΛCDM predicts $S_{\frac{1}{2}} \simeq 42000\mu\text{K}^4$.

Parity Asymmetry

The parity properties of the temperature field can be investigated by means of the difference in power between even and odd multipoles in the CMB due to the properties of the spherical hamonics decomposition. An even or odd preference indicates parity violation [29]. Since ΛCDM predicts the parity neutrality of primordial perturbations, very large scales in the CMB (which correspond to very long wavelengths) are expected to be parity neutral.

This feature is quantified by means of the following quantity

$$R^{TT}(\ell_{\text{max}}) = \frac{D_+(\ell_{\text{max}})}{D - (\ell_{\text{max}})}, \tag{3.7}$$

where

$$D_\pm(\ell_{\text{max}}) \equiv \frac{1}{\ell^\pm_{\text{tot}}} \sum_{\ell=2,\ell_{\text{max}}}^{\pm} \frac{\ell(\ell+1)}{2\pi} C_\ell, \tag{3.8}$$

$\pm$ refer to even or odd multipoles and $\ell^\pm_{\text{tot}}$ is the total number of multipoles in the sum. Therefore, $R^{TT}(\ell_{\text{max}}) = 1$ indicates parity neutrality, $R^{TT}(\ell_{\text{max}}) > 1$ indicates even parity preference and $R^{TT}(\ell_{\text{max}}) < 1$ indicates odd parity preference. The latter is what is observed in both WMAP [8] and Planck [11].

Dipolar Asymmetry

The dipolar asymmetry refers to correlations between the multipoles ℓ and $\ell + 1$. The name of the anomaly is related to dipole modulation and not to the dipole $\ell = 1$, which appears in the data due to our motion with respect to CMB. This type of correlation indicates a violation of isotropy or, in other words, a departure from ΛCDM.

In order to undedrstand how this anomaly is quantified, let us introduce the Bipolar Spherical Harmonics (BipoSH) $\{Y_{\ell_1}(\hat{n}_1) \otimes Y_{\ell_2}(\hat{n}_2)\}_{LM}$, which are

related to the usual spherical harmonics via

$$\{Y_{\ell_1}(\hat{n}_1) \bigotimes Y_{\ell_2}(\hat{n}_2)\}_{LM} \equiv \sum_{m_1 m_2} C^{LM}_{\ell_1 m 1 \ell_2 m_2} Y_{\ell_1 m 1}(\hat{n}_1) Y_{\ell_2 m 2}(\hat{n}_2), \tag{3.9}$$

where $C^{LM}_{\ell_1 m 1 \ell_2 m_2}$ are the so-called Clebsch-Gordan coefficients.

We can use the BipoSH as a basis to decompose the temperature fluctuations, namely

$$\left\langle \delta T(\hat{n}_1) \delta T(\hat{n}_2) \right\rangle = \sum_{\ell_1 \ell_2 LM} A^{LM}_{\ell_1 \ell_2} \{Y_{\ell_1}(\hat{n}_1) \bigotimes Y_{\ell_2}(\hat{n}_2)\}_{LM}, \tag{3.10}$$

from where we obtain the BipoSH coefficients $A^{LM}_{\ell_1 \ell_2}$. These coefficients are related to the usual $a_{\ell m}$ via

$$A^{LM}_{\ell_1 \ell_2} = \sum_{m_1 m_2} \left\langle a_{\ell_1 m_1} a^*_{\ell_2 m_2} \right\rangle (-1)^{m_2} C^{LM}_{\ell_1 m_1, \ell_2, -m_2}. \tag{3.11}$$

In ΛCDM cosmology, one can use the properties of the Clebsh-Gordan coefficients to obtain [29]

$$A^{LM}_{\ell_1 \ell_2} = (-1)^{\ell_1} \sqrt{2\ell_1 + 1} C_{\ell_1} \delta_{L0} \delta_{M0} \delta_{\ell_1 \ell_2}, \tag{3.12}$$

meaning that only $A^{00}_{\ell\ell}$ exist. Therefore, a BipoSH coefficient of $L > 0$ indicates departure from ΛCDM. The WMAP [8] and Planck [11] data report a non-vanishing BipoSH coefficient $A^{1M}_{\ell\ell+1}$.

3.1.2 Alleviating the CMB Anomalies in a Bouncing Cosmology

Let us now review the scenario proposed in [29, 125], which introduces a bouce preceeding inflation. Instead of focusing in one specific theoretical bouncing model, the authors make use of a quite general parametrization of the scale factor

$$a(t) = a_B (1 + bt^2)^n, \tag{3.13}$$

where b is a constant related to the Ricci scalar at the bounce, $R_B = 12nb$, and n is a constant that encodes the new physics that generates the bounce. As examples, in Chapter 2 we have obtained the scale factor (2.44) in the scope of the Wheeler-DeWitt equation, while $n = 1/6$ has been obtained in the context of LQC [127].

This bounce modifies the initial condition at the onset of inflation, since the adiabatic vacuum is now set much before the bounce. The new initial state for the inflationary phase has non-Gaussianities, which correlate super-horizon and very large scale modes. Such non-Gaussianities can be described

in Fourier space by

$$\Phi_{\vec{k}}(t) = \phi_{\vec{k}}(t) + \frac{1}{2}\int \frac{d^3q}{(2\pi)^3}\bar{f}_{NL}(\vec{q},\vec{k}-\vec{q})\phi_{\vec{q}}(t)\phi_{\vec{k}-\vec{q}}(t), \tag{3.14}$$

where $\bar{f}_{NL}$ quantifies the magnitude and shape of the non-Gaussianity, $\phi_{\vec{k}}$ is Gaussian field and the subscript NL stands for non-linear.

The effects caused by the presence of the non-Gaussianity can be investigated by considering a spectator mode (a concrete realization) of the Bardeen potential $\Phi_{\vec{q}}$. This spectator mode is a super-horizon mode, which is correlated to other modes $\vec{k}$ by means of the non-Gaussianity, therefore affecting their statistical properties. In the case of the two-point correlation function, we obtain[1] [29]

$$\begin{aligned}\left\langle \Phi_{\vec{k}_1}\Phi^*_{\vec{k}_2}\right\rangle|_{\Phi_{\vec{q}}} &= (2\pi)^3\delta(\vec{k}_1-\vec{k}_2)P_\phi(\vec{k}_1) + \\ &+ \bar{f}_{NL}(\vec{k}_1,-\vec{k}_2)\frac{1}{2}\left[P_\phi(\vec{k}_1)+P_\phi(\vec{k}_2)\right]\phi_{\vec{q}},\end{aligned} \tag{3.15}$$

where we have used $\phi^*_{\vec{q}} = \phi_{-\vec{q}}$, i.e. $\phi(\vec{x}) \in \mathbb{R}$, and $\left\langle \phi(\vec{k}_1)\phi^*(\vec{k}_2)\right\rangle = (2\pi)^3\delta(\vec{k}_1 - \vec{k}_2)P_\phi(\vec{k}_1)$ (therefore, $\vec{q} = \vec{k}_1 - \vec{k}_2$ is required). The second term is the extra contribution that appears because of the spectator mode, which is known as the non-Gaussian modulation of the two-point function.

The above modulation is forwarded to the temperature covariance matrix $\left\langle a_{\ell m}a^*_{\ell' m'}\right\rangle$, since the coefficients $a_{\ell m}$ are related to the Bardeen potential $\Phi_{\vec{k}}$ via

$$a_{\ell m} = 4\pi\int\frac{d^3k}{(2\pi)^3}(-i)^\ell\mathcal{T}(k,\ell)Y^*_{\ell m}(\hat{k})\Phi_{\vec{k}}, \tag{3.16}$$

where $\mathcal{T}(k,\ell)$ are the so-called temperature radiation transfer functions. In [29] it is shown that, for $|\vec{q}| < |\vec{k}_1|$, the temperature covariance matrix reads

$$\left\langle a_{\ell m}a^*_{\ell' m'}\right\rangle = C_\ell\delta_{\ell\ell'}\delta_{mm'} + (-1)^{m'}\sum_{LM}A^{LM}_{\ell\ell'}C^{LM}_{\ell m\ell'-m'}. \tag{3.17}$$

Therefore, the non-Gaussianities introduced by the presence of the bounce before inflation induce anisotrpies in the CMB.

In the angular power spectrum, the monupolar modulation (i.e. $L = 0$) takes the form

$$C^{\text{mod}}_\ell = C_\ell\left(1 + \frac{1}{C_\ell}(-1)^\ell\frac{A^{00}_{\ell\ell}}{\sqrt{2\ell+1}}\right), \tag{3.18}$$

where C_ℓ is the usual Gaussian power spectrum.

[1] We neglect contributions that are higher order in $\bar{f}_{NL}$.

The square mean value of such modulation reads

$$\sigma_0^2(\ell) \equiv \frac{1}{C_\ell^2}\frac{\left\langle |A_{\ell\ell}^{00}|^2 \right\rangle}{2\ell+1} \tag{3.19}$$

$$= \frac{1}{C_\ell^2}\frac{1}{8\pi^2}\int dq q^2 P_\phi(q)|C_{\ell\ell}^0(q)|^2, \tag{3.20}$$

where

$$C_{\ell\ell'}^L(q) \equiv \frac{2}{\pi}\int dk_1 k_1^2 (i)^{\ell-\ell'}\mathcal{T}(k_1,\ell)\mathcal{T}(k_1,\ell')P_\phi(k_1)\times$$
$$\times \int_{-1}^{1} d\mu \bar{f}_{NL}(k_1,q,\mu)P_L(\mu), \tag{3.21}$$

$P_L(\mu)$ are Legendre polynomials and $\mu \equiv \vec{k}_1 \cdot \vec{q}$. See [29] for more details. The larger the non-Gaussianity (encoded in the parameter $\bar{f}_{NL}$), the higher the square mean value σ_0^2, and therefore, the higher the probability that a suppression of the observed power spectrum happens in a concrete realization of the temperature map. This is the reason why these bounce scenarios mitigate the power suppression anomaly - they make the suppression more likely (or less anomalous), without affecting the homogeneity and isotropy of the undedrlying cosmology. Therefore, one can compute the amount of non-Gaussianity required in order to have a p-value of, for instance, 20%.

By requiring a p-value of 20% to the power suppression, the authors of [29] also alleviated the dipole anomaly (due to an analogous dipole modulation for $L = 1$), the parity anomaly and the issue with the lensing parameter in the Planck data[2].

3.2 The Bispectrum in a Bouncing Model

3.2.1 The Theoretical Expressions

The bouncing model discussed in [29] has the following dimensionless power spectrum, $\mathcal{P}_\mathcal{R}(k)$, and bispectrum, $B(k_1,k_2,k_3)$, of the curvature fluctuations in Fourier space.

[2]The lensing parameter A_L was introduced in the Planck analysis as a consistency check. It was kept as a free parameter to be best fitted, but the expect value for internal consistency is $A_L = 1$. This value is more than 2σ away from the obtained best fit.

n	γ	q	$f_{\rm nl}$ for $R_B = 1\, l_{Pl}^{-2}$	$f_{\rm nl}$ for $R_B = 10^{-3}\, l_{Pl}^{-2}$
1/6	0.6468	-0.7	3326	8518
0.21	0.751	-1.24	959	4372

TABLE 3.1: The values of the parameters considered in this work. The $f_{\rm nl}$ parameter is chosen according to [29] in order to alleviate the power suppression anomaly (with a p-value of 20%). The two different values correspond, respectively, to the space-time curvature at the bounce R_B equal to $1\, l_{Pl}^{-2}$ and to $10^{-3}\, l_{Pl}^{-2}$, where l_{Pl} is the Planck length.

$$\mathcal{P}_{\mathcal{R}}(k) = A_s \begin{cases} (k/k_i)^2 (k_i/k_b)^q & \text{if } k \leq k_i \\ (k/k_b)^q & \text{if } k_i < k \leq k_b \\ (k/k_b)^{n_s - 1} & \text{if } k > k_b \,. \end{cases} \tag{3.22}$$

$$B(k_1, k_2, k_3) = \frac{3}{5}(2\pi^2)^2 f_{\rm nl} \left[\frac{\mathcal{P}_{\mathcal{R}}(k_1)}{k_1^3} \frac{\mathcal{P}_{\mathcal{R}}(k_2)}{k_2^3} + \frac{\mathcal{P}_{\mathcal{R}}(k_1)}{k_1^3} \frac{\mathcal{P}_{\mathcal{R}}(k_3)}{k_3^3} + \right.$$
$$\left. + \frac{\mathcal{P}_{\mathcal{R}}(k_3)}{k_3^3} \frac{\mathcal{P}_{\mathcal{R}}(k_2)}{k_2^3} \right] \exp\left(-\gamma \frac{k_1 + k_2 + k_3}{k_b} \right) . \tag{3.23}$$

Here $n_s = 0.9659$ and $A_s = 2.3424 \times 10^{-9}$, corresponding to the Planck values [5]. The inflation and bounce (pivot) scales are, respectively, $k_i = 10^{-6}\text{Mpc}^{-1}$ and $k_b = 0.002\text{Mpc}^{-1}$. Note that $k_i = 10^{-6}$ Mpc^{-1}, is a very large scale, below which perturbations are significantly suppressed. Our results are not sensitive to this scale. The scale $k_b = 0.002$ Mpc^{-1} is the pivot scale above which the bispectrum is exponentially suppressed. Its value is related to $f_{\rm NL}$. Making it smaller in order to suppress also lower k-values, we have to increase $f_{\rm NL}$ to achieve the goal of removing the CMB anomalies. On the other hand, by making it larger we would obtain a power spectrum which no longer agrees with the Planck observations. We therefore choose the largest possible value for k_b which is of the order of the smallest values of k which are well measured in the CMB power spectrum observed by Planck. The parameters q, $f_{\rm nl}$ and $\gamma = \sqrt{n\pi/2}\Gamma\left[1-n\right]/\Gamma\left[3/2-n\right]$ depend on the details of the bounce, being related to the parameter n in Eq. (3.1). The values of q and $f_{\rm nl}$ used in this chapter are shown in Table 3.1. The power spectrum for $n = 1/6$ is shown in Figure 3.1.

The bispectrum (3.23) is decaying exponentially for $k > k_b$. Since k_b is close to the horizon scale, the authors of [29] argue that the model is not excluded by observations, even for quite large values of $f_{\rm nl}$. Apart from this exponential decay, which is of course crucial to render a bispectrum with such a large value of $f_{\rm nl}$ viable, the bispectrum (3.23) is actually just the local bispectrum. Due to the strong exponential decay, however, its overlap with the local bispectrum is small. The values requested for $f_{\rm nl}$ given in Table 3.1

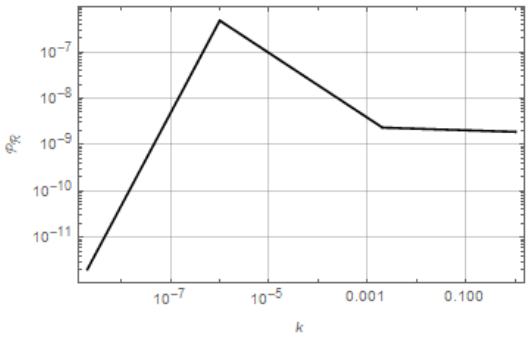

FIGURE 3.1: The power spectrum $\mathcal{P}_\mathcal{R}(k)$ versus k for $n = 1/6$. Note the three different regimes separated by the inflationary and the bounce scales.

are much larger than the Planck limit for the local shape which is $f_{\rm nl} \lesssim 10$ [128]. This is in principle possible since most of the Planck constraint comes from smaller scales, where the LQC bispectrum is exponentially suppressed.

In this work we check quantitatively whether the LQC bispectrum with the parameters given in Table 3.1 is compatible with observations. Clearly, this non-Gaussianity is best constrained on very large scales corresponding to $k \lesssim k_b$. This motivates us to compute the CMB bispectrum induced by it, concentrating on the largest angular scales. Expanding the CMB temperature fluctuations in spherical harmonics,

$$\frac{\Delta T}{T}(\mathbf{n}) = \sum_{\ell m} a_{\ell m} Y_{\ell m}(\mathbf{n})\,, \tag{3.24}$$

the bispectrum is defined by

$$\langle a_{\ell_1 m_1} a_{\ell_2 m_2} a_{\ell_2 m_3} \rangle = \mathcal{G}^{\ell_1 \ell_2 \ell_3}_{m_1 m_2 m_3} b_{\ell_1 \ell_2 \ell_3} = \begin{pmatrix} \ell_1 & \ell_2 & \ell_3 \\ m_1 & m_2 & m_3 \end{pmatrix} B_{\ell_1 \ell_2 \ell_3}\,. \tag{3.25}$$

Here $\mathcal{G}^{\ell_1 \ell_2 \ell_3}_{m_1 m_2 m_3}$ is the so-called Gaunt factor which can be expressed in terms of the Wigner $3j$-symbols as

$$\mathcal{G}^{\ell_1 \ell_2 \ell_3}_{m_1 m_2 m_3} = \sqrt{\frac{\prod_{j=1}^{3}(2\ell_j + 1)}{4\pi}} \begin{pmatrix} \ell_1 & \ell_2 & \ell_3 \\ 0 & 0 & 0 \end{pmatrix} \begin{pmatrix} \ell_1 & \ell_2 & \ell_3 \\ m_1 & m_2 & m_3 \end{pmatrix} \tag{3.26}$$

$$= g_{\ell_1 \ell_2 \ell_3} \begin{pmatrix} \ell_1 & \ell_2 & \ell_3 \\ m_1 & m_2 & m_3 \end{pmatrix}. \tag{3.27}$$

The m_i-dependent prefactor is a consequence of statistical isotropy [124]. The model dependent quantity $b_{\ell_1 \ell_2 \ell_3}$ is called the reduced bispectrum. It depends only on the values ℓ_1, ℓ_2, ℓ_3 and vanishes if these do not satisfy the triangle inequality, $|\ell_1 - \ell_2| \leq \ell_3 \leq \ell_1 + \ell_2$ or if the sum $\ell_1 + \ell_2 + \ell_3$ is odd.

Within linear perturbation theory, the reduced CMB bispectrum is entirely

determined by the primordial bispectrum of the curvature fluctuations in Fourier space. More precisely,

$$b_{\ell_1\ell_2\ell_3} = \left(\frac{2}{\pi}\right)^3 \int_0^\infty dx\, x^2 \int_0^\infty dk_1 \int_0^\infty dk_2 \int_0^\infty dk_3 \times \left[\prod_{j=1}^{3} \mathcal{T}(k_j,\ell_j) j_{\ell_j}(k_j x)\right] (k_1k_2k_3)^2 B(k_1,k_2,k_3)\,, \tag{3.28}$$

where $\mathcal{T}(k,\ell)$ is the CMB transfer function and j_ℓ is the spherical Bessel function of index ℓ [124]. On large scales, considering only the Sachs Wolfe term, we can approximate the transfer function by

$$\mathcal{T}(k,\ell) \simeq \frac{1}{5} j_\ell(k(t_0 - t_{\rm dec}))\,. \tag{3.29}$$

The times t_0 and $t_{\rm dec}$ are the (conformal) present time and the decoupling time respectively, given by (we set the speed of light to $c = 1$)

$$t_0 \simeq 14093.023\ \text{Mpc}, \qquad t_{\rm dec} \simeq 279.529\ \text{Mpc}\,. \tag{3.30}$$

Our bispectrum in k-space is separable, i.e., it can be written as a sum of products of functions of k_i,

$$\frac{B(k_1k_2k_3)}{B_0} = \frac{[f(k_1)f(k_2)g(k_3) + f(k_1)f(k_3)g(k_2) + f(k_3)f(k_2)g(k_1)]}{(k_1k_2k_3)^2} \tag{3.31}$$

where

$$B_0 = \frac{3}{5}(2\pi^2)^2 f_{\rm nl}, \tag{3.32}$$

$$f(k) = \frac{\mathcal{P}_\mathcal{R}(k)}{k}\exp(-\gamma k/k_b) \qquad \text{and} \tag{3.33}$$

$$g(k) = k^2 \exp(-\gamma k/k_b). \tag{3.34}$$

Setting

$$X_\ell(x,k) = \mathcal{T}(k,\ell) j_\ell(kx) f(k) \qquad \text{and} \tag{3.35}$$

$$Z_\ell(x,k) = \mathcal{T}(k,\ell) j_\ell(kx) g(k) \tag{3.36}$$

with Eq. (3.28) we obtain

$$\begin{aligned} b_{\ell_1\ell_2\ell_3} &= \left(\frac{2}{\pi}\right)^3 B_0 \int_0^\infty dx\, x^2 \int_0^\infty dk_1 \int_0^\infty dk_2 \int_0^\infty dk_3 \times \\ &\times \Big[X_{\ell_1}(x,k_1) X_{\ell_2}(x,k_2) Z_{\ell_3}(x,k_3) + \\ &+ X_{\ell_1}(x,k_1) X_{\ell_3}(x,k_3) Z_{\ell_2}(x,k_2) + \\ &+ X_{\ell_3}(x,k_3) X_{\ell_2}(x,k_2) Z_{\ell_1}(x,k_1)\Big]. \end{aligned} \tag{3.37}$$

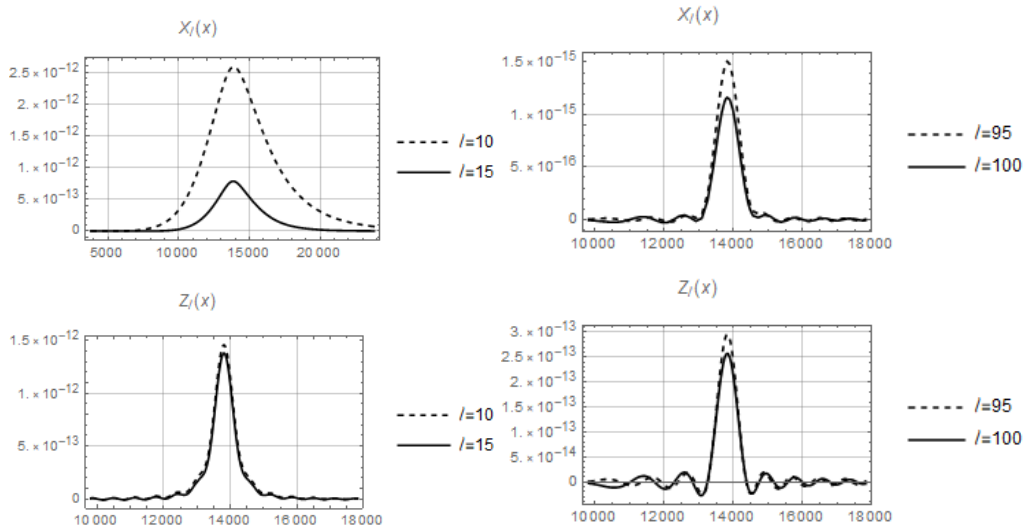

FIGURE 3.2: The functions $X_\ell(x)$ and $Z_\ell(x)$ for $n = 1/6$ with the integration over k performed up to $k_{\max} = 10^{-2}$ Mpc^{-1}. Note the sharp peaks at $x = t_0 - t_{\rm dec}$ and the oscillatory behavior that is especially visible for higher multipoles. Left: $\ell = 10$ and $\ell = 15$; right: $\ell = 95$ and $\ell = 100$.

This is the sum of three separable k-integrals. We introduce

$$X_\ell(x) = \int_0^\infty dk X_\ell(x,k) \qquad \text{and} \tag{3.38}$$

$$Z_\ell(x) = \int_0^\infty dk Z_\ell(x,k), \tag{3.39}$$

such that the bispectrum becomes the following integral:

$$\begin{aligned} b_{\ell_1\ell_2\ell_3} &= \left(\frac{2}{\pi}\right)^3 B_0 \int_0^\infty dx\, x^2 \Big[X_{\ell_1}(x) X_{\ell_2}(x) Z_{\ell_3}(x) + \\ &+ X_{\ell_1}(x) X_{\ell_3}(x) Z_{\ell_2}(x) + X_{\ell_3}(x) X_{\ell_2}(x) Z_{\ell_1}(x) \Big] . \end{aligned} \tag{3.40}$$

3.2.2 Numerical Calculations

The functions $X_\ell(x,k)$ and $Z_\ell(x,k)$ are heavily oscillating as functions of k (containing products of two Bessel functions of different arguments) and difficult to integrate. However when $x = t_0 - t_{\rm dec}$ the product $j_\ell(k(t_0 - t_{\rm dec}))j_\ell(kx)$ becomes a square and both $X_\ell(x,k)$ and $Z_\ell(x,k)$ are positive definite functions of k for this value of x. We therefore expect that the integrals over k, $X_\ell(x)$ and $Z_\ell(x)$ peak at $x = t_0 - t_{\rm dec}$. As an example, see the functions $X_\ell(x)$ and $Z_\ell(x)$ in Figure 3.2 for $n = 1/6$ and in Figure 3.3 for $n = 0.21$. We see that both functions decay rapidly for growing $|x - (t_0 - t_{\rm dec})|$ for the two values of n considered. One might hope, that due to this feature which is

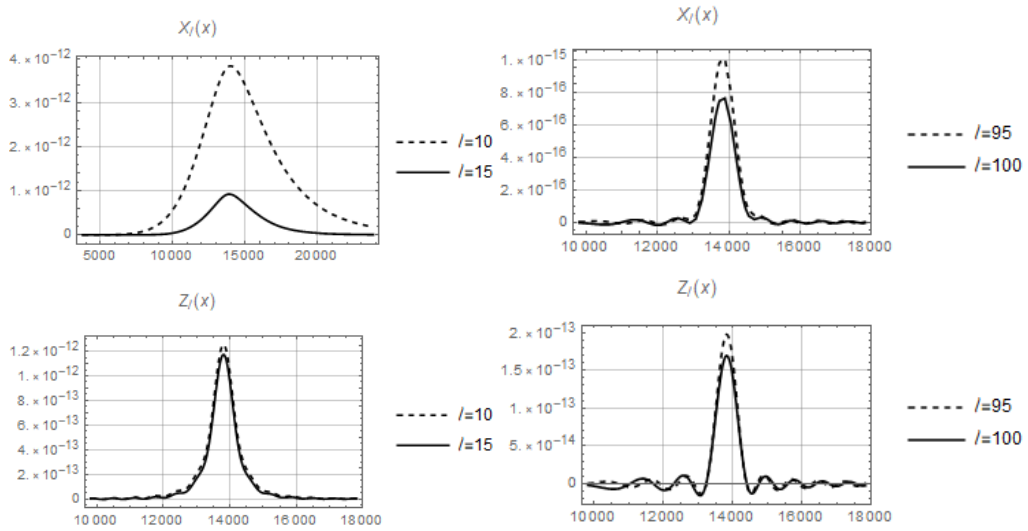

FIGURE 3.3: The functions $X_\ell(x)$ and $Z_\ell(x)$ for $n = 0.21$ with the integration over k performed up to $k_{\max} = 10^{-2}$ Mpc^{-1}. Again we see the sharp peaks at $x = t_0 - t_{\rm dec}$ and the oscillatory behavior for higher multipoles. Left: $\ell = 10$ and $\ell = 15$; right: $\ell = 95$ and $\ell = 100$.

the basic idea behind the Limber approximation, the Limber approximation might be relatively good. However, as we show in Section 3.2.5 this is not the case. The Limber approximation actually overestimates the signal by more than one order of magnitude at low ℓ.

The bispectrum (3.40) can be computed numerically if one takes into account the peaked behavior described above, restricting the integration range for the integral over x to an interval around $x = t_0 - t_{\rm dec}$. As we can see in Figs. 3.2 and 3.3, the width of the central peak is larger for low values of the multipole ℓ. For this reason we choose an x-range around $t_0 - t_{\rm dec}$ of 10^4 Mpc for $\ell_1 + \ell_2 + \ell_3 \leq 90$ and 2000 Mpc for $\ell_1 + \ell_2 + \ell_3 > 90$, encompassing a large percentage of the total contribution. For the latter cases, the difference with respect to the width 10^4 is less than 1%. Also for the low ℓ's the difference between the ranges 10^4 and 1.5×10^4 is always less than 1%. We first perform the computation for a number of allowed sets of multipoles, i.e. with an even sum and satisfying the triangle inequality, starting from the value $\ell_j = 4$, $j = 1, 2, 3$, and such that $\ell_2 = \ell_3 = \ell$. This is a suitable choice in order to depict the bispectrum in a three-dimensional plot. Configurations with $\ell_2 \neq \ell_3$ are considered in Section 3.2.4. The results are plotted in Figure 3.4 both for $n = 1/6$ (left) and $n = 0.21$ (right), where we identify a fast decaying behavior as the multipoles increase. The dots represent the values of the bispectrum obtained via numerical computation for $f_{\rm nl} = 8518$ in the case $n = 1/6$ and $f_{\rm nl} = 4372$ in the case $n = 0.21$. The gray planes correspond to the fits obtained in Section 3.2.4, namely Eqs. (3.48) and (3.50).

We want to compare the present model and the bispectrum for the local

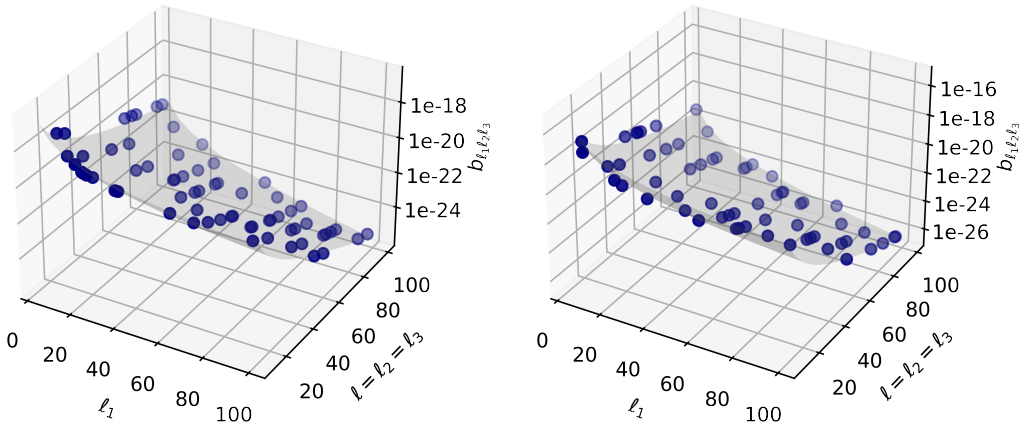

FIGURE 3.4: The bispectrum $b_{\ell_1\ell_2\ell_3}$ as a function of ℓ_1 and $\ell = \ell_2 = \ell_3$ for $n = 1/6$ (left) and $n = 0.21$ (right). The dots correspond to numerical results for $f_{\rm nl} = 8518$ in the case $n = 1/6$ and $f_{\rm nl} = 4372$ in the case $n = 0.21$. For the other values of $f_{\rm nl}$ in Table 3.1, the plots are re-scaled by the ratios of the $f_{\rm nl}$'s, the factors of 0.390 and 0.219 for $n = 1/6$ and $n = 0.21$, respectively. The gray planes correspond to the product fits obtained in Section 3.2.4, Eqs. (3.48) and (3.50).

shape. To do so, we first fix $\ell_1 = 4$, require $\ell_2 = \ell_3 = \ell$ and perform the numerical computations for the bispectrum of the current work. Then, recalling that the reduced bispectrum of the local shape is given by [124]

$$b^{(\rm local)}_{\ell_1\ell_2\ell_3} = \frac{3 f_{\rm nl}(2\pi^2 A_s)^2}{4\times 5^4}\Big(\frac{1}{\ell_1(\ell_1+1)\ell_2(\ell_2+1)} + \\ + \frac{1}{\ell_1(\ell_1+1)\ell_3(\ell_3+1)} + \frac{1}{\ell_2(\ell_2+1)\ell_3(\ell_3+1)}\Big), \qquad (3.41)$$

we substitute $\ell_1 = 4$, $\ell_2 = \ell_3 = \ell$ and $f_{\rm nl} = 5.0$, this value of $f_{\rm nl}$ is chosen based on the Planck constraint on local non-Gaussianity [121]. In Figure 3.5, we plot the power spectra versus ℓ.

The bispectrum of the bounce followed by an inflationary phase is larger than the local bispectrum for all the low multipoles considered here. However, this does not mean that it is ruled out by the Planck observations, as most of the observational power from Planck limiting the bispectrum comes from higher values of ℓ which are not present in this plot and for which $b^{(\rm local)}$ is much larger than the bispectrum from our bouncing models.

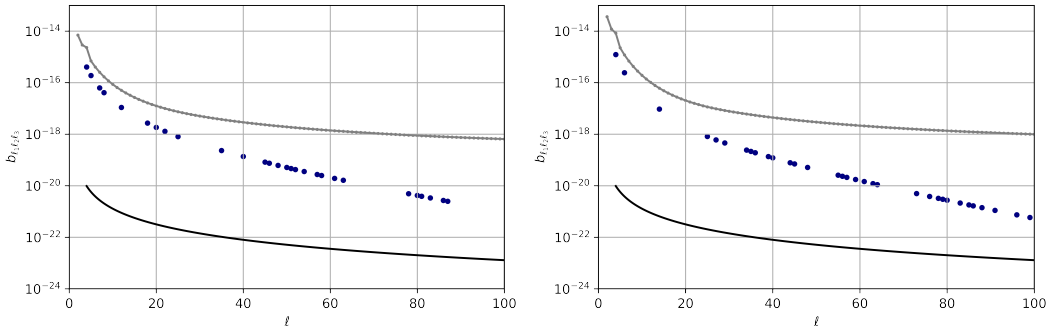

FIGURE 3.5: The bispectrum of the current work with $n = 1/6$ (left) and $n = 0.21$ (right) and the local bispectrum with $f_{\rm nl} = 5.0$, considering multipoles such that $\ell_1 = 4$ and $\ell_2 = \ell_3 = \ell$. The dots correspond to $f_{\rm nl} = 8518$ for $n = 1/6$ and to $f_{\rm nl} = 4372$ for $n = 0.21$. For the other values of $f_{\rm nl}$ in Table 3.1, the bispectrum is re-scaled by factors of 0.390 for $n = 1/6$ and 0.219 for $n = 0.21$. The local bispectrum and cosmic variance are depicted as the black and gray lines, respectively.

3.2.3 Cosmic Variance

In order to decide whether the bispectrum of the bouncing models discussed here can be ruled out, we consider its SNR by adding cosmic variance as the dominant noise source on large scales. This is the minimal error on $b_{\ell_1\ell_2\ell_3}$. Here we follow [129]. Let us introduce the random variable

$$\hat{B}_{\ell_1\ell_2\ell_3} = \sum_{m_1 m_2 m_3} \begin{pmatrix} \ell_1 & \ell_2 & \ell_3 \\ m_1 & m_2 & m_3 \end{pmatrix} a_{\ell_1 m_1} a_{\ell_2 m_2} a_{\ell_2 m_3} \,. \tag{3.42}$$

This is an estimator of $B_{\ell_1\ell_2\ell_3}$ defined in (3.25), i.e. $\langle \hat{B}_{\ell_1\ell_2\ell_3} \rangle = B_{\ell_1\ell_2\ell_3}$. In the same way as

$$\hat{C}_\ell = (2\ell+1)^{-1} \sum_m |a_{\ell m}|^2 \tag{3.43}$$

is an estimator of the power spectrum $C_\ell = \langle |a_{\ell m}|^2 \rangle$. Using identities of the Wigner 3j symbols and neglecting terms involving the bispectrum, which are much smaller than the terms from the power spectrum to the third power, one finds for the variance of our estimator $\hat{B}_{\ell_1\ell_2\ell_3}$

$$\begin{aligned} \mathrm{var}(B_{\ell_1\ell_2\ell_3}) &= \langle \hat{B}^2_{\ell_1\ell_2\ell_3} \rangle \\ &\simeq C_{\ell_1} C_{\ell_2} C_{\ell_3} \left(1 + \delta_{\ell_1\ell_2} + \delta_{\ell_1\ell_3} + \delta_{\ell_3\ell_2} + 2\delta_{\ell_1\ell_2}\delta_{\ell_2\ell_3}\right) . \end{aligned} \tag{3.44}$$

For the reduced bispectrum this yields

$$\mathrm{var}\left(b_{\ell_1\ell_2\ell_3}\right) \simeq g^{-2}_{\ell_1\ell_2\ell_3} C_{\ell_1} C_{\ell_2} C_{\ell_3} \left(1 + \delta_{\ell_1\ell_2} + \delta_{\ell_1\ell_3} + \delta_{\ell_3\ell_2} + 2\delta_{\ell_1\ell_2}\delta_{\ell_2\ell_3}\right) . \tag{3.45}$$

Of course this equality is only valid when $g_{\ell_1\ell_2\ell_3} \neq 0$, i.e., for values of ℓ_1, ℓ_2, ℓ_3 which satisfy the triangle inequality and are such that $\ell_1 + \ell_2 + \ell_3$ is even, since otherwise $b_{\ell_1\ell_2\ell_3} = 0$ with vanishing variance.

The minimal error on $b_{\ell_1\ell_2\ell_3}$ for an experiment measuring all $a_{\ell_1 m_1} a_{\ell_2 m_2} a_{\ell_2 m_3}$ with negligible instrumental noise is (the square root of) the cosmic variance. The latter is computed using the values of C_ℓ obtained with the Cosmic Linear Anisotropy Solving System (CLASS) [130, 131] and compared to the amplitude of the bispectrum of the bouncing model in Figure 3.5. Clearly, the amplitude of the square root of the cosmic variance is larger than the bispectrum for all values of ℓ. This precludes a measurement of the individual $b_{\ell_1\ell_2\ell_2}$'s, but in order to investigate whether the model can be ruled out due to its non-Gaussianity, we have to go on and compute the total SNR.

3.2.4 Signal-to-Noise Ratio

For each individual triple (ℓ_1, ℓ_2, ℓ_3) with $\ell_i \geqslant 4$, $i = 1, 2, 3$, cosmic variance is larger than the value of the bispectrum. However, this does not mean that such a bispectrum is not detectable. To decide on that, we estimate the cumulative SNR of the entire bispectrum for $\ell_i \leq \ell_{\mathrm{max}}$. We choose $\ell_{\mathrm{max}} = 80$ to make sure that the Sachs-Wolfe term calculated here really is the dominant contribution. However, as we shall see, the SNR saturates already at $\ell_{\mathrm{max}} \sim 30$.

$$\left(\frac{S}{N}\right)^2 (\ell_{\mathrm{max}}) = \sum_{\ell_1\ell_2\ell_3=2}^{\ell_{\mathrm{max}}} \frac{b^2_{\ell_1\ell_2\ell_3}}{\mathrm{var}\left(b_{\ell_1\ell_2\ell_3}\right)}\,. \tag{3.46}$$

In order to perform this computation, we fit the numerical results of the bispectrum obtained for different sets of multipoles by a product ansatz, including the ones where $\ell_1 \neq \ell_2 \neq \ell_3$. The fits of our product approximation read

$$\ln(b_{\ell_1\ell_2\ell_3}) \;=\; -3.727 \times 10^{-6}(\ell_1\ell_2\ell_3) - 2.225\ln(\ell_1\ell_2\ell_3) - 25.607 \tag{3.47}$$

for $n = 1/6$ and $f_{\mathrm{nl}} = 3326$,

$$\ln(b_{\ell_1\ell_2\ell_3}) \;=\; -3.727 \times 10^{-6}(\ell_1\ell_2\ell_3) - 2.225\ln(\ell_1\ell_2\ell_3) - 24.667 \tag{3.48}$$

for $n = 1/6$ and $f_{\mathrm{nl}} = 8518$,

$$\ln(b_{\ell_1\ell_2\ell_3}) = -3.204 \times 10^{-6}(\ell_1\ell_2\ell_3) - 2.661\ln(\ell_1\ell_2\ell_3) - 22.491 \tag{3.49}$$

for $n = 0.21$ and $f_{\mathrm{nl}} = 959$ and

$$\ln(b_{\ell_1\ell_2\ell_3}) = -3.204 \times 10^{-6}(\ell_1\ell_2\ell_3) - 2.661\ln(\ell_1\ell_2\ell_3) - 20.974 \tag{3.50}$$

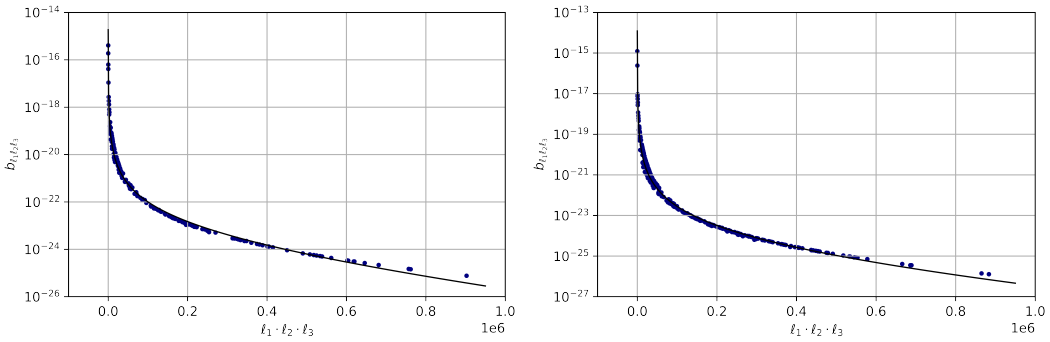

FIGURE 3.6: The bispectrum $b_{\ell_1\ell_2\ell_3}$ vs $\ell_1\ell_2\ell_3$ for $n = 1/6$ (left) and $n = 0.21$ (right). The dots correspond to $f_{\rm nl} = 8518$ for $n = 1/6$ and to $f_{\rm nl} = 4372$ for $n = 0.21$. The lines represent the fits, given by Eqs. (3.48) and (3.50). For the other values of $f_{\rm nl}$ in Table 3.1, the approximations are simply re-scaled by the ratios of the $f_{\rm nl}$ values, namely the factors 0.390 for $n = 1/6$ and 0.219 for $n = 0.21$.

for $n = 0.21$ and $f_{\rm nl} = 4372$. Two of them are shown in Figure 3.6, while the other two are simply re-scaled by the ratios of the $f_{\rm nl}$ values.

The variance is obtained from Eq. (3.45), as before. Summing all the terms corresponding to allowed sets of multipoles, i.e. with $\ell_1 + \ell_2 + \ell_3$ even and $|\ell_1 - \ell_2| \leq \ell_3 \leq \ell_1 + \ell_2$, we obtain the cummulative SNR as a function of the maximum multipoles $\ell_{\rm max}$.

Our purpose it to investigate whether we achieve a value of order $\mathcal{O}(10)$ within the low ℓ regime, i.e. $\ell \ll 200$, which corresponds to the validity of the transfer function given in Eq. (3.29), and which is also the regime in which the non-Gaussianitiy of these models is larger. The results are shown in Figure 3.7. In order to consider a sky coverage of 70%, we multiply the cosmic variance by $1/0.70$. Clearly, the SNR saturates very fast, namely roughly at $\ell_{\rm max} = 30$, but it achieves a value larger than 25, both for $n = 1/6$ and $n = 0.21$ for the larger value of $f_{\rm nl}$. For the smaller values of $f_{\rm nl}$ the cumulative SNR for $n = 1/6$ is 10.3 while for $n = 0.21$ it is 10.6. In all cases these bispectra should be detectable in the Planck data.

Even though the individual $b_{\ell_1\ell_2\ell_3}$ are below cosmic variance if $\ell_i \geqslant 4$, $i = 1, 2, 3$, the cumulative SNR of the bispectrum with $\ell_{\rm max} = 30$ is larger than 10 for all the models proposed, when assuming a sky coverage of 70% and considering only temperature data. Note that the largest contributions to the SNR come from triples (ℓ_1, ℓ_2, ℓ_3) where at least one multipole is smaller than 4, for which the signal is larger than or comparable to the square root of the variance. For the higher values of $f_{\rm nl}$ the cumulative SNR is about 26.5 ($n = 1/6$) and 48.2 ($n = 0.21$) respectively. To get an impression of the amplitude of the SNR of these models, one may want to compare it to the one of CMB lensing, which is about 40 in the Planck 2015 data [132]. Note

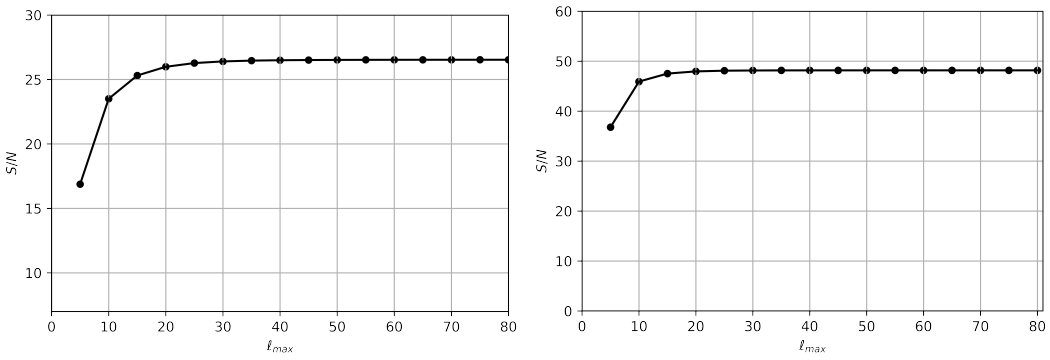

FIGURE 3.7: The signal-to-noise ratio, considering 70% of sky coverage, versus maximum values of the multipoles $\ell_{\rm max}$ for $n = 1/6$ (left) and $n = 0.21$ (right). The dots correspond to $f_{\rm nl} = 8518$ for $n = 1/6$ and to $f_{\rm nl} = 4372$ for $n = 0.21$. For the other values of $f_{\rm nl}$ in Table 3.1, the bispectrum is re-scaled by factors of 0.390 for $n = 1/6$ and 0.219 for $n = 0.21$.

that already at $\ell_{\rm max} = 5$ the SNR is larger than 15 ($n = 1/6$) and 35 ($n = 0.21$). But also for the two models with the lower value of $f_{\rm nl}$, the cumulative SNR is actually just slightly above 10, so that the bispectrum can in principle be detected. In order to obtain an undetectable bispectrum one would have to reduce the $f_{\rm nl}$ by about a factor of 10, so that the cumulative SNR would become of order unity. However, when reducing $f_{\rm nl}$ to these values, the CMB large scale anomalies can no longer be resolved efficiently by these models and they lose one of their main attractive features.

These findings motivate us to perform a search for this bispectrum in the actual Planck data. Before doing so, let us consider the reduced bispectrum computed by means of the Limber approximation.

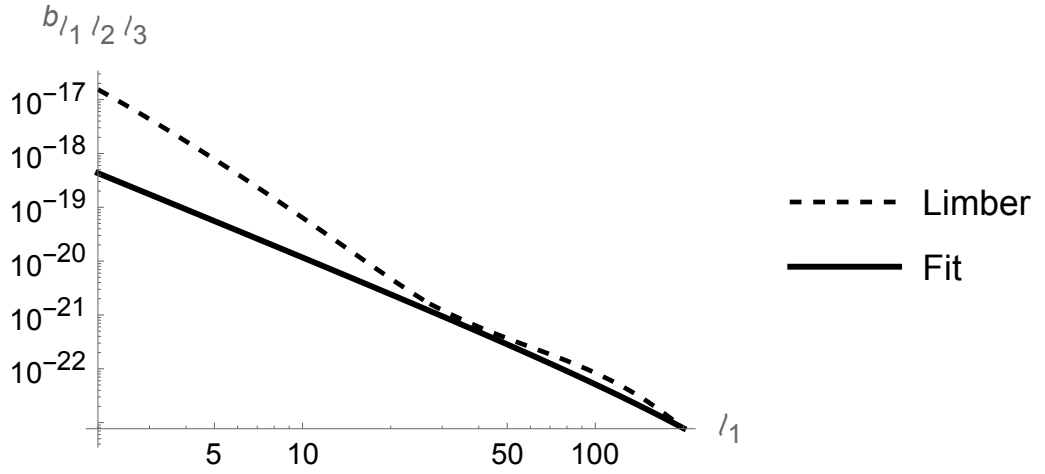

FIGURE 3.8: The Limber approximation (dashed) is compared with our product approximation (solid) for $\ell_2 = \ell_3 = 30$ fixed, as a function of ℓ_1. Even though the Limber approximation is probably better for $\ell > 50$, it is much worse than our excellent product approximation in the relevant regime, $\ell_i < 30$.

3.2.5 Limber Approximation

Let us now solve the integrals (3.38) and (3.39) with $\mathcal{T}(k,\ell) = j_\ell(k(t_0 - t_{\rm dec}))/5$ using the Limber approximation [133]. This yields

$$\begin{aligned}
X_\ell(x) &= \int dk T(k,\ell) j_\ell(kx) f(k) \simeq \frac{1}{5}\int dk j_\ell(k(t_0-t_{\rm dec})) j_\ell(kx) f(k) \\
&\simeq \frac{\pi}{10}\frac{\delta(t_0-t_{\rm dec}-x)}{(\ell+1/2)^2} f\left(\frac{\ell+1/2}{t_0-t_{\rm dec}}\right) \\
&= \frac{\pi}{10}\delta(t_0-t_{\rm dec}-x)\frac{t_0-t_{\rm dec}}{(\ell+1/2)^3}\mathcal{P}_{\mathcal{R}}\left(\frac{\ell+1/2}{t_0-t_{\rm dec}}\right) e^{-\gamma\frac{\ell+1/2}{k_b(t_0-t_{\rm dec})}} \\
Z_\ell(x) &= \int dk T(k,\ell) j_\ell(k) g(k) \simeq \frac{1}{5}\int dk j_\ell(k(t_0-t_{\rm dec})) j_\ell(kx) g(k) \\
&\simeq \frac{\pi}{10}\frac{\delta(t_0-t_{\rm dec}-x)}{(\ell+1/2)^2} g\left(\frac{\ell+1/2}{t_0-t_{\rm dec}}\right) \\
&= \frac{\pi}{10}\delta(t_0-t_{\rm dec}-x)\frac{1}{(t_0-t_{\rm dec})^2} e^{-\gamma\frac{\ell+1/2}{k_b(t_0-t_{\rm dec})}} .
\end{aligned} \tag{3.51}$$

Here we used the functions f and g defined in Eqs. (3.33) and (3.34). Of course, the product of three delta functions cannot be integrated, but replacing them by narrow Gaussians we obtain up to an unknown constant A, related to the

width of the Gaussian,

$$\begin{aligned} b_{\ell_1\ell_2\ell_3)} &= \left(\frac{2}{\pi}\right)^3 B_0 \int dx x^2 X_{\ell_1}(x) X_{\ell_2}(x) Z_{\ell_3}(x) \\ &\sim \frac{AB_0}{125} \exp\left(-\gamma \frac{\ell_1+\ell_2+\ell_3}{k_b(t_0-t_{\rm dec})}\right) \times \\ &\times \left[\frac{\mathcal{P}_{\mathcal{R}}\left(\frac{\ell_1+1/2}{t_0-t_{\rm dec}}\right)}{(\ell_1+1/2)^3} \frac{\mathcal{P}_{\mathcal{R}}\left(\frac{\ell_2+1/2}{t_0-t_{\rm dec}}\right)}{(\ell_2+1/2)^3} + \circlearrowleft\right] . \end{aligned} \tag{3.52}$$

Here $\circlearrowleft$ indicates that the two permutations $(\ell_1,\ell_2) \to (\ell_1,\ell_3)$ and $(\ell_1,\ell_2) \to (\ell_3,\ell_2)$ have to be added. We have tested this approximation with our numerical computations and found that for the relevant values of ℓ, $\ell < 30$, which contribute most to the SNR, it is much less accurate than the product approximation that we have used in Section 3.2.4, as seen from Figure 3.8.

3.3 Limits from Planck

In order to adapt the parameters of the bouncing model to the Planck conventions [134], we rewrite the bispectrum (3.23) as

$$\begin{aligned} B(k_1,k_2,k_3) &= -\frac{6}{5}(2\pi^2)^2 f_{\rm NL} \left[\frac{\mathcal{P}_{\mathcal{R}}(k_1)}{k_1^3}\frac{\mathcal{P}_{\mathcal{R}}(k_2)}{k_2^3} + \right. \\ &+ \left. \frac{\mathcal{P}_{\mathcal{R}}(k_1)}{k_1^3}\frac{\mathcal{P}_{\mathcal{R}}(k_3)}{k_3^3} + \frac{\mathcal{P}_{\mathcal{R}}(k_3)}{k_3^3}\frac{\mathcal{P}_{\mathcal{R}}(k_2)}{k_2^3}\right] \times \\ &\times \exp\left(-\gamma \frac{k_1+k_2+k_3}{k_b}\right) . \end{aligned} \tag{3.53}$$

Therefore, the definition of $f_{\rm NL}$ in (3.23) differs by a factor -2 from the one used here. This explains for example why there is a factor $+3/5$ instead of $-6/5$ in the expression (3.23) and why the numbers in Table 3.2 differ by a factor of -2 from the ones in Table 3.1. In addition, we change the notation in (3.28) from $b_{l_1 l_2 l_3}$ to $B_{l_1 l_2 l_3}$ to keep notation consistency with the Planck analysis.

From now on we consider the two scenarios included in Table 3.1 and add a third model for completeness. As previously mentioned, the parameters of model 2, with $q = -0.7$, correspond to LQC, while model 3, with $q = -1.24$, is a phenomenological bouncing model which provides the best fit to the Planck data in a Markov Chain Monte Carlo (MCMC) analysis performed with Planck TT and low-ℓ EE power spectra carried out in [29]. The fit is excellent, even somewhat better than ΛCDM. This value is also close to the smallest value of q which can still resolve the large-scale anomalies as we

model	q	γ	$f_{\rm NL}$ 20%	$f_{\rm NL}$ 10%	$f_{\rm NL}$ 5%
1	-0.5	0.588	-2516	-1661	-1283
2	-0.7	0.6468	-1663	-1098	-848
3	-1.24	0.751	-480	-317	-245

TABLE 3.2: The values of the parameters considered in this section. The $f_{\rm NL}$ parameters are chosen according to [29] in order to alleviate the power suppression anomaly (but note the factor -2 difference in definition here as compared to [29]). We also give the values of $f_{\rm NL}$ needed to obtain a probability of 10% and 5%, respectively, to observe the power suppression anomaly using the definition of [29].

require here. The value of $|f_{\rm NL}|$ needed in this model is significantly smaller. Finally, we also study a somewhat larger value than the one of LQC, $q = -0.5$, which correspondingly requires a larger value of $f_{\rm NL}$ to resolve the large-scale anomalies. We call this model 1. In all three cases we assume the smallest possible values for $f_{\rm NL}$ such that the large-scale anomalies appear with a probability of 20%. This requires that the curvature scale of the bounce is the Planck scale. We also give the values of $f_{\rm NL}$ for the 10% and 5% probabilities. Note, however, that in standard ΛCDM this probability is about 2%, hence not so much smaller than the last value. The analysis in the next section is performed for $f_{\rm NL}$ of 20% in Table 3.2. The results for the other probabilities can be obtained by linear rescaling.

The reduced CMB bispectrum is obtained in terms of the Fourier space bispectrum via (3.28), where one uses $\mathcal{T}(k,\ell)$, the CMB transfer function, which is defined such that the CMB temperature power spectrum is given by

$$C_\ell = 4\pi \int dk\, k^2 (\mathcal{T}(k,\ell))^2 \mathcal{P}_{\mathcal{R}}(k)\,, \tag{3.54}$$

where $\mathcal{P}_{\mathcal{R}}$ is the dimensionless curvature power spectrum [124]. Note that the normalization of the transfer functions depends on the definition. This transfer function, e.g., differs by a factor $\sqrt{\ell(\ell+1)/2}$ from the one given in [135].

Now let us compute the CMB bispectrum exactly using the numerical transfer functions as determined by CAMB[3] (or CLASS[4]) and search for the signal in the truly observed Planck data. The comparison between the approximated and fully numerical transfer functions can be seen in Figure 3.9 for $\ell = 2$ and $\ell = 15$. We employ the binned bispectrum estimator described in [136, 137] and used in the Planck analyses [138, 128, 121]. We analyze the cleaned CMB temperature and E-polarization maps of the Planck 2018

[3] http://camb.info

[4] https://lesgourg.github.io/class-tour-Tokyo.html

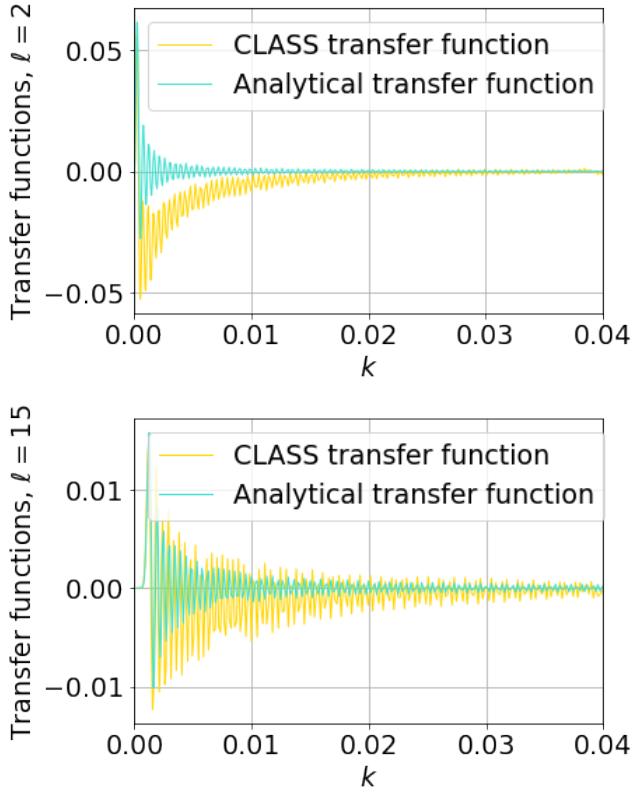

FIGURE 3.9: Comparison between the analytical transfer function (2.35) and the fully numerical transfer function obtained from CLASS(or CAMB) for $\ell = 2$ and $\ell = 15$. Although the agreement is relatively good for $\ell = 15$, for lower multipoles the difference is not negligible.

release, created by the SMICA component separation method [139], which have an angular resolution of 5′. We mask them using the common masks of the Planck 2018 analysis, which leave a sky fraction of 78%. Error bars and linear correction terms are computed using 300 simulations. For more details about the data, see [121].

Figure 3.10 shows the comparison between the bispectrum fit from Section 3.2.4 and the exact numerical bispectrum. While there are obvious differences, we see that the fit gives a reasonable approximation, despite the shortcomings of the analytic approximations on which it was based. These shortcomings are for example the fact that the integrated Sachs-Wolfe effect was ignored, even though it is important at the lowest values of ℓ where this template peaks. Also the contributions from the acoustic peaks are not accounted for in the previous sections. However, we expect these to be negligible due to the exponential decay of the bispectrum. Furthermore, the integration routine used previously was different and computationally much more demanding, so that it cannot be used efficiently with the full numerical transfer functions. In Section 3.2.4 simple fits for the bispectra as functions of the product $L \equiv \ell_1 \cdot \ell_2 \cdot \ell_3$ were

introduced. While these capture well the overall shape of the numerical results, they somewhat overestimate it at high L and also, more importantly, at the dominant lowest values of L. Here the analytical fit is just shown for illustration but it is not used in the data analysis.

The bispectrum amplitude $f_{\rm NL}$ is determined from the data by template fitting. The theoretical bispectrum template (3.28) determined from (3.53) is multiplied by the observed bispectrum $B_{\ell_1\ell_2\ell_3}$ of the CMB and divided by the expected bispectrum variance (which in the case of weak non-Gaussianity is just a product of the three measured power spectra $C_{\ell_1}C_{\ell_2}C_{\ell_3}$), summing over all values of ℓ_1, ℓ_2, ℓ_3. This expression must finally be multiplied by a factor to normalize the inverse-variance weights, and this factor is exactly the expected variance of $f_{\rm NL}$. In the case that polarization data is included as well as temperature data, the division by the variance becomes a multiplication with the inverse covariance matrix, and the sum is also over polarization indices. The whole expression for $f_{\rm NL}$ can simply be viewed as the normalized inner product of the bispectrum template with the observed bispectrum of the CMB:

$$f_{\rm NL} = \frac{\left\langle B^{\rm th}, B^{\rm obs}\right\rangle}{\left\langle B^{\rm th}, B^{\rm th}\right\rangle}. \tag{3.55}$$

In the simple case of temperature only and no binning, this inner product is given by

$$\left\langle B^A, B^B\right\rangle = \sum_{\ell_1\leq\ell_2\leq\ell_3} \frac{B^A_{\ell_1\ell_2\ell_3} B^B_{\ell_1\ell_2\ell_3}}{V_{\ell_1\ell_2\ell_3}}, \tag{3.56}$$

where V is the variance of the observed bispectrum, which depends on the noise and beam characteristics of the experiment. For the explicit definitions of the inner product in the case of binning or when polarization is included, as well as for other expressions and more detailed explanations, see e.g. [137].

Computing the observed bispectrum for all values of ℓ_1, ℓ_2, ℓ_3 is computationally too expensive, hence estimators must use approximations. The binned bispectrum estimator used in this paper makes the approximation that the bispectrum templates we are looking for are sufficiently smooth and slowly changing, that it is enough to only compute the average value of the bispectrum in each bin of ℓ values. This is a good approximation for the bouncing bispectrum under consideration: it was explicitly tested that the standard binning with 57 bins used for the Planck 2018 analysis [121] gives a negligible increase in variance compared to the exact non-binned template. The Planck binning was determined by minimizing the increase in the theoretical variance for the local, equilateral and orthogonal shapes due to the binning, taking into account the noise and beam characteristics of the Planck experiment for both temperature and polarization.

The bouncing bispectrum template has the property that it decreases extremely fast as a function of ℓ because of the exponential factor in (3.53). It was shown that cutting off the analysis at $\ell_{\rm max} = 36$ does not change the

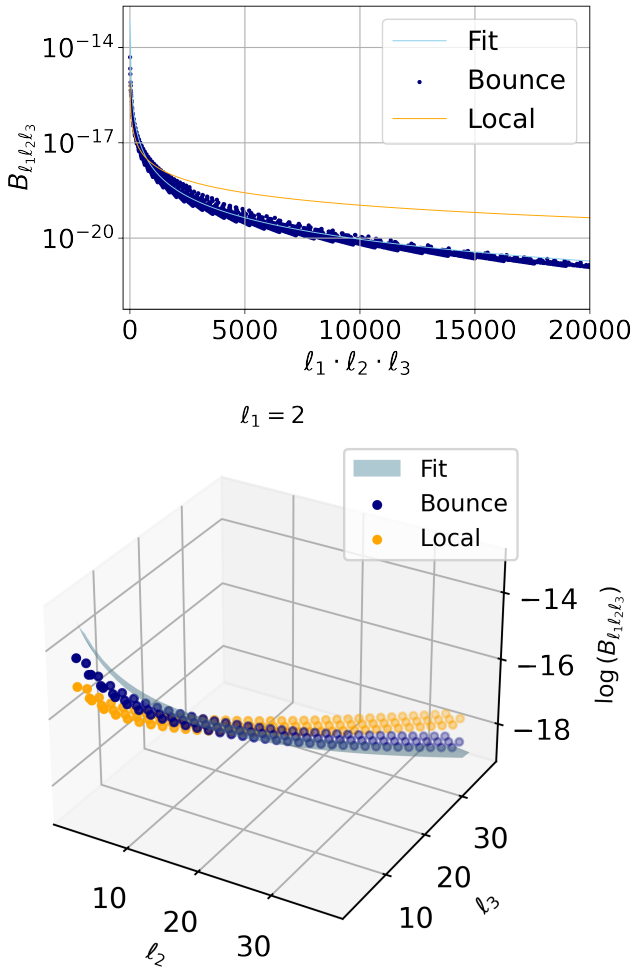

FIGURE 3.10: *Top panel:* The bouncing bispectrum computed with the numerical transfer functions (blue dots), fit to the bispectrum obtained in [35] (cyan) and the local bispectrum (yellow), for $q = -0.7$ (multiplication by $f_{\rm NL}$ included). The bispectrum is plotted as a function of the product $L \equiv \ell_1\ell_2\ell_3$, which allows plotting all values of the 3D bispectrum in a 2D plot, at the price of having multiple (ℓ_1, ℓ_2, ℓ_3) configurations corresponding to the same value of the product L.
Bottom panel : The same bispectrum for $\ell_1 = 2$ fixed as a function of ℓ_2 and ℓ_3, compared to the local bispectrum with the same value for $f_{\rm NL}$. Only values of ℓ_i which satisfy the triangle inequality are plotted. The fitting formula is indicated as a cyan surface.

	bouncing ($q = -0.5$)	bouncing ($q = -0.7$)	bouncing ($q = -1.24$)
local	0.018	0.013	0.006
equilateral	0.011	0.006	-0.002
orthogonal	-0.046	-0.039	-0.028
point sources	-10^{-10}	-10^{-10}	-10^{-11}
CIB	-10^{-7}	-10^{-7}	-10^{-8}
galactic dust	-0.13	-0.11	-0.066
lensing	-0.002	-0.002	-0.001
bouncing ($q = -0.5$)		0.98	0.82
bouncing ($q = -0.7$)			0.91

TABLE 3.3: Correlation coefficients of the bouncing template (for the three different values of q) with the standard primordial and foreground bispectrum templates of the Planck analysis [121], as well as with the galactic dust bispectrum template from [140].

expected Fisher error bar at all compared to the $\ell_{\rm max} = 2500$ used in the Planck analysis. However, in the actual data analysis it is still important to use this much higher $\ell_{\rm max}$ in order to disentangle the bouncing bispectrum from other sources of non-Gaussianity that are present in the data, like extra-galactic point sources and the lensing bispectrum. Table 3.3 gives the correlation coefficients of the bouncing template (for the three different values of q) with the standard primordial and foreground templates of the Planck analysis (for temperature only, in order to also show extragalactic point sources and the Cosmic Infrared Background). These correlations coefficients are defined as

$$C_{IJ} = \frac{F_{IJ}}{\sqrt{F_{II}F_{JJ}}}, \tag{3.57}$$

where I and J are indices labeling the templates and F is the Fisher matrix defined as $F_{IJ} = \langle B^I, B^J \rangle$. We see that, once the full Planck range is used, the correlation with all the other templates is very small (although the 3-5% correlation with the orthogonal shape is not completely negligible). Not surprisingly, the correlation between the three bouncing templates, on the other hand, is very large. There is also some correlation with the galactic dust template from [140], but as the analysis was performed on the cleaned CMB map from which the dust has been removed, this has no impact on our final results.

Table 3.4 presents the final results for the analysis of the Planck 2018 SMICA CMB maps with the bouncing template. They have been computed using a full temperature plus E-mode polarization analysis. However, the addition of polarization does not help at all, one obtains exactly the same error bars using temperature only. We see that there is no detection of any of the three templates. Given the size of the error bars in this Table and the

template	$f_{\rm NL}$
bouncing ($q = -0.5$)	240 ± 470
bouncing ($q = -0.7$)	160 ± 260
bouncing ($q = -1.24$)	19 ± 34

TABLE 3.4: $f_{\rm NL}$ (with 1σ error bars) of the bouncing template (for the three different values of q) as determined from the 2018 Planck SMICA CMB temperature and polarization maps using the binned bispectrum estimator.

predicted values of $f_{\rm NL}$ (20%) given in Table 3.2, we see that model 1 with $q = -0.5$ is ruled out at 5.4σ, the LQC model with $q = -0.7$ is ruled out at 6.4σ, while model 3 with $q = -1.24$ is ruled out at 14σ.

3.4 Conclusions and Discussion

In this chapter we have investigated the non-Gaussianities of bouncing models that mitigate the large-scale anomalies in the CMB data. Despite the fact that the bispectrum of these scenarios decays exponentially below the pivot scale, for $k > k_b = 0.002$ Mpc^{-1}, these models are excluded by the Planck data with high significance. This shows the sensitivity of the Planck data to scales beyond the pivot scale. This is especially evident when comparing models 2 and 3. While the LQC model has much larger $f_{\rm NL}$ and therefore a larger bispectrum on all scales $k > k_b$, it is less significantly excluded, namely by 6.4σ, than the third model with $q = -1.24$ which is excluded at 14σ. The bispectrum of this model is smaller than the one from LQC for $k > k_b$, but is larger for $k < k_b/3.3$. These large scales are imprinted in the CMB since the CMB transfer function is by no means a Dirac delta and a given ℓ value obtains contributions from a rather broad band of wave numbers k.

As lowering $f_{\rm NL}$ in these models goes in pair with rendering q even more negative, this implies that solving the large-scale anomaly puzzle with these models is excluded by the Planck data.

If one reduces the probability for the large-scale anomalies to appear from 20% to 10 % or even 5%, this reduces the exclusion by the same factor as $f_{\rm NL}$, see Table 3.2, leading to only 3.5σ or 2.7σ exclusion for model 1 but still 9.3σ and 7.2σ for model 3. For the LQC model 2 the corresponding limits are 4.2σ and 3.3σ, respectively.

It is very likely that our results actually go beyond the models studied here. If we want the large-scale anomalies to be less improbable by skewed statistics, this introduces a bispectrum. Even if this bispectrum is significant only on very large scales, the Planck data are sufficiently precise to exclude it.

It is of course possible that this might be evaded by some very exceptional, faster than exponential decay of the bispectrum. Nevertheless, ours does appear to be a quite solid conclusion.

Chapter 4

Inflation in the Presence of Holographic Dark Energy

4.1 Introduction

In 1998, observations of type Ia supernovae led to the conclusion that the Universe is under an accelerated expansion [19, 20], which gave rise to the concept of dark energy [21]. In the following years, the presence of this dark component was corroborated by many other observations, such as the Cosmic Microwave Background (CMB) radiation [141, 9, 10, 11], the large scale structure [142], the late-time integrated Sachs-Wolfe effect [143, 144] and the direct measurement of the Hubble parameter [145]. However, although its existence is widely evidenced, the nature of dark energy remains unknown. The standard cosmological model, namely ΛCDM, is currently favoured by observations [146, 147], meaning that a cosmological constant Λ would be responsible for driving the accelerated expansion.

On the other hand, the holographic principle [148, 149], which states that the physics inside a volume can be described by a theory on its boundary, has been considered as a principle of quantum gravity and, therefore, could shed some light on the dark energy problem. According to the holographic principle, the vacuum energy density arising from the quantum fluctuation of the UV cut-off quantum field theory should relate to the boundary surface of a system in the way [150],

$$\rho \propto M_p^2 L^{-2}, \tag{4.1}$$

where M_p is the reduced Planck mass and L is a length scale. On the UV side, the quartic divergence of the vacuum energy is cut off at the scale $\Lambda \sim M_p/L$. Therefore, it can serve as one of the solutions to the cosmological constant problem [151]. It was suggested to adopt the future event horizon R_h as the IR cut-off scale of the universe [152], and the cosmic expansion is speeded up by the associated vacuum energy given by eq. (4.1). The model is dubbed as Holographic Dark Energy (HDE), and has drawn a lot of attention, being widely studied. See [153] for a comprehensive review on the topic.

A general covariant local field theory of HDE was presented in [37], where it is shown that the low energy effective theory corresponds to a massive gravity, whose graviton has 3 polarisations, including 1 scalar and 2 tensor. The UV cut-off of the HDE stems from the strong coupling nature of the scalar mode above some certain energy scale that relates to the graviton's Compton wavelength. It provides a physical interpretation for the UV-IR correspondence of HDE.

Given the general covariant local field theory of HDE, it is thus possible to analyse its local dynamics. The structure formation in the framework of the effective field theory of HDE was studied in [154], and it has been found that the equation of motion for the matter density contrast $\delta_m \equiv \delta\rho_m/\rho_m$ of the Cold Dark Matter (CDM) is the same as the one in GR up to the leading order in the small scale limit $k \gg aH$, provided the equation of state is Quintessence-like.

Since HDE is present during the whole cosmic history, including the early Universe, it is expected that it alters the dynamics during inflation [155, 156, 3, 157, 158], which is the most accepted solution to the horizon and flatness problems in cosmology, encompassing models in great agreement with the observed scalar power spectrum and with the not yet detected primordial gravitational waves. It has been pointed out that the the cosmic coincidence problem can also be solved, provided a minimal number of e-folds during inflation [152]. The corrections of HDE to the primordial curvature perturbations were analysed in [159], leading to the conclusion that the scalar power spectrum is generically red-tilted. However, this analysis is incomplete as the local field theory of HDE was still missing at that time, and the analyses did not include the perturbations of HDE itself. In this chapter, with the general covariant and ghost free action obtained in [37] in hands, which takes into account also the contribution of perturbations of HDE, we compute the inflationary background and both scalar and tensor power spectra[1].

The chapter is organized as follows: the main ideas behind inflation are introduced in Section 4.1.1. In Section 4.2 we discuss the validity of the low energy effective field theory obtained in [37] during the inflationary phase. In Section 4.3 we obtain the background evolution of the inflaton and of the dark components numerically. In Section 4.4 we compute the cosmological perturbations on a FLRW background and present the quadratic actions for the scalar and tensor parts. In Section 4.5 we compute the scalar and tensor power spectra and discuss their compatibility with observational constraints. Finally, in Section 4.6 we summarize the results and discussions.

[1] In [160] the authors propose that HDE is the responsible for driving the inflationary phase, which differs from the approach developed here.

4.1.1 Introduction to Inflation

Although we have introduced some aspects related to inflation (namely the horizon and flatness problems) in Chapter 2, a brief introduction to the inflationary physics remains to be done. This is covered by the present section.

As we have seen in Chapter 2, the horizon and flatness problems can be addressed if the Universe suffered an exponential expansion in its beginning. This expansion is usually driven by a scalar field, which is called inflaton. Let us now understand the properties of such field and how it generates the quasi-de Sitter background that we are interested in. Consider the following action for the inflaton χ [2]:

$$S = \int d^4x\sqrt{-g}\left[-\frac{1}{2}g^{\mu\nu}\partial_\mu\chi\partial_\nu\chi - V(\chi)\right]. \tag{4.2}$$

The corresponding energy-momentum tensor leads to the following energy density and pressure

$$\rho = \frac{\dot{\chi}^2}{2} + V(\chi) \tag{4.3}$$

$$p = \frac{\dot{\chi}^2}{2} - V(\chi), \tag{4.4}$$

from where we see that, if the inflaton moves slowly along the potential and the potential energy dominates, we have $p < 0$. Therefore, for a slowly-rolling field, an exponential expansion of the scale factor can happen.

The Friedman equation is therefore given by

$$H^2 = \frac{1}{3}\left[\frac{\dot{\chi}^2}{2} + V(\chi)\right], \tag{4.5}$$

where we have used $M_p^2 = 1$.

From the action (4.2) we also get the equation of motion, which reads

$$\ddot{\chi} + 3H\dot{\chi} + V_\chi = 0, \tag{4.6}$$

where $V_\chi \equiv dV/d\chi$ and H is the Hubble parameter.

Since the inflaton moves slowly, we have an almost flat potential (with exactly flat corresponding to de Sitter space-time). In order to simplify the equation of motion of the scalar field and the Friedman equation, one can perform an expansion around de Sitter by means of the so-called slow-roll

[2] The inflaton is usually denoted in the literature by ϕ. However, due to a notation coincidence in the next sections, we use χ.

parameters

$$\epsilon \equiv -\frac{\dot{H}}{H^2} \simeq \frac{\dot{\chi}^2}{2H^2} \tag{4.7}$$

$$\eta \equiv -\frac{\ddot{\chi}}{H\dot{\chi}} \tag{4.8}$$

by requiring $\epsilon, |\eta| \ll 1$. Alternatively, one can also express the slow-roll conditions via the potential slow-roll parameters

$$\epsilon_V \equiv \frac{1}{2}\left(\frac{V_\chi}{V}\right)^2 \tag{4.9}$$

$$\eta_V \equiv \frac{V_{\chi\chi}}{V}, \tag{4.10}$$

with $\epsilon_V, |\eta_V| \ll 1$. They relate to ϵ and η via $\epsilon \simeq \epsilon_V$ and $\eta \simeq \eta_V - \epsilon_V$.

By considering this expansion, we obtain

$$H^2 \simeq \frac{1}{3}V(\chi) \simeq \text{constant} \tag{4.11}$$

$$\dot{\chi} \simeq -\frac{V_\chi}{3H}, \tag{4.12}$$

corresponding to a quasi-de Sitter space-time, where the scale factor behaves as

$$a(t) \simeq \exp Ht. \tag{4.13}$$

The duration of the inflationary phase can be quantified by means of the number of e-folds, which can be obtained via

$$N \equiv \ln\frac{a_{\text{end}}}{a} \tag{4.14}$$

$$= \int_t^{t_{\text{end}}} H dt = \int_\chi^{\chi_{\text{end}}} \frac{H}{\dot{\chi}} d\chi \simeq \int_{\chi_{\text{end}}}^{\chi} \frac{V}{V_\chi} d\chi, \tag{4.15}$$

where we have used (4.11).

4.2 Validity of the Effective Field Theory During the Inflationary Phase

In obtaining equation (4.1) via the holographic principle, one sets an UV cut-off Λ to the local quantum field theory [153] and a UV-IR correspondence takes place. In essence, one requires the energy within a Schwarzschild radius, i.e. $L^3\Lambda^4$, to be smaller than the mass of a corresponding black hole, i.e. LM_p^2, so that $\Lambda \lesssim \sqrt{M_p/L}$. As mentioned in Section 4.1, the IR cut-off is chosen to

be the future event horizon $R_h = aL$, so that $\Lambda \sim \sqrt{M_p/R_h}$. Since the later varies in time, the UV cut-off Λ is also time dependent.

The relevance of HDE to the cosmological scenario depends on whether $\Lambda > H$ is satisfied, where H is the Hubble parameter. Recalling that $\Omega_{\rm hde} \propto 1/(H^2 R_h^2)$, where $\Omega_{\rm hde}$ is the fractional density of the holographic term, one finds that this condition can be rewritten as

$$\Omega_{\rm hde} > \frac{H^2}{M_p^2}. \tag{4.16}$$

As we are going to show in Section 4.3, during inflation the holographic component constitutes a tiny amount of the total energy density, i.e. $\Omega_{\rm hde} \ll 1$. Recalling that it scales as a^{-2}, we see that for large field inflation, for which $H^2/M_p^2 \sim 10^{-12}$, the effective field theory breaks down some time around 10 to 12 e-folds after the beginning of inflation, which is the moment when the inflaton energy density dominates over the one of HDE. Although this time interval is quite limited, it is enough to cover the CMB scales. For small field inflation, the ratio H^2/M_p^2 is much smaller and, therefore, the effective theory has a much longer validity.

In what follows we assume that the inflationary phase continues even after the break down of the effective theory, since it does not necessarily mean a pathology, but rather that an UV completion is required.

4.3 Inflationary Background

We start with the covariant and ghost free action of the HDE model, as obtained in [37], and the action of the matter sector corresponding to the inflaton χ:

$$\begin{aligned} S &= \int d^4x\sqrt{-g}\Bigg\{\frac{\mathcal{R}}{2} - \varphi^{-2}\left[(c+\lambda)Z + \lambda\partial^\mu\varphi\partial_\mu\varphi + \frac{3d}{8Z}\bar{\delta}Z^{ab}\bar{\delta}Z^{cd}\delta_{ac}\delta_{bd}\right] + \\ &- \frac{1}{2}\partial_\mu\chi\partial^\mu\chi - V(\chi)\Bigg\}. \end{aligned} \tag{4.17}$$

Here g is the determinant of the metric, $M_p^2 \equiv 8\pi G = 1$, $\mathcal{R}$ is the 4 dimensional Ricci scalar, $V(\chi)$ is the inflaton potential and c and d are constants. The extra field φ is a time-like Stueckelberg field, which arises to recover general covariance, together with other three space-like Stueckelberg fields ϕ^a, where a, b are indices in the field space described by the metric δ_{ab}. Z^{ab} is another

building block of the theory, given by

$$Z^{ab} \equiv \partial_\mu \phi^a \partial^\mu \phi^b - \frac{(\partial_\mu \varphi \partial^\mu \phi^a)(\partial_\nu \varphi \partial^\nu \phi^b)}{\partial_\mu \varphi \partial^\mu \varphi}. \tag{4.18}$$

As discussed in [37], when the four Stueckelberg scalar fields assume their Vacuum Expectation Values (VEVs), $\langle \varphi \rangle$ and $\langle \phi^a \rangle$, they break the diffeomorphism invariance. This introduces a massless boson for each broken symmetry, according to the Goldstone theorem. We then have $\varphi = \langle \varphi \rangle + \pi^0$ and $\phi^a = \langle \phi^a \rangle + \pi^a/\sqrt{3}$, where π^0 and π^a are the time-like and space-like Goldstone bosons, respectively. These Goldstone excitations satisfy the symmetry

$$\pi^i(t, \mathbf{x}) \to \pi^i(t, \mathbf{x}) + \xi^i(t), \tag{4.19}$$

which eliminates the dynamics of the 3 would-be ghosty bosons π^i. In the unitary gauge, the bosons are muted, and the graviton becomes massive. With this gauge choice, eq. (4.18) is rewritten as $Z^{ab} = h^{ij}\delta^a_i \delta^b_j/3$, where h^{ij} is the induced metric of the spatial hypersurfaces in the ADM decomposition and δ^a_i is a pullback mapping between the space-time and the field space. The quantities Z and $\bar{\delta} Z^{ab}$ are defined, respectively, as $Z \equiv Z^{ab}\delta_{ab}$ and $\bar{\delta} Z^{ab} \equiv Z^{ab} - 3Z^{ac}Z^{db}\delta_{cd}/(Z^{cd}\delta_{cd})$.

In a Friedmann-Lemaître-Robertson-Walker background $ds^2 = -dt^2 + a^2 d\mathbf{x}^2$, the equations of motion read

$$3H^2 = \frac{c}{a^2\varphi^2} + \frac{\lambda}{2a^4} + \frac{1}{2}\dot{\chi}^2 + V(\chi), \tag{4.20}$$

$$-\dot{H} = \frac{c}{3a^2\varphi^2} + \frac{\lambda}{3a^4} + \frac{1}{2}\dot{\chi}^2 \tag{4.21}$$

and

$$\dot{\varphi} = -\frac{1}{a}, \qquad \dot{\lambda} = -\frac{4ca}{\varphi^3}, \tag{4.22}$$

where overdot denotes derivative with respect to cosmic time t and the Lagrangian multiplier was re-scaled as $\lambda \to \lambda \frac{\varphi^2}{4a^2}$ for simplicity. Note that the energy density of the dark sector includes two components,

$$\rho_{dark} = \frac{c}{a^2 L^2} + \frac{\lambda}{2a^4}, \tag{4.23}$$

where the first term is the holographic term, and the second term is the dark radiation term which scales as radiation at late times, when λ is approximately constant. For this reason, from now on we refer to the above contributions as the holographic term $\rho_{\rm hde}$ and the dark radiation term $\rho_{\rm rad}$ respectively.

In order to obtain the background evolution numerically, we define the following dimensionless quantities, in analogy to [161]:

$$\tilde{\varphi} \equiv H_i \varphi, \qquad \tilde{\lambda} \equiv \frac{\lambda}{H_i^2}, \qquad E(z) \equiv \frac{H}{H_i}, \tag{4.24}$$

where H_i is the Hubble parameter at the beginning of the inflationary epoch. In terms of the above quantities, the Friedmann equation reads

$$E^2 = \frac{3H^2}{3H_i^2} = \frac{\rho_\chi + ca^{-2}\varphi^{-2} + \lambda(2a^4)^{-1}}{3H_i^2} = \tilde{\rho}_\chi + \frac{1}{3}\left(\frac{c}{a^2\tilde{\varphi}^2} + \frac{\tilde{\lambda}}{2a^4}\right), \tag{4.25}$$

where ρ_χ is the energy density of the inflaton, $\tilde{\rho}_\chi \equiv \rho_\chi/\rho_c(t_i)$, and $\rho_c(t_i) \equiv 3H_i^2$ is the critical density at the beginning of inflation.

In the redshift space, equations (4.22) are rewritten as

$$\frac{d\tilde{\varphi}}{dz} = \frac{1}{E(z)}, \qquad \frac{d\tilde{\lambda}}{dz} = \frac{4c}{(1+z)^2 E(z)\tilde{\varphi}^3}, \tag{4.26}$$

while the equation of motion for $\tilde{\rho}_\chi$ is given by

$$\frac{d\tilde{\rho}_\chi}{dz} = 6(1+z)^{-1}(\tilde{\rho}_\chi - \tilde{V}), \tag{4.27}$$

where $\tilde{V} \equiv V/\rho_c(t_i)$. For the latter the equation of motion reads

$$\frac{d\tilde{V}}{dz} = \frac{2\tilde{m}\sqrt{\tilde{V}(\tilde{\rho}_\chi - \tilde{V})}}{(1+z)E(z)}, \tag{4.28}$$

where $\tilde{m} \equiv m/H_i$ and we have assumed the simplest chaotic inflation with $V = \frac{1}{2}m^2\chi^2$.

Numerically solving equations (4.25), (4.26), (4.27) and (4.28) we obtain Figure 4.1 and Figure 4.2, where we parametrized the scale factor as $a_i = 1$ at the beginning of inflation. As initial conditions, we used the initial values of the time-like Stueckelberg field $\tilde{\varphi}_i \equiv \tilde{\varphi}(0)$, the inflaton energy density $\tilde{\rho}_{\chi i} \equiv \tilde{\rho}_\chi(0)$, the inflaton potential $\tilde{V}_i \equiv \tilde{V}(0)$ and the Lagrange multiplier $\tilde{\lambda}_i \equiv \tilde{\lambda}(0)$ such that $E(z=0) = 1$. The values of the constant c were chosen according to the observational constraint obtained in [161], given by

$$1.41 < c < 3.09 \tag{4.29}$$

with 95.4% CL. Note that the initial conditions determine the future event horizon L, and not the other way around. The constraint equation that allows us to obtain L is given by $\dot{L} = -N/a$. We could, in principle, integrate it from $-\infty$ to nowadays

$$L = \int_{-\infty}^{t} \frac{-N dt'}{a(t')} + L(-\infty), \tag{4.30}$$

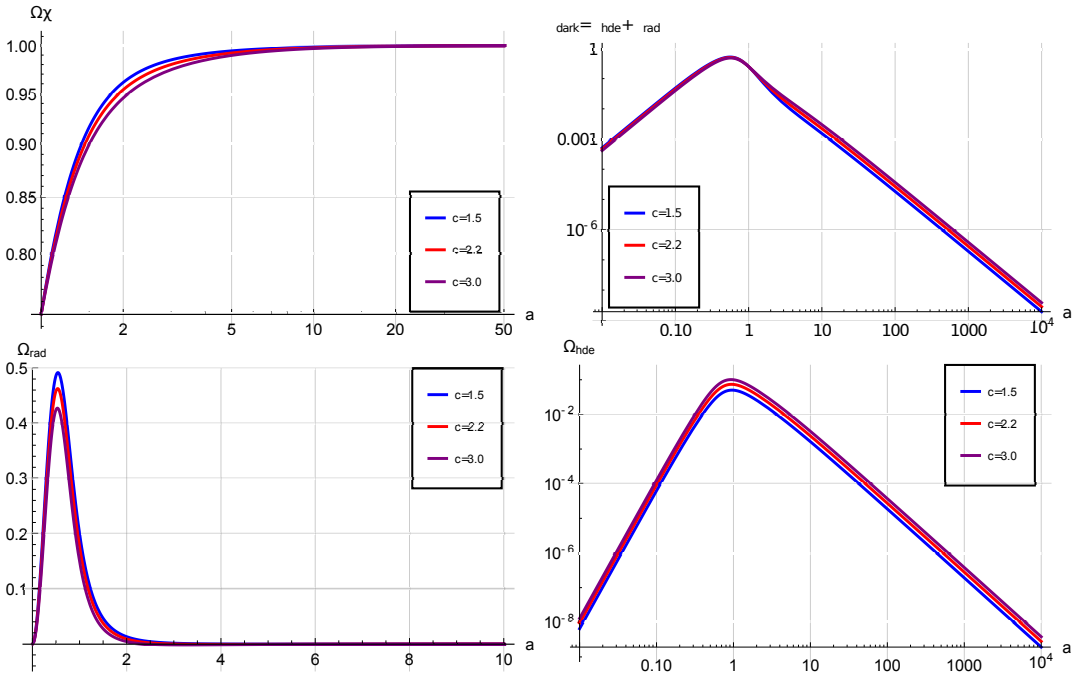

FIGURE 4.1: Evolution of the fractional energy densities of the inflaton Ω_χ, the dark radiation $\Omega_{\rm rad}$, the holographic component $\Omega_{\rm hde}$ and their sum $\Omega_{\rm dark}$. The inflaton eventually dominates over the dark components after the beginning of inflation ($a_i = 1$ in our convention). In these plots, $\tilde{m} = 0.1$, $\tilde{\varphi}_i = \frac{1}{\sqrt{0.1}}$, $\tilde{\rho}_i = 0.75$ and $\tilde{V} = 0.7$.

where $L(-\infty)$ is the initial condition in the infinite past. However, this initial condition is not known and, in practice, we perform the integration from the other side:

$$L = \int_t^\infty \frac{N dt'}{a(t')} + L(\infty). \tag{4.31}$$

Equations (4.30) and (4.31) are equivalent, if both boundary conditions are known. In our case, $L(-\infty)$ remains unkonwn due to our ignorance about the quantum gravity. On the other hand, we do know the asymptotic value of $L(\infty) = 0$, as it is model independent [162].

From the numerical results we conclude that the inflaton eventually dominates over the dark radiation and holographic components, regardless of the hierarchy between them. In other words, at the background level the inflationary phase is not spoiled by the presence of the dark sector, making the HDE compatible with inflation. We can also see, from Figure 4.2, that $\Omega_{\rm rad}$ may become negative during the inflationary phase, but the density of the total dark sector $\Omega_{\rm dark} = \Omega_{\rm hde} + \Omega_{\rm rad}$ is nonetheless positive. The equation of state parameter of the inflaton, as expected, achieves $\omega_\chi = -1$ in the inflationary epoch, as shown in Figure 4.3.

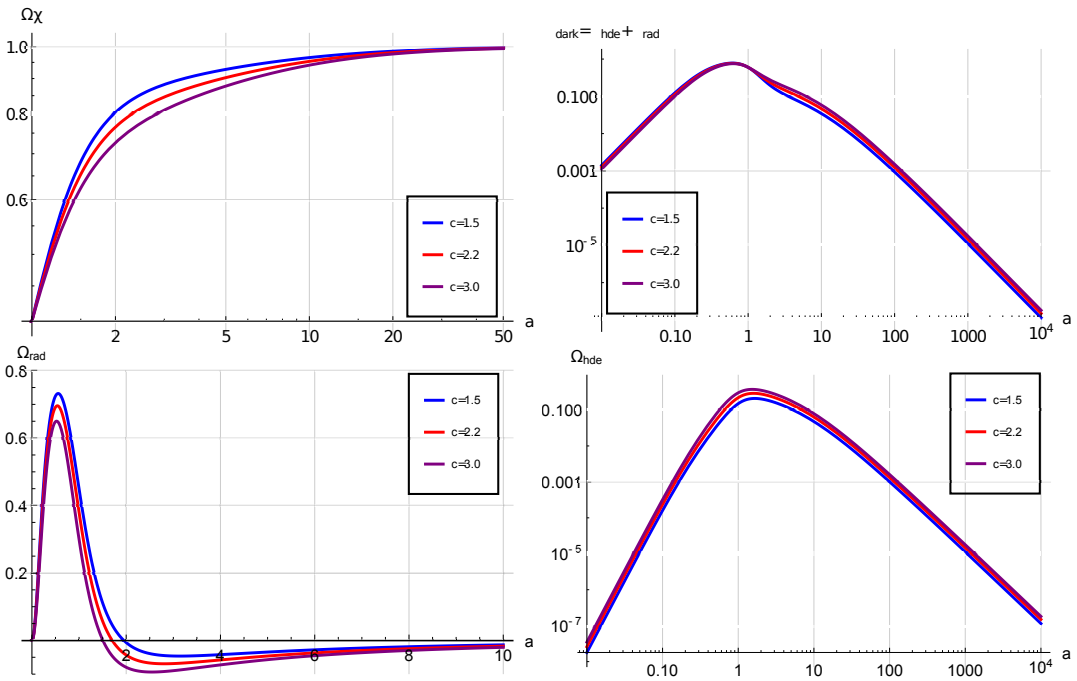

FIGURE 4.2: Evolution of the fractional energy densities of the inflaton Ω_χ, the dark radiation $\Omega_{\rm rad}$, the holographic component $\Omega_{\rm hde}$ and their sum $\Omega_{\rm dark}$ with $\tilde{m} = 0.1$, $\tilde{\varphi}_i = \frac{1}{\sqrt{0.3}}$, $\tilde{\rho}_i = 0.4$ and $\tilde{V} = 0.36$.

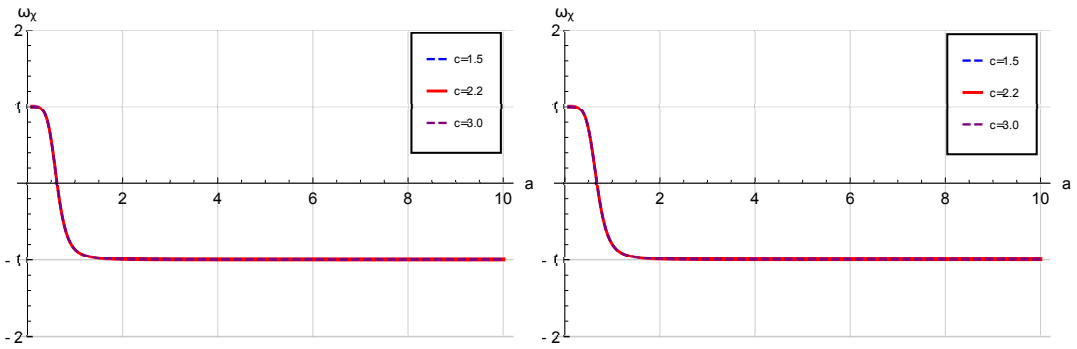

FIGURE 4.3: Equation of state parameter of the inflaton χ for $\tilde{m} = 0.1$, $\tilde{\varphi}_i = \frac{1}{\sqrt{0.1}}$, $\tilde{\rho}_i = 0.75$ and $\tilde{V} = 0.7$ (left) and $\tilde{m} = 0.1$, $\tilde{\varphi}_i = \frac{1}{\sqrt{0.3}}$, $\tilde{\rho}_i = 0.4$ and $\tilde{V} = 0.36$ (right). As expected, $\omega_\chi = -1$ in the inflationary phase.

4.4 Cosmological Perturbations

In this section, the general covariant and ghost free action (4.17) is used to compute the cosmological perturbations in the unitary gauge around a Friedmann-Lemaître-Robertson-Walker background. We use the following metric decomposition

$$\begin{aligned} g_{00} &= -a(t)^2(1+2\alpha), \\ g_{0i} &= a(t)^2(\partial_i\beta + S_i), \\ g_{ij} &= a(t)^2\left[\delta_{ij} + 2\psi\delta_{ij} + \partial_i\partial_j E + \frac{1}{2}(\partial_i F_j + \partial_j F_i) + \gamma_{ij}\right], \end{aligned} \tag{4.32}$$

where the scalar perturbations are represented by the variables α, β, ψ and E, the tensor perturbation is represented by γ_{ij} and the vector perturbations are represented by S_i and F_i. The latter obey $\partial_i S_i = 0$ and $\partial_i F_i = 0$, while γ_{ij} obeys $\gamma_{ii} = \partial_i\gamma_{ij} = 0$, being traceless and transverse. As mentioned in Section 4.3, in the unitary gauge we keep all the perturbation variables, while the Goldstone bosons are muted and the graviton acquires a mass.

4.4.1 Scalar Perturbations

For the scalar perturbations, the quadratic action reads

$$S^{(2)}_{\text{scalar}} = \int d^4x \ \left(\mathcal{L}_{\text{EH}} + \mathcal{L}_{\text{mass}} + \mathcal{L}_\chi\right), \tag{4.33}$$

where $\mathcal{L}_{\text{EH}}$ is the Einstein-Hilbert lagrangian density, $\mathcal{L}_{\text{mass}}$ is the lagrangian density related to the graviton mass and $\mathcal{L}_\chi$ is the lagrangian density for the inflaton χ. They read, respectively,

$$\begin{aligned} \frac{\mathcal{L}_{\text{EH}}}{a^3} &= -3\dot{\psi}^2 + \frac{k^2}{a^2}\left[\psi^2 - \frac{1}{2}a^2\dot{E}(H\psi - 2\dot{\psi}) - \frac{1}{2}a^2HE(\dot{\psi} + 3H\psi)\right] \\ &+ \alpha\left[\frac{2k^2\beta H}{a} + \frac{k^2}{a^2}(2\psi - a^2H\dot{E}) + 6H\dot{\psi} - 3H^2\alpha\right] - \frac{2k^2\beta\dot{\psi}}{a}, \end{aligned} \tag{4.34}$$

$$\begin{aligned} \mathcal{L}_{\text{mass}} &= \varphi^{-2}\left[-\frac{3c+d}{36}k^4aE^2 - \frac{1}{6}ck^2aE(2\alpha+\psi) + ca\psi(2\alpha+\psi)\right] \\ &+ \lambda\left[-\frac{k^4E^2}{48a} + \frac{k^2E(\psi-\alpha)}{12a} + \frac{(\alpha+\psi)^2}{4a}\right] + \\ &+ \delta\lambda\left(\frac{\psi-\alpha}{2a} - \frac{k^2E}{12a}\right) \end{aligned} \tag{4.35}$$

and

$$\begin{aligned}\frac{\mathcal{L}_\chi}{a^3} &= \frac{1}{2}\dot{\delta\chi}^2 - \frac{1}{2}\dot{\chi}\dot{\delta\chi}(k^2E + 2\alpha - 6\psi) + \frac{1}{4}\dot{\chi}^2(2\alpha^2 + k^2E\psi) \\ &+ \delta\chi\left[-\frac{k^2\beta\dot{\chi}}{a} - \frac{1}{2}V_{,\chi}(-k^2E + 2\alpha + 6\psi)\right] + \\ &+ \delta\chi^2\left(-\frac{k^2}{2a^2} - \frac{V_{,\chi\chi}}{2}\right), \end{aligned} \tag{4.36}$$

where the Lagrangian multiplier λ was again re-scaled to $\lambda\frac{\varphi^2}{4a^2}$, overdot denotes derivative with respect to cosmic time and the sub-index $_{,\chi}$ denotes derivative with respect to the inflaton χ.

The constraints can be obtained by varying the action with respect to the non-dynamical variables of the theory, namely α, $\delta\lambda$ and β. We then have the following set of equations:

$$\begin{aligned} H(6\dot{\psi} - k^2\dot{E}) + \frac{2c\psi}{a^2\varphi^2} + \frac{k^2}{a^2}\left(2\psi - \frac{cE}{3\varphi^2}\right) + \frac{\lambda}{12a^4}(6\psi - k^2E) & \\ -\frac{\delta\lambda}{2a^4} + \alpha\left(\frac{\lambda}{2a^4} - 6H^2 + \dot{\chi}^2\right) + \frac{2k^2H\beta}{a} - \dot{\chi}\dot{\delta\chi} - \delta\chi V_{,\chi} &= 0, \quad (4.37) \\ k^2E + 6\alpha - 6\psi &= 0, \quad (4.38) \\ -\frac{\dot{\chi}\delta\chi}{2} + H\alpha - \dot{\psi} &= 0. \quad (4.39) \end{aligned}$$

Solving them simultaneously and substituting the solution back in the action, we find an expression of the form

$$S^{(2)}_{\text{scalar}} = \int d^4x\left[\frac{a^3}{2}\dot{\delta\chi}^2 + \frac{a^3\varphi^2\dot{\chi}^2 - 2(c+d)a}{2H^2\varphi^2}\dot{\psi}^2 - \frac{a^3\dot{\chi}}{H}\dot{\psi}\dot{\delta\chi} + ...\right], \tag{4.40}$$

where the ellipsis stand for potential, gradient and (non-kinetic) interaction terms. The diagonalization of the kinetic terms is performed by redefining the $\delta\chi$ variable as follows

$$\delta\chi \to \delta\chi - \frac{C}{2A}\psi, \tag{4.41}$$

where A and C are, respectively, the coefficients of $\dot{\delta\chi}^2$ and $\dot{\psi}\dot{\delta\chi}$. The quadratic diagonalized action then reads

$$S^{(2)}_{\text{scalar}} = \int d^4x\left[-\frac{(c+d)a}{H^2\varphi^2}\dot{\psi}^2 + \frac{a^3}{2}\dot{\delta\chi}^2 + ...\right], \tag{4.42}$$

which requires $c + d < 0$ to avoid ghost instabilities. Defining the constant $b \equiv -2(c+d)$ for convenience and the canonical variables $\delta\chi_c$ and ψ_c as

$$\delta\chi_c \equiv a\delta\chi, \qquad \psi_c \equiv \frac{\sqrt{b}}{H\varphi}\psi, \tag{4.43}$$

we rewrite the action as

$$\begin{aligned} S^{(2)}_{\rm scalar} &= \int dtd^3k\frac{1}{2}\Bigg[a\dot{\psi_c}^2 + a\delta\dot{\chi_c}^2 + \left(-\frac{k^2c_s^2}{a^2} - aM_s^2\right)\psi_c^2 + \\ &+ \left(-\frac{k^2}{a^2} - aM_\chi^2\right)\delta\chi_c^2 + I_1\delta\chi_c\psi_c + I_2\delta\dot{\chi}_c\psi_c\Bigg], \end{aligned} \tag{4.44}$$

where the sound speed of the scalar graviton is given by

$$c_s^2 = \frac{2c}{3b}\left(1 + \frac{2\rho_{\rm rad}}{\rho_{\rm hde}}\right), \tag{4.45}$$

with $\rho_{\rm rad} = \lambda/(2a^4)$ and $\rho_{\rm hde} = c/(a^2\varphi^2)$. The latter is plotted in Figure 4.4, where we can see that it is positive definite during the inflationary phase. The mass of the scalar mode reads

$$\begin{aligned} M_s^2 &= 2H^2\Bigg[\frac{6c}{b} + \frac{2c-b}{bHR_h} - \frac{-6c^2+6b+cb}{6bH^2R_h^2} - \frac{c^2}{9H^4R_h^4} + \\ &+ \Omega_{\rm rad}\left(1 + \frac{8c}{b} - \frac{2}{HR_h} - \frac{4c}{3H^2R_h^2}\right) + \Omega_{\rm rad}^2\left(\frac{4c}{b\Omega_{\rm hde}} - 4\right)\Bigg] + \\ &+ \dot{\chi}^2\Bigg[\frac{1}{6} - \frac{6H^2R_h^2\Omega_{\rm hde}}{b}\left(1 + \frac{2\Omega_{\rm rad}}{3}\right) - \frac{\Omega_{\rm hde}}{2}\left(1 + \frac{2\Omega_{\rm rad}}{\Omega_{\rm hde}}\right) + \\ &- \frac{R_h^2H^2\Omega_{\rm hde}^2}{b}\left(1 + \frac{4\Omega_{\rm rad}^2}{\Omega_{\rm hde}^2}\right)\Bigg] - \frac{2V}{3}, \end{aligned} \tag{4.46}$$

while for the inflaton term we have

$$\begin{aligned} M_\chi^2 &= 2H^2\left(-1 + \Omega_{\rm rad} + \frac{\Omega_{\rm hde}}{2}\right) + \frac{2V_{,\chi}\dot{\chi}}{H} + \frac{7\dot{\chi}^2}{2} + \\ &- \frac{\Omega_{\rm hde}\dot{\chi}^2}{2}\left(1 + \frac{3b}{2c}\right) - \Omega_{\rm rad}\dot{\chi}^2 - \frac{\dot{\chi}^4}{2H^2} + V_{,\chi\chi}, \end{aligned} \tag{4.47}$$

with $R_h \equiv a\varphi$, $\Omega_{\rm rad} = \rho_{\rm rad}/(3H^2)$ and $\Omega_{\rm hde} = \rho_{\rm hde}/(3H^2)$. For the coefficients of the interaction terms we find

$$\begin{aligned} I_1 &= \Big\{-4\left[3ba^3H\varphi - (3b+8c)a^4H^2\varphi^2 + b\lambda\varphi^2 + a^2(bc - 2H^2\lambda\varphi^4)\right]\dot{\chi} + \\ &- a^2\varphi^2\left[(3b+2c)a^2 + 2\lambda\varphi^2\right]\dot{\chi}^3 + 2a^2H\varphi^2\left[(3b+2c)a^2 + 2\lambda\varphi^2\right]V_{,\chi}\Big\} \times \\ &\times \left\{6a^4H^2\varphi^3\sqrt{b}\right\}^{-1} \end{aligned} \tag{4.48}$$

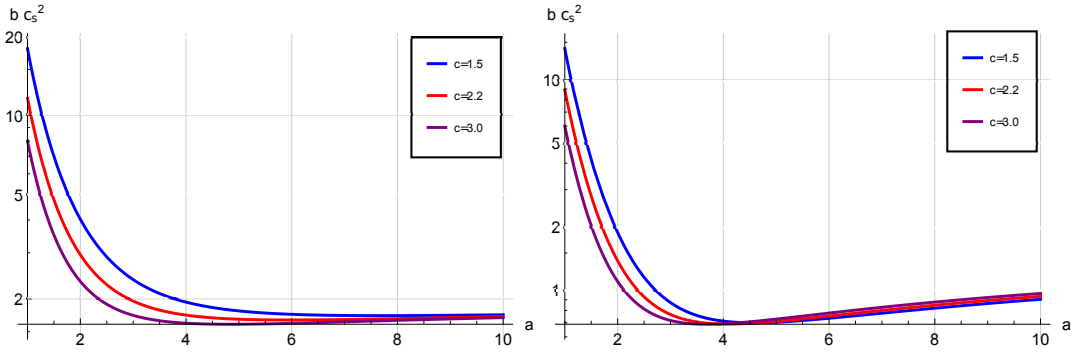

FIGURE 4.4: Sound speed of the scalar graviton ψ for $\tilde{m} = 0.1$, $\tilde{\varphi}_i = \frac{1}{\sqrt{0.1}}$, $\tilde{\rho}_i = 0.75$ and $\tilde{V} = 0.7$ (left) and $\tilde{m} = 0.1$, $\tilde{\varphi}_i = \frac{1}{\sqrt{0.3}}$, $\tilde{\rho}_i = 0.4$ and $\tilde{V} = 0.36$ (right).

and

$$I_2 = \frac{\left[(2c-3b)a^2 + 2\lambda\varphi^2\right]\dot{\chi}}{3a^2 H\varphi\sqrt{b}}. \tag{4.49}$$

From the background evolution we know that the inflaton density dominates over the dark sector, namely $\Omega_{\rm rad}$ and $\Omega_{\rm hde}$. Therefore, in order to simplify the quadratic action, we rewrite the Lagrangian multiplier λ and the time-like Stueckelberg field φ in terms of the fractional densities and expand up to zero order in $\Omega_{\rm rad}$ and $\Omega_{\rm hde}$. We then end up with the following action:

$$\begin{aligned} S^{(2)}_{\rm scalar} &= \int dt d^3k \Bigg\{ \frac{1}{2} a \delta\dot{\chi_c}^2 + \frac{1}{2} a \dot{\psi_c}^2 + \\ &- \left[\frac{ck^2}{3ba}\left(1 + \frac{2\Omega_{\rm rad}}{\Omega_{\rm hde}}\right) + \frac{H^2 a(6c-b)}{b} + \frac{a\dot{\chi}^2(b-4c)}{4b} \right] \psi_c^2 + \\ &+ \left[-\frac{k^2}{2a} + \frac{a}{4}\left(4H^2 - \frac{4V_{,\chi}\dot{\chi}}{H} - 7\dot{\chi}^2 + \frac{\dot{\chi}^4}{H^2} - 2V_{,\chi\chi} \right) \right] \delta\chi_c^2 \Bigg\} \end{aligned} \tag{4.50}$$

where the graviton ψ_c, which corresponds to the scalar degree of the HDE, and the inflaton perturbation $\delta\chi_c$ decouple. With the above expression we compute the scalar power spectrum in Section 4.5.1.

4.4.2 Tensor Perturbations

The quadratic action for the tensor perturbation, obtained from (4.17), is given by

$$S^{(2)}_{\rm tensor} = \frac{1}{8}\int d\tau d^3k a^2 \left[\gamma'^{ij}\gamma'_{ij} - (k^2 + M^2_{GW}a^2)\gamma_{ij}\gamma^{ij} \right], \tag{4.51}$$

where τ is the conformal time, prime denotes derivative with respect to τ and the mass of the tensor mode reads

$$M_{\rm GW}^2 = \frac{6c - b + 12H^2R_h^2\Omega_{\rm rad}}{6R_h^2}. \tag{4.52}$$

We then define the normalized Mukhanov variable as $v_k \equiv a\gamma_k/2$and rewrite the action in the form

$$S^{(2)}_{\rm tensor} = \int d\tau d^3k \frac{1}{2}\left[{v_k}'^2 + v_k^2\left(-k^2 - \frac{\lambda}{3a^2} + \frac{b-6c}{6\varphi^2} + \frac{a''}{a}\right)\right], \tag{4.53}$$

which allows us to compute the power spectrum in Section 4.5.2.

4.5 Power Spectra

4.5.1 Scalar Power Spectrum

As we have seen in Section 4.4.1, the graviton ψ_c and the inflaton perturbation $\delta\chi_c$ decouple when one considers an expansion of the action for low values of $\Omega_{\rm rad}$ and $\Omega_{\rm hde}$, which is corroborated by the results for background evolution. In this case, we are able to compute the power spectrum for ψ and $\delta\chi$ separately.

Power Spectrum of the Inflaton Perturbation

Let us start by computing the power spectrum related to $\delta\chi_c$. From the decoupled quadratic action (4.50) we have the action corresponding to the inflaton perturbation, which reads

$$S^{(2)}_{\delta\chi_c} = \int d\tau d^3k \left[\frac{{\delta\chi_c}'^2}{2} - \frac{k^2}{2}\delta\chi_c^2 + F(\tau)\delta\chi_c^2\right] \tag{4.54}$$

in terms of the conformal time τ, where $F(\tau)$ is given by

$$F(\tau) = \frac{1}{4}\left[-\frac{4aV_{,\chi}\chi'}{H} - 7\chi'^2 + \frac{\chi'^4}{a^2H^2} + a^2\left(4H^2 - 2V_{,\chi\chi}\right)\right]. \tag{4.55}$$

The corresponding equation of motion reads

$$\delta\chi_{ck}'' + \left[k^2 - 2F(\tau)\right]\delta\chi_{ck} = 0, \tag{4.56}$$

which is simplified to

$$\delta\chi_c'' + \left[k^2 - 2a^2H^2\left(1+\epsilon-\frac{3}{2}\eta\right)\right]\delta\chi_c = 0 \tag{4.57}$$

up to first order in slow-roll approximation, where ϵ and η are the slow-roll parameters and we have used $V \simeq 3H^2$.

Defining $x \equiv k/(aH)$ we obtain

$$x^2(1-2\epsilon)\frac{d^2\delta\chi_c}{dx^2} + \left[x^2 - 2\left(1+\epsilon-\frac{3}{2}\eta\right)\right]\delta\chi_c = 0, \tag{4.58}$$

which leads to the following leading order solution:

$$\delta\chi_c = -\frac{1}{2}\sqrt{\frac{\pi x}{k}}\left[J_\nu(x) + iY_\nu(x)\right], \tag{4.59}$$

where J_ν and Y_ν are Bessel functions of the first and second kind, respectively, and

$$\nu \simeq \frac{3}{2} + 2\epsilon - \eta \tag{4.60}$$

up to first order in slow-roll approximation. The initial conditions were fixed in order to obtain the commutation relation between the annihilation and creation operators and the Bunch-Davis vacuum in the infinite past.

Considering the solution (4.59), we obtain the corresponding solution to $\delta\chi_k$ via equation (4.43), which, in terms of x and the Hankel function of the first kind $H_\nu^{(1)}$, reads

$$\delta\chi_k = -\frac{1}{2a}\sqrt{\frac{\pi x}{k}}H_\nu^{(1)}(x). \tag{4.61}$$

In the superhorizon regime, i.e. $x \ll 1$, the two-point correlation function of $\delta\chi$ is given by

$$\langle\delta\chi_k(\tau)\delta\chi_{k'}(\tau)\rangle = (2\pi)^3\delta(\vec{k}+\vec{k'})\frac{4^{-1+\nu}x^{1-2\nu}\Gamma(\nu)^2}{k\pi a^2} \tag{4.62}$$

where Γ represents the gamma function. Therefore the dimensionless power spectrum reads

$$\Delta^2_{\delta\chi} = \left.\frac{2^{-3+2\nu}x^{3-2\nu}\Gamma(\nu)^2H^2}{\pi^3}\right|_{k=aH}, \tag{4.63}$$

where $k = aH$ indicates that it must be evaluated at horizon crossing. Therefore, the scalar spectral index is obtained as

$$n_s - 1 = 3 - 2\nu = 4\epsilon - 2\eta, \tag{4.64}$$

which corresponds to the standard single field result.

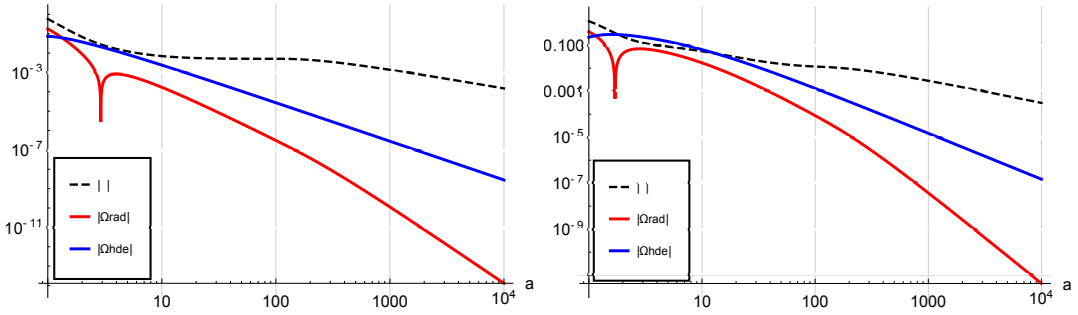

FIGURE 4.5: Comparison between the dark densities $\Omega_{\rm rad}$ and $\Omega_{\rm hde}$ and the slow-roll parameter ϵ. Here $c = 2.2$, $\tilde{m} = 0.1$, $\tilde{\varphi}_i = \frac{1}{\sqrt{0.1}}$, $\tilde{\rho}_i = 0.75$ and $\tilde{V} = 0.7$ (left) and $c = 2.2$, $\tilde{m} = 0.1$, $\tilde{\varphi}_i = \frac{1}{\sqrt{0.3}}$, $\tilde{\rho}_i = 0.4$ and $\tilde{V} = 0.36$ (right).

The next-to-leading order contribution to the equation of motion is of order $\sqrt{\Omega_i}$, $i = \text{hde}, \text{rad}$, and can be considered as a source term. In the slow-roll regime we find

$$\begin{aligned} \delta\chi_c'' + (k^2 - 2a^2H^2)\delta\chi_c &= \psi_c \frac{a^2H^2\sqrt{\epsilon}}{\sqrt{6cb\Omega_{hde}}}\left[(10c - 3b)\Omega_{hde} + 4c\Omega_{rad}\right] + \\ &+ \psi_c' \frac{aH\sqrt{\epsilon}}{\sqrt{6cb\Omega_{hde}}}\left[(3b - 2c)\Omega_{hde} - 4c\Omega_{rad}\right]. \quad (4.65) \end{aligned}$$

Therefore in the equation of motion this contribution is not only suppressed by the square root of the fractional densities related to the HDE, but also by $\sqrt{\epsilon}$. For the power spectrum this means a correction of order $\Omega_i\epsilon$, which is even smaller than the slow-roll correction of order ϵ^2, as one can see in Figure 4.5.

Power Spectrum of the Graviton

Now let us compute the power spectrum related to the graviton ψ. From the quadratic action (4.50) we have the following action for ψ_c in terms of the conformal time τ:

$$S^{(2)}_{\psi_c} = \int d\tau d^3k \left[\frac{{\psi_c}'^2}{2} - \frac{k^2c_s^2}{2}\psi_c^2 + G(\tau)\psi_c^2\right], \quad (4.66)$$

where prime denotes derivative with respect to τ and

$$G(\tau) = \frac{4(b - 6c)a^2H^2 - (b - 4c)\chi'^2}{4b} \quad (4.67)$$

The corresponding equation of motion is given by

$$\psi_{ck}'' + \left[k^2 c_s^2 - 2G(\tau)\right]\psi_{ck} = 0, \tag{4.68}$$

which, when considering slow-roll approximation up to first order, reduces to

$$\psi_{ck}'' + \left[k^2 c_s^2 - 2a^2H^2 + \frac{12ca^2H^2 + \epsilon(b-4c)a^2H^2}{b}\right]\psi_{ck} = 0. \tag{4.69}$$

Defining $x \equiv c_s k/(aH)$ and $s \equiv \dot{c}_s/(Hc_s)$ we rewrite the equation of motion as

$$x^2(1-2\epsilon)\frac{d^2\psi_{ck}}{dx^2} - sx\frac{d\psi_{ck}}{dx} + \left[-2 + x^2 - \frac{4c(-3+\epsilon)}{b} + \epsilon\right]\psi_{ck} = 0, \tag{4.70}$$

which leads to the following solution:

$$\psi_{ck} = -\frac{1}{2}\sqrt{\frac{\pi}{2}}\left[\frac{x(2-4\epsilon)}{c_s k}\right]^{\frac{1+s-2\epsilon}{2-4\epsilon}}\left[J_\nu(x) + iY_\nu(x)\right], \tag{4.71}$$

where

$$\nu = -\frac{\sqrt{-16c(3-7\epsilon) + b(9+2s-24\epsilon)}}{2\sqrt{b}(-1+2\epsilon)}. \tag{4.72}$$

If ν is imaginary, the power spectrum is highly suppressed, since in this case the solution is in terms of hyperbolic trigonometric functions that decay instead of oscillating. Therefore, from now on we assume that ν is real.

Recalling the definition of the canonical variable given by (4.43), we have the expression for the graviton ψ, with which we calculate the power spectrum. In terms of the Hankel function of the first kind $H_\nu^{(1)}$ and the variable $x \equiv -c_s k\tau$, the solution reads

$$\psi_k = -\frac{H\varphi}{2}\sqrt{\frac{\pi x}{c_s k b}}H_\nu^{(1)}(x), \tag{4.73}$$

where we have neglected the parameters ϵ and s in the exponent.

The two-point correlation function of the variable ψ in the superhorizon regime, i.e. $x \ll 1$, is given by

$$\langle\psi_k(\tau)\psi_{k'}(\tau)\rangle = (2\pi)^3\delta(\vec{k}+\vec{k}')\frac{4^{-1+\nu}x^{1-2\nu}\Gamma(\nu)^2H^2\varphi^2}{bc_s k\pi}, \tag{4.74}$$

which corresponds to the power spectrum

$$\Delta_\psi^2 = \left.\frac{2^{-3+2\nu}x^{3-2\nu}\Gamma(\nu)^2a^2H^4\varphi^2}{b\pi^3c_s^3}\right|_{c_S k = aH}, \tag{4.75}$$

to be evaluated at horizon crossing.

Comoving Curvature Power Spectrum

In order to obtain the comoving curvature perturbation, which is given by

$$R = -\psi - \frac{H}{\rho + p}\delta q, \tag{4.76}$$

we compute δq via $\partial_i \delta q \equiv \delta T^0_i$, where $T_{\mu\nu}$ is the energy-momentum tensor. Perturbing the latter, which encompasses the inflaton and the holographic and radiation terms, we find[3]

$$\delta q = -\dot{\chi}\delta\chi, \tag{4.77}$$

while the total density and pressure read respectively

$$\rho = \frac{1}{2}\dot{\chi}^2 + V + \frac{c}{a^2\varphi^2} + \frac{\lambda}{2a^4}, \tag{4.78}$$

$$p = \frac{1}{2}\dot{\chi}^2 - V - \frac{c}{3a^2\varphi^2} + \frac{\lambda}{6a^4}. \tag{4.79}$$

Therefore, the curvature perturbation is given by

$$R = \frac{\dot{\chi}}{2\epsilon a H}\delta\chi_c - \sqrt{\frac{c}{3b\Omega_{\rm hde}}}\frac{\Omega_{\rm hde} + 2\Omega_{\rm rad}}{\epsilon a}\psi_c, \tag{4.80}$$

where we have used both the re-scaling (4.41) and the canonical transformation (4.43).

As a result, the power spectrum reads

$$\begin{aligned}\Delta^2_R &= \frac{\dot{\chi}^2}{4\epsilon^2 a^2 H^2}\Delta^2_{\delta\chi_c} + \frac{c(\Omega_{\rm hde} + 2\Omega_{\rm rad})^2}{3b\epsilon^2 a^2 \Omega_{\rm hde}}\Delta^2_{\psi_c} \\ &= \frac{1}{2\epsilon a^2}\left(1 - \frac{\Omega_{\rm hde} + 2\Omega_{\rm rad}}{\epsilon}\right)\Delta^2_{\delta\chi_c} + \frac{c(\Omega_{\rm hde} + 2\Omega_{\rm rad})^2}{3\epsilon^2 b a^2 \Omega_{\rm hde}}\Delta^2_{\psi_c}.\end{aligned} \tag{4.81}$$

Note that the contribution coming from ψ_c decays away, as the dark radiation and the holographic components in the prefactor are dominated by the inflaton. Therefore, although $\Delta^2_{\psi_c}$ is approximately frozen after horizon crossing, the overall contribution becomes extremely small. Note also that (4.80) corresponds to the comoving curvature power spectrum at the end of inflation, which is not conserved in the presence of entropy perturbations. However, since the second term in the right hand size of (4.80) decays rapidly, becoming negligible after the very first e-folds, the majority of modes is approximately

[3]Note that in this step $\delta\chi$ corresponds to the original perturbation, i.e. the one defined previously to the re-scaling (4.41).

frozen after horizon crossing. The modes that leave the horizon during the first e-folds might still evolve, but they correspond to the lowest multipoles in the CMB power spectrum, which are not tightly constraint due to cosmic variance. Finally, in terms of (4.63) and (4.75), we have

$$\Delta_R^2 = \frac{1}{2\epsilon}\left(1 - \frac{\Omega_{\rm hde} + 2\Omega_{\rm rad}}{\epsilon}\right)\Delta_{\delta\chi}^2 + \frac{c(\Omega_{\rm hde} + 2\Omega_{\rm rad})^2}{3\epsilon^2 a^2 H^2 \varphi^2 \Omega_{\rm hde}}\Delta_\psi^2 \simeq \frac{1}{2\epsilon}\Delta_{\delta\chi}^2. \quad (4.82)$$

4.5.2 Tensor Power Spectrum

The quadratic action (4.53) leads to the following equation of motion:

$$v_k'' + v_k\left(k^2 + \frac{\lambda}{3a^2} - \frac{b}{6\varphi^2} + \frac{c}{\varphi^2} - \frac{a''}{a}\right) = 0. \quad (4.83)$$

In a pure de Sitter universe, it is rewritten as

$$v_k'' + \left(k^2 - \frac{2}{\tau^2} + M^2\right)v_k = 0, \quad (4.84)$$

where M is approximately constant[4] and related to the mass of the tensor mode (4.52) as

$$M^2 = M_{\rm GW}^2 a^2 = \frac{\lambda H^2 \tau^2}{3} - \frac{b}{6\varphi^2} + \frac{c}{\varphi^2}. \quad (4.85)$$

The solution satisfying both equation (4.84) and the commutation relation for the annihilation and creation operators, i.e. $[\hat{a}_{\vec{k}}, \hat{a}^\dagger_{\vec{k}'}] = (2\pi)^3\delta(\vec{k} - \vec{k}')$, reads

$$v_k = \frac{e^{-i\sqrt{k^2+M^2}\tau}}{\sqrt{2}(k^2+M^2)^{\frac{1}{4}}}\left(1 - \frac{i}{\sqrt{k^2+M^2}\tau}\right). \quad (4.86)$$

The two-point correlation function of the tensor perturbation γ_k is readily obtained as

$$\begin{aligned}\langle \gamma_k \gamma_k' \rangle &= (2\pi)^3\delta(k+k')4\frac{|v_k|^2}{a^2} \\ &= 16\pi^3\delta(k+k')\frac{H^2(1+k^2\tau^2+M^2\tau^2)}{(k^2+M^2)^{\frac{3}{2}}}, \end{aligned} \quad (4.87)$$

[4]Note from equation (4.52) that the dominant terms in the mass of the tensor mode are proportional to a^{-2}, while $\Omega_{\rm rad}$ decays faster, as one can see in Figure 4.5. Therefore, after a few e-folds, $M^2 = M_{\rm GW}^2 a^2$ is approximately constant.

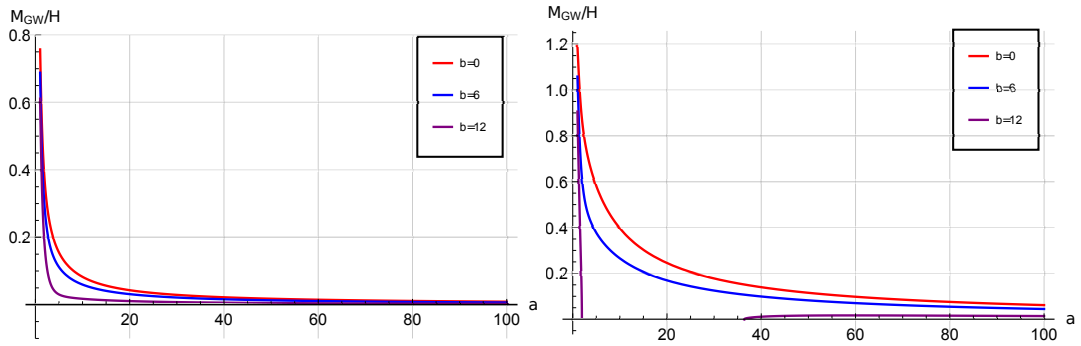

FIGURE 4.6: M_{GW}/H for $c = 2.2$. Here $\tilde{m} = 0.1$, $\tilde{\varphi}_i = \frac{1}{\sqrt{0.1}}$, $\tilde{\rho}_i = 0.75$ and $\tilde{V} = 0.7$ (left) and $c = 2.2$, $\tilde{m} = 0.1$, $\tilde{\varphi}_i = \frac{1}{\sqrt{0.3}}$, $\tilde{\rho}_i = 0.4$ and $\tilde{V} = 0.36$ (right).

leading to the following dimensionless power spectrum:

$$\Delta_t^2 = 2\Delta_\gamma^2 = 2\frac{H^2k^3(1+k^2\tau^2+M^2\tau^2)}{\pi^2(k^2+M^2)^{\frac{3}{2}}}. \tag{4.88}$$

For superhorizon modes, we have

$$\Delta_t^2 = 2\Delta_\gamma^2 = 2\frac{H^2k^3}{\pi^2(k^2+M^2)^{\frac{3}{2}}}\bigg|_{\sqrt{k^2+M^2}=aH} = \frac{2H^2}{\pi^2}\left(1-\frac{M_{GW}^2}{H^2}\right)^{\frac{3}{2}}, \tag{4.89}$$

where the second equality must be evaluated at horizon crossing, i.e. $\sqrt{k^2+M^2} = aH$. The ratio M_{GW}/H is plotted in figure 4.6, where we see that it decays rapidly.

The spectral index n_t can be obtained from the superhorizon power spectrum (4.89) via

$$n_t = \frac{d\ln\Delta_t^2}{d\ln k}, \tag{4.90}$$

which can be computed using the chain rule

$$n_t = \frac{d\ln\Delta_t^2}{dN}\frac{dN}{d\ln k}, \tag{4.91}$$

where N is the number of e-folds. The first factor is obtained directly from the power spectrum, while the second comes from $\ln k = N + \ln H + \frac{1}{2}\ln\left(1-\frac{M^2}{a^2H^2}\right)$,

leading to

$$\begin{aligned}\frac{dN}{d\ln k} &= \left[1+\frac{d\ln H}{dN}+\frac{1}{2}\frac{d\ln\left(1-\frac{M^2}{a^2H^2}\right)}{dN}\right]^{-1}= \\ &\simeq \left[(1-\epsilon)\left(1+\frac{M_{GW}^2}{H^2}\right)-\frac{\epsilon_M M_{GW}^2}{H^2}\right]^{-1}, \end{aligned} \tag{4.92}$$

up to leading order in M_{GW}^2/H^2, where $\epsilon_M \equiv M_{,N}/M$.

Using that $H_{,N}/H = -\epsilon$, where $_{,N}$ represents derivative with respect to N, one finds

$$\begin{aligned} n_t &= -\frac{2\epsilon}{(1-\epsilon)\left(1+\frac{M^2}{a^2H^2}\right)-\frac{\epsilon_M M^2}{a^2H^2}}+ \\ &+ \frac{3M^2(-\epsilon_M k\tau^2\sqrt{1-M^2\tau^2}+M\tau^3 M_{,N}+\tau_{,N})}{k\tau^2\sqrt{1-M^2\tau^2}(k^2+M^2)\left[(1-\epsilon)\left(1+\frac{M^2}{a^2H^2}\right)-\frac{\epsilon_M M^2}{a^2H^2}\right]}= \\ &\simeq -2\epsilon+\frac{M_{GW}^2}{H^2}(3-3\epsilon_M+2\epsilon) \end{aligned} \tag{4.93}$$

up to first order in ϵ and ϵ_M, and up to second order in M_{GW}/H. In the last equality we have used that $\tau_{,N} = -(1-\epsilon)\tau$, $\tau = -1/(aH)$ and $\sqrt{k^2+M^2} = aH$. Therefore, since $M_{GW} \ll H$ from the very beginning of inflation on, we obtain a tensor spectral index similar to the standard one for single field inflation.

4.6 Conclusions and Discussion

In this chapter we analyzed the effects of the two components of the HDE model, namely the holographic and the dark radiation terms, in a single field slow-roll inflation, both in the scalar and tensor sectors. We started by numerically computing the evolution of the components at the background level, which led to the conclusion that the inflaton dominates after a few e-folds, while the holographic and (especially) the dark radiation terms decay rapidly. Therefore, at the background level, the inflationary phase is not spoiled by the presence of HDE.

For the scalar perturbation we showed that the two scalar degrees of freedom, i.e. the inflaton perturbation and the graviton, decouple when expanding the quadratic action up to zero order in $\Omega_{\rm hde}$ and $\Omega_{\rm rad}$. The next-to-leading order correction to this expansion is of order $\sqrt{\Omega_i\epsilon}$, $i = {\rm hde, rad}$, i.e. a correction suppressed not only by the square root of the tiny fractional densities of the dark sector, but also by the square root of the first slow-roll

parameter. The correction to the curvature power spectrum coming from the graviton decays rapidly, as the dark radiation and holographic components are dominated by the inflaton. Moreover, the correction to the inflaton power spectrum also decays as Ω_{hde} and Ω_{rad} become smaller than ϵ.

For the tensor power spectrum we find a dependence on the mass of the tensor mode, which decays rapidly in the beginning of inflation. The resulting power spectrum for $M_{GW} \ll H$ is the usual single field result.

Taking all the above features into account, we conclude that HDE is compatible with single field slow-roll inflation, being in agreement with the current constraints on the scalar power spectrum, since the extra contributions decay quite fast, and on primordial gravitational waves, since it leads to the usual tensor amplitude. In case of detection of primordial gravitational waves, the tensor spectral index can be used as evidence in favour or against HDE, constraining the mass of the tensor mode.

Chapter 5

Graviton to Photon Conversion via Parametric Resonance

5.1 Introduction

Parametric resonance is a well-known effect in classical mechanics: an oscillator with a periodically varying contribution to the mass will be exponentially excited if the frequency of the oscillator lies in certain resonance bands determined by the frequency of the variation of the mass. If the amplitude of the varying part of the mass is small compared to the magnitude of the time-independent part, we speak of narrow band resonance, if it is large then we are in the realm of broad resonance. Parametric resonance is a special case of the Floquet theory of instability of a dynamical system in the presence of a periodic time-dependence of one of the coefficients. The equation of motion for the special case is called the Mathieu equation.

In early univere cosmology, parametric resonance plays a crucial role in the transfer of energy to regular matter at the end of a hypothetical period of inflation [163, 164]. At the end of inflation, the scalar field ϕ which drives inflation will be oscillating about the minimum of its potential. This oscillation can induce a parametric resonance instability for any field χ which couples in an appropriate way to ϕ, e.g. via a $\phi^2\chi^2$ coupling in the case of a matter scalar field χ. In the case of a self-interacting scalar field ϕ, excitation of fluctuations of ϕ will also occur (see [165, 166] for reviews). This instability is known as preheating [167, 168, 169]. Note that the preheating instability can occur for both bosons and fermions, although because of Pauli blocking the resonance for fermions is less efficient [170].

In an expanding universe the equation of motion for a matter field χ contains a Hubble damping term, and hence the parametric resonance analysis does not directly apply. However, if we rescale the matter field by a power of the cosmological scale factor and also work in conformal time τ instead of physical time t, we obtain an equation of motion without damping term. However, the bare mass term of the equation in terms of the original field now acquires a scale factor dependence which greatly reduces the efficiency

of the Floquet resonance. On the other hand, for massless fields we obtain a standard Mathieu equation for the rescaled field.

Gravitational waves induce oscillating terms in the equations of motion for all matter fields. In the case of massless matter fields such as the photon, it is hence expected that these gravitational wave can induce instabilities. These instabilities, in turn, will drain energy from the gravitational waves. In the Standard Model, the only massless field is the photon[1]. Here, we will study the parametric resonance instability of the photon field in the presence of a gravitational wave. We find that there is indeed a resonance effect. In vacuum, the resonance occurs only in the second resonance band and is hence highly inefficient. On the other hand, in a medium in which the speed of fluctuations of the electromagnetic field is smaller than unity[2], the instability occurs in the first resonance band and is hence much more efficient. In the current chapter, we estimate the decay rate of a packet of gravitational waves passing through a medium.

In the following we will be studying the effects of gravitational waves on matter fields in a Minkowski space-time backgound. Provided that the time scale of the instability is shorter than the duration which a mode spends in the instability band, the effects of the expansion of space are small, the main effect being that modes slowly enter and exit the resonance bands, as argued already in the original article [163]. Note that our analysis does not make use of any physics beyond Standard Model particle physics and Einstein gravity.

In Section 5.1.1 we review the phenomenon of parametric resonance. Then we apply the concepts to the cases of a massless scalar field in Section 5.2 and of an electromagnetic field in Section 5.3. The estimate of the damping rate is computed in Section 5.4. Finally, the conclusions are presented in Section 5.5.

5.1.1 Parametric Resonance

Let us now introduce the parametric resonance mechanism in order to present the main ideas explored in the gravitational wave damping (Sections 5.2 and 5.3) and amplification (Chapter 6).

As mentioned in the previous section, parametric resonance is a classical phenomenon that an oscillator experiences when it receives a periodically varying contribution to its mass. The result is an exponential amplification of the oscillator's amplitude if its frequency is within the so called resonance bands, which depend on the frequency by which the mass varies.

[1] If there is a massless neutrino there can also be an instability to neutrino production, but because of Pauli blocking it will be less efficient than for photons.

[2] We use units in which the speed of light, Planck's constant and Boltzmann's constant are 1.

As an example, let us consider a generic oscillator $x(t)$ governed by the following equation of motion

$$\ddot{x} + Ax - 2q\cos(2t)x = 0, \tag{5.1}$$

where A and q are parameters determined by details of the dynamics of $x(t)$ and dot denotes derivative with respect to t. This type of equation is known as Mathieu equation and can be investigated by means of the Floquet instability theory, which can be used to estimate the oscillator's amplification. The exponential growth is quantified by means of the so called Floquet exponent μ, which appears in the solution as

$$x(t) \propto \exp(\mu t). \tag{5.2}$$

It can be computed by using the fundamental matrix, i.e. a matrix representing the independent solutions [171]. The eigenvalues $\sigma^{\pm}$ of this matrix at $t_0 + T$, where t_0 is the initial time and T is the period of the oscillating function in (5.1), are related to the Floquet exponent μ via

$$\mathbb{R}[\mu^{\pm}] = \frac{1}{T}\ln|\sigma^{\pm}|, \tag{5.3}$$

where the superscript $\pm$ represents the growing and decaying solutions to (5.1). When $\mathbb{R}[\mu^{\pm}] > 0$, $x(t)$ is exponentially amplified, as seen from (5.2). By following this procedure, we find the values of A that correspond to the resonance bands and the dependence of μ on q, which is given by

$$\mu \propto \begin{cases} q & \text{if} \quad A \subset (1-q, 1+q) \\ q^2 & \text{if} \quad A \subset (4-q^2, 4+q^2) \end{cases}. \tag{5.4}$$

Figure 5.1 shows the dependence of the Floquet exponent on the parameters A and q, defining the so-called resonance bands.

If q, i.e. the periodically varying contribution to the mass term, is small compared to A, the parametric resonance is said to happen in a narrow band. As we will see in this chapter and in Chapter 6, this is exactly the case of the gravitational wave resonance and, therefore, the first resonance band, i.e. $A \subset (1-q, 1+q)$, is the most efficient when it comes to the amplification factor.

5.2 Massless Scalar Field Resonance

Here we consider a gravitational wave of frequency ω exciting a scalar field ϕ with mass m_ϕ. We consider a gravitational wave with metric tensor $h_{\mu\nu}$ travelling in Minkowski space-time. The full metric is

$$g_{\mu\nu} = \eta_{\mu\nu} + h_{\mu\nu}. \tag{5.5}$$

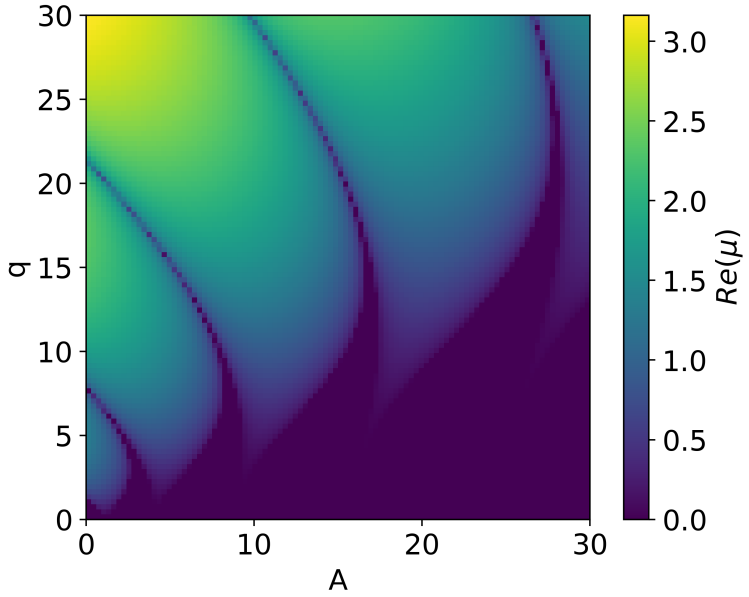

FIGURE 5.1: Floquet exponent μ as a function of the parameters A and q of the Mathieu equation. The light regions, i.e. regions where $Re(\mu) > 0$, are the so-called resonance bands, which are centered around $A = 1, 4, 9$ and so on.

Specifically, we consider a standing gravitational wave with frequency ω:

$$h_{ij} = h_0 \cos \omega t \cos \omega z \cdot \epsilon_{ij}, \qquad h_{0\mu} = 0, \tag{5.6}$$

where h_0 is the amplitude, and ϵ_{ij} is the polarisation tensor

$$\epsilon_{ij} = \begin{pmatrix} 1 & 1 & 0 \\ 1 & -1 & 0 \\ 0 & 0 & 0 \end{pmatrix}. \tag{5.7}$$

The equation of motion of a scalar field of mass m in this gravitational wave background is

$$\ddot{\phi} - \left(\delta_{ij} - h_{ij}\right) \partial_i \partial_j \phi + m_\phi^2 \phi = 0. \tag{5.8}$$

This equation is reminiscent of the sound speed resonance mechanism [172][173], where the sound speed of scalar modes or tensor modes receives an oscillatory correction which eventually triggers the resonance instability. In Fourier space, the equation becomes

$$\ddot{\phi}_{\mathbf{k}} + \left(k^2 + m_\phi^2\right) \phi_{\mathbf{k}} - \frac{h_0}{2} k_\epsilon^2 \cos \omega t \cdot \left[\phi_{\mathbf{k}-\mathbf{p}} + \phi_{\mathbf{k}+\mathbf{p}}\right] = 0, \tag{5.9}$$

where $k_\epsilon^2 \equiv \epsilon_{ij} k_i k_j$ and $\mathbf{p}$ is a 3-dimensional vector defined by $\mathbf{p} = (0, 0, \omega)$. Let us define the variable

$$\Phi\left(t, k_x, k_y, k_z\right) \equiv \phi\left(t, k_x, k_y, k_z\right) + \phi\left(t, k_x, k_y, -k_z\right), \tag{5.10}$$

and let us choose $k_z = \omega/2$. Then, quite remarkably, its equation of motion is

$$\ddot{\Phi}_{k_z} + \left(k^2 + m_\phi^2\right)\Phi_{k_z} - \frac{h_0}{2} k_\epsilon^2 \cos\omega t \left(\Phi_{k_z} + \Phi_{3k_z}\right) = 0, \tag{5.11}$$

which is a Mathieu equation with a source term proportional to Φ_{3k_z}. To avoid notational clutter we have defined $\Phi_{k_z} \equiv \Phi\left(t, k_x, k_y, k_z\right)$. In a first approximation, the source term can be neglected as the mode $\Phi\left(t, k_x, k_y, 3k_z\right)$ does not receive a parametric resonance amplification and thus remains small[3].

Inserting the value of k_z, the equation of motion (5.11) then becomes the standard Mathieu equation

$$\Phi_{k_z}{}'' + \left[A_k - 2q\cos(2\tau)\right]\Phi_{k_z} = 0, \tag{5.12}$$

with the rescaled time variable being $\tau \equiv \frac{\omega t}{2}$, the prime denotes the derivative with respect to τ, and

$$A = 1 + \frac{4\left(k_x^2 + k_y^2 + m_\phi^2\right)}{\omega^2}, \qquad q = \frac{h_0 k_\epsilon^2}{\omega^2}. \tag{5.13}$$

The Mathieu equation (5.12) undergoes broad resonance for $q > 1$, where the exponential instability occurs for all sufficiently long wavelength modes, and narrow resonance for $q < 1$, where the exponential instability occurs only for narrow bands of k modes. We are interested in the weak field limit where the amplitudes of both polarisations are small, i.e. $h_0 \ll 1$. Hence, $q \ll 1$ and we are dealing with narrow band resonance. It is clear that we are outside of the first resonance band where $A \subset (1-q, 1+q)$. However, parametric resonance may still occur at the second resonance band where $A \subset \left(4 - q^2, 4 + q^2\right)$. For resonance in the second band, the amplitude of Φ grows as $\exp[\mu_k^{(2)}\tau]$, where $\mu_k^{(2)}$ is the Floquet exponent of the second resonance band $\mu_k^{(2)} \simeq \frac{q^2}{4}$, which is parametrically suppressed compared to the Floquet exponent in the first resonance band which is $\mu_k^{(1)} \simeq \frac{q}{2}$.

There is, however, a way to obtain resonance in the first band: if we consider the propagation of the scalar field ϕ in a medium which leads to a

[3]We can include the $\Phi\left(t, k_x, k_y, 3k_z\right)$ term and add in the equation of motion for this mode, thus obtaining a set of coupled differential equations. In the context of a study of the effects of inhomogeneous noise on the strength of parametric resonance, it has been shown that considering the inhomogeneous system actually boosts the growth rate of the instability [174]. This is an consequence of Furstenberg's Theorem [175] (see [176]). As an application, this leads to a new proof of Anderson Localization in condensed matter systems [177].

reduced speed of propagation $c_s < 1$, then A becomes

$$A = c_s^2 + c_s^2 \frac{4(k_x^2 + k_y^2)}{\omega^2} + \frac{4m_\phi^2}{\omega^2}\,. \tag{5.14}$$

In this case, for a massive scalar field it will remain impossible to obtain resonance in the first band, unless $m_\phi^2 < (1 - c_s^2)\omega^2/4$, which in our case is not reasonable for masses of Standard Model particles, given that the wavelengths of gravitational waves emitted by the most of astrophysical events are of macroscopic scale. However, for photons (which are massless) there will be a band of (k_x, k_y) values which lie in the first resonance band. Thus, in the following we will focus on gravitational waves exciting the electromagnetic field.

One may be confused at this point, as quantum field theory tells us a massless particle does not decay to a massive particle in the vacuum; The process is simply forbidden by energy momentum conservation. Nevertheless, two colliding massless particles do decay to massive particles, as now this process is allowed (for instance a pair of colliding high-energy photons can decay into an electron-positron pair). This is precisely the case in our analysis, where a standing gravitational wave, which can be understood as the collective behaviour of two groups of massless gravitons travelling in the opposite direction, decays into massive scalar particles (provided that mass is smaller than the frequency of gravitational wave) due to the collision of massless gravitons.

In passing, we shall mention that for a traveling gravitational wave in vacuum, the parametric resonance does not occur, even if the scalar field is massless. This is because the lightcones of the gravitational wave and the scalar field overlap with each other. Sitting on the wavefront of the scalar wave, one does not "feel" the oscillation induced by the gravitational wave. However, in a medium where the scalar wave is sub-luminal, the two lightcones do not overlap and that opens up the channel converting energy from the gravitational wave sector to the scalar field sector, even for a pure traveling wave. The similar effect has been observed in the framework of the modified gravity too [178].

5.3 Electromagnetic Resonance

Here we consider the excitation of the electromagnetic field by a gravitational wave in a medium with speed of light $c_s < 1$. The metric which enters the kinetic part of gauge field equation of motion is

$$g_{\mu\nu} = \tilde{\eta}_{\mu\nu} + h_{\mu\nu}, \tag{5.15}$$

where $\tilde{\eta}_{\mu\nu} = (-1, 1/c_s^2, 1/c_s^2, 1/c_s^2)$. Generally c_s^2 is dependent on the frequency. In our idealised case where a mono-frequency gravitational wave is considered, c_s^2 is just a constant. It can be a good approximation if the frequency spread in a wave packet is small.

The Coulomb gauge is unavailable in the presence of the gravitational wave, and thus we adopt the Weyl gauge instead, where $A_0 = 0$. The $i-th$ component of the equation of motion reads

$$\begin{aligned} 0 &= g_{i\alpha}\partial_\mu \left(F_{\rho\sigma} g^{\alpha\rho} g^{\mu\sigma}\right) \\ &= \partial_t^2 A_i - c_s^2 \partial_t h_{ij} \cdot \partial_t A_j + c_s^2 \partial_j F_{ij} \\ &\quad -c_s^4 h_{jk}\partial_j F_{ik} - c_s^4 F_{kj}\partial_j h_{ik}\,, \end{aligned} \tag{5.16}$$

and the $0-th$ component gives the modified Gauss law,

$$\partial_i E_i = c_s^4 h_{ij}\partial_i E_j. \tag{5.17}$$

We consider an unpolarised standing gravitational wave

$$h_{ij} = h_0 \cos\omega t \cos\omega z \cdot \epsilon_{ij}\,. \tag{5.18}$$

The generalizations to other waves and other types of polarisation are straightforward.

Translating (5.16) to momentum space and defining

$$\begin{aligned} \mathcal{A}_x\left(t, k_x, k_y, k_z\right) &\equiv A_x\left(t, k_x, k_y, k_z\right) + A_x\left(t, k_x, k_y, -k_z\right), \\ \mathcal{A}_y\left(t, k_x, k_y, k_z\right) &\equiv A_y\left(t, k_x, k_y, k_z\right) + A_y\left(t, k_x, k_y, -k_z\right), \\ \mathcal{A}_z\left(t, k_x, k_y, k_z\right) &\equiv A_z\left(t, k_x, k_y, k_z\right) - A_z\left(t, k_x, k_y, -k_z\right), \end{aligned} \tag{5.19}$$

then for $k_z = \omega/2$ these equations (5.16) can be written in matrix form

$$\ddot{\mathcal{Y}} + c_s^2 \mathcal{G}\mathcal{Y} + c_s^2 \mathcal{F}\dot{\mathcal{Y}} + c_s^4 \mathcal{M}\mathcal{Y} \simeq 0, \tag{5.20}$$

where

$$\mathcal{Y} = \begin{pmatrix} \mathcal{A}_x \\ \mathcal{A}_y \\ \mathcal{A}_z \end{pmatrix} \tag{5.21}$$

$\mathcal{G}$ is the gradient matrix

$$\mathcal{G} = \begin{pmatrix} k_y^2 + \frac{\omega^2}{4} & -k_x k_y & -k_x k_z \\ -k_x k_y & k_x^2 + \frac{\omega^2}{4} & -k_y k_z \\ -k_x k_z & -k_y k_z & k_x^2 + k_y^2 \end{pmatrix} \tag{5.22}$$

$\mathcal{F}$ is the friction matrix

$$\mathcal{F} = \frac{1}{2} h_0 \omega \sin \omega t \begin{pmatrix} 1 & 1 & 0 \\ 1 & -1 & 0 \\ 0 & 0 & 0 \end{pmatrix}, \tag{5.23}$$

and $\mathcal{M}$ is defined by

$$\begin{aligned} \mathcal{M} &= \frac{1}{4} h_0 \cos \omega t \times \\ &\times \begin{pmatrix} -2k_x k_y + 2k_y^2 + \omega^2 & 2k_x^2 - 2k_x k_y + \omega^2 & -2\omega \left(k_x + k_y\right) \\ 2k_x k_y + 2k_y^2 + \omega^2 & -2k_x^2 - 2k_x k_y - \omega^2 & -2\omega \left(k_x - k_y\right) \\ -\left(k_x + k_y\right) \omega & \left(k_y - k_x\right) \omega & 2k_\epsilon^2 \end{pmatrix}. \end{aligned} \tag{5.24}$$

Note of that only two of the variables are independent since the photon has only two dynamical degrees of freedom. Thus we need to decouple one of variables from the other two. The gradient matrix $\mathcal{G}$ has only two non-vanishing eigenvalues,

$$\mathcal{S}\mathcal{G}\mathcal{S}^{-1} = \begin{pmatrix} 0 & 0 & 0 \\ 0 & k_x^2 + k_y^2 + k_z^2 & 0 \\ 0 & 0 & k_x^2 + k_y^2 + k_z^2 \end{pmatrix}, \tag{5.25}$$

where

$$\mathcal{S} = \begin{pmatrix} \frac{k_x}{k_z} & \frac{k_y}{k_z} & 1 \\ -\frac{k_z}{k_x} & 0 & 1 \\ -\frac{k_y}{k_x} & 1 & 0 \end{pmatrix}. \tag{5.26}$$

Introducing the new variables,

$$\mathcal{S}\mathcal{Y} \equiv \begin{pmatrix} a_x \\ a_y \\ a_z \end{pmatrix}, \tag{5.27}$$

and linearly transforming (5.20),

$$\mathcal{S}\left(\ddot{\mathcal{Y}} + c_s^2 \mathcal{G}\mathcal{Y} + c_s^2 \mathcal{F}\dot{\mathcal{Y}} + c_s^4 \mathcal{M}\mathcal{Y}\right) = 0, \tag{5.28}$$

and noting that $k_z \dot{a}_x = k_i E_i = \mathcal{O}(h_{ij})$, then up to first order in the gravitational wave amplitude we have the following two coupled differential equations which decouple from the third variable,

$$y'' + c_s^2 \tilde{\mathcal{F}} y' + c_s^2 \tilde{k}^2 y + c_s^4 \tilde{\mathcal{M}} y = 0, \tag{5.29}$$

where $y = (a_y, a_z)^T$, a prime denotes the derivative with respect to $\tau \equiv \frac{\omega t}{2}$, $\tilde{k}^2 \equiv 4k^2/\omega^2$, and

$$\begin{aligned}\tilde{\mathcal{F}} =& h_0 \sin 2\tau \begin{pmatrix} \frac{\omega^2(k_x+k_y)}{4k_x k^2} & -\frac{\omega(k_x^2-k_xk_y+k_z^2)}{2k_x k^2} \\ \frac{\omega(-k_x^2+2k_xk_y+k_y^2)}{2k_x k^2} & \frac{-4k_xk_\epsilon^2-\omega^2(k_x+k_y)}{4k_x k^2} \end{pmatrix}, \\ \tilde{\mathcal{M}} =& h_0 \cos 2\tau \begin{pmatrix} \frac{2k_\epsilon^2}{\omega^2}+1+\frac{k_y}{k_x} & \frac{-2k_x+2k_y}{\omega}-\frac{\omega}{2k_x} \\ \frac{2k_y^2}{\omega k_x}-\frac{2k_x-4k_y}{\omega} & \frac{-2\epsilon_{ij}k_ik_j}{\omega^2}-1-\frac{k_y}{k_x} \end{pmatrix}, \end{aligned} \tag{5.30}$$

Note that $a_y \propto F_{xz}$ and $a_z \propto F_{xy}$ are proportional to the gauge field strength and thus gauge invariant.

The equation of motion (5.29) has the form of a Mathieu type matrix equation with a friction term. The friction term can be removed via a field rescaling in a similar way to how the Hubble friction term in a scalar field equation can be removed by rescaling the field. The solution of the rescaled variable will then display exponential growth with a Floquet exponent μ_k in narrow resonance bands of k. In terms of the original variables, the exponential growth is modulated by the rescaling function. As shown explicitly in [174] in the case of inflationary reheating, the exponential growth of the solutions trivially extends from the scalar case to the matrix case.

We have numerically solved the equation (5.29), and the solutions for a_y and a_z are shown in Figure 5.2, in the first case for propagation in the vacuum ($c_s = 1$) and in the second case for propagation in a medium (the value $c_s = 1/1.333$ for water was chosen). For $c_s = 1$ the resonance occurs only in the second band, while for $c_s = 1/1.333$ we have resonance in the first band. The growth rate in the case of first band resonance is much larger and it takes a much shorter time for the instability to develop.

As is apparent by comparing the two figures, for $c_s^2 < 1$ (the value for water was chosen), the amplication is much stronger (the Floquet exponent is much larger). The time scale in the second figure is two orders of magnitude smaller than in the first, and the amplitude at the end of the evolution period is of the same order. The horizontal axis in the graphs is the re-scaled dimensionless time $\tau = \omega t/2$.

Our analysis in this section is based on an un-polarized gravitational standing wave in the flat space-time. The main conclusion also applies to the traveling waves which are of more relevance in various astrophysical phenomena. Namely a traveling gravitational wave can trigger parametric resonance in the photon sector, at the first band in a medium where the refractive index of light differs from unity. In this sense our mechanism is somewhat similar to Cherenkov radiation. However, an essential difference is that the resonant decay rate in our case is proportional to the amount of photon produced at earlier times: namely, it grows exponentially. Moreover, the exponential instability only occurs in a very narrow band in the Mathieu

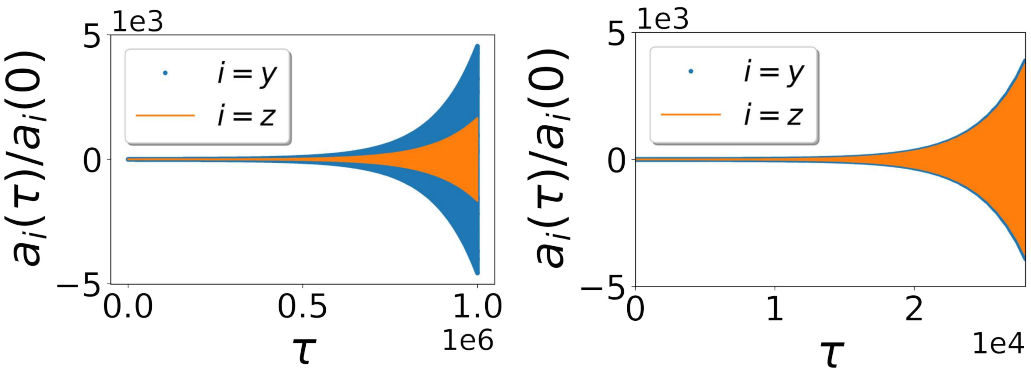

FIGURE 5.2: The left figure: the exponential instability of a_y and a_z in the vacuum where $c_s = 1$. The resonance occurs at the 2nd band where $A = 4$. We set $\tilde{k}_x^2 = \tilde{k}_y^2 = 3/2$ in the numerical plots, and we have adopted a unrealistically large value for $h_0 = 0.01$ to reduce the CPU computing time. The initial condition is set to $a_y(0) = a_y'(0) = a_z(0) = a_z'(0) = 1$. The right figure: the exponential instability of a_y and a_z, where speed of light in the water $c_s = 1/1.333$, $\tilde{k}_x^2 = \tilde{k}_y^2 = 0.388$, and thus we have $A \simeq 1$ in the Mathieu equation. We have adopted an unrealistically large value for $h_0 = 0.01$ to reduce the CPU computing time. The initial condition is set to $a_y(0) = a_z(0) = 1$ and $a_y'(0) = a_z'(0) = 0$.

equation, while Cherenkov radiation occurs within a wide frequency range allowed by energy momentum conservation[4].

[4]Note that the inverse process, namely the production of gravitational waves via parametric resonance from an oscillating scalar field, does not occur in a Minkowski background in a vacuum since the scalar field only enters the source term in the gravitational wave equation and not in the mass term (see e.g. equation (44) of [179]). However, in an expanding background, there is the possibility of parametric resonance of gravitational waves if the oscillating scalar fields lead to small amplitude periodic fluctuations of the Hubble expansion rate $H(t)$ superimposed on the regular decrease of H (see e.g. [180]).

5.4 Estimate of the Damping Rate

In this section we will estimate the decay rate of a wave packet of gravitational waves peaked at frequency ω with a frequency spread of $\Delta\omega \sim \omega$ due to excitation of electromagnetic fluctuations in a medium with effective speed of light c_s. The energy density in gravitational waves is

$$\rho_{GW} \sim G^{-1}\omega^2 h_0^2 . \tag{5.31}$$

In the semiclassical approximation, we consider vector fields A_i initially in their vacuum state, i.e. with an initial amplitude $A_k(t_i) \sim k^{-1/2}$. In this case, the energy density in the produced gauge fields is

$$\rho_A \sim \Delta\omega \int_{\mathcal{P}} d^2k k^{-1} k^2 e^{2\mu_k \tau} , \tag{5.32}$$

where the integral runs over the two-dimensional phase space $\mathcal{P}$ of (k_x, k_y) modes which undergo resonance.

For each specific plane wave of frequency ω, resonance occurs for a fixed value of k_z, namely $k_z = \omega/2$, and for a band of (k_x, k_y) with width $r_{max}^2 - r_{min}^2 \simeq \frac{q\omega^2}{4c_s^2}$ and radius r determined by

$$r^2 = k_x^2 + k_y^2 \simeq \frac{1 - c_s^2}{4c_s^2}\omega^2 . \tag{5.33}$$

These two equations determine the range of values of (k_x, k_y) for which $A_k = 1$ modulo q. Thus, in (5.32) we make the approximations of replacing the modulus k by $\omega/2$ and taking μ_k to be independent of k. Inserting equation (5.33), $\delta\omega \sim \omega$ and the value $q \sim c_s^2(1 - c_s^2)h_0$ we obtain

$$\rho_A \sim \omega^4 c_s^4 (1 - c_s^2) h_0 e^{2\mu\tau} . \tag{5.34}$$

The decay rate of the gravitational wave amplitude h_0 can then be determined by equating the energy gain in ρ_A with the energy loss in ρ_{GW}. Neglecting the time dependence of h_0 in ρ_A (the time dependence is dominated by the Floquet term and including the time dependence of h_0 would yield only a higher order correction) yields

$$\log(h_0)' \sim -G\omega^2 c_s^6 (1 - c_s^2)^2 e^{2\mu\tau} . \tag{5.35}$$

Thus, we see that the decay rate of h_0 on the gravitational wave oscillation time scale is suppressed by $G\omega^2$ and also by the factor $(1 - c_s^2)^2$.

5.5 Conclusions and Discussion

We have shown that gravitational waves can be damped by exciting a parametric resonance instability of the electromagnetic gauge field. In vacuum, the resonance is very weak since the resonant modes lie in the second resonance band. In a medium in which electromagnetic waves travel with a speed smaller than 1, on the other hand, the resonance is in the first band and hence stronger. We have estimated the decay rate which a wavepacket of gravitational waves undergoes.

The analysis is based on a single gravitational wave with fixed frequency. The extension to several gravitational wave modes is straightforward. As to be expected from the general theory of Floquet instability and also studied explicitly for inflationary reheating in [174], the instability remains, and the Floquet exponent for a fixed value of $k_z = \omega/2$ is boosted if gravitational waves of different frequencies are added.

The conversion of gravitational waves into plasma waves has been studied in the literature focusing on linear resonant conversion [181] or the non-linear interaction of two plasma and one gravitational wave [182, 183, 184, 185], in the presence of strong background magnetic fields. Our analysis fits nicely into this area providing a new conversion process with the same order of magnitude for the growth parameter as for the three wave interaction [183], without requiring a strong background magnetic field to exist, provided that the plasma mass is sufficiently small compared to the frequency of the gravitational wave, $m^2_{\rm plasma} < (1 - c_s^2)\omega^2/4$.

Our result is a first step in the direction of investigating possible implications of gravitational wave conversion via parametric resonance in cosmology and astrophysics. The biggest challenge in finding straightforward applications is to achieve the necessary conditions that lead to a non-negligible conversion rate: namely a refractive index sufficiently larger than 1 in a context where there is enough time for the instability to develop. In a black hole binary, for instance, the orbital decay is faster than the time required for a non-negligible conversion, while the refractive index in the accretion disk is generally not large enough. In the early universe, during radiation domination, the refractive index is indeed significant, and a field redefined in order to incorporate the background expansion satisfies a Mathieu equation with $q \sim h_0/\omega^2$. It would be interesting to carefully investigate the possibility of suppression of B-modes in the Cosmic Microwave Background if the instability is well developed until matter-radiation equality. Another potential application consists in a novel type of gravitational wave detector, in which gravitational waves turn into possibly detectable electromagnetic waves whose amplitude grows as $\exp(\epsilon h_0 \omega t)$ due to the exponential instability induced by parametric resonance, where h_0 and ω are the amplitude and frequency of gravitational waves respectively, and ϵ is an order one constant depending on the relation between the momentum of electromagnetic waves

and gravitational waves. Given the amplitude of gravitational waves, the electromagnetic signals grow faster for high frequency gravitational waves. It remains a challenge to detect the high frequency gravitational waves with natural origin [186]. Nevertheless, there are already some ideas about lab generation of high frequency gravitational waves [187, 188]. Finally, we shall mention that the methodology developed in this chapter can be applied to investigate the inverse process, namely the amplification of gravitational waves due to parametric resonance.

Chapter 6

Gravitational Wave Resonance in ULDM Halos

6.1 Introduction

The nature of dark matter represents one of the most intriguing open questions in Cosmology and Astrophysics. Although abundant evidence points to its existence, a detection was never made, leading to a wide range of possibilities with regard to its fundamental character [189, 190, 191]. CDM is currently used in the Standard Cosmological Model (ΛCDM), which is very successful in describing the Universe on large scales. However, on sub-galactic scales there still remain incompatibilities between the CDM description and the observed data, as CDM predicts more structure on small scales than what we observe [192]. An interesting solution to this problem comes from Ultralight Dark Matter (ULDM), namely Ultralight Axions (ULAs) of mass 10^{-22}eV as a dark matter candidate [193, 194, 195]. Apart from that, different ULA masses can be obtained in the scope of string theory [196] and might constitute the totality or a fraction of dark matter in the cases where $m \gtrsim 10^{-27}$ [197, 198].

On the other hand, gravitational waves have been providing us with unprecedented tools to test our Universe and it is natural to ask how they can shed light into the dark matter problem. A number of different dark matter candidates have already been investigated by using gravitational wave physics [199, 200, 201, 202], including ULDM [203, 204, 205, 206].

In this chapter we focus on a peculiar property of ULDM halos constituted by ULAs - the time-oscillation of the generated gravitational potentials - to show its relation with gravitational wave resonance in the halo. The mechanism corresponds to narrow band parametric resonance, enhancing gravitational waves of frequencies equal to the ULA masses.

The chapter is organised as follows: Section 6.2 presents the description of the ULDM halo, resulting in the expressions for the gravitational potentials. Section 6.3 applies parametric resonance to the context of a gravitational wave in a ULDM halo. Finally, a summary of the results is presented in Section

6.4. Natural units with $M_p = 1$ are used throughout the text, except when explicitly said otherwise.

6.2 Description of the ULDM Halo

In this section we present the mathematical description of the ULDM halo, which leads to the expressions for the oscillating gravitational potentials. As shown in Section 6.3, this feature is of major importance for the occurrence of resonance.

We start from an almost Minkowski space-time given by

$$ds^2 = -(1+2U)dt^2 + (1-2\bar{U})(dx^2+dy^2+dz^2), \tag{6.1}$$

as the expansion of the Universe is negligible on the scales considered. The quantities U and $\bar{U}$ are the gravitational potentials generated by the ULDM halo, which are treated perturbatively. This assumption holds even inside the halo, where the condition $U, \bar{U} \ll 1$ is still satisfied.

The ULDM is represented by an ULA field

$$\phi(t) = \phi_0 \cos(mt), \tag{6.2}$$

where the spatial dependence of the amplitude ϕ_0 was neglected at leading order [203, 207]. The oscillating frequency corresponds to the particle's energy, which can be approximated by the particle's mass m in the non-relativistic limit. The corresponding energy-momentum tensor is

$$T_{\mu\nu} = \mathrm{diag}(\rho, p, p, p), \tag{6.3}$$

where

$$\rho = \frac{1}{2}m^2\phi_0^2, \tag{6.4}$$
$$p = -\rho\cos(2mt). \tag{6.5}$$

The oscillating pressure leads to an oscillating contribution to the gravitational potentials U and $\bar{U}$, in such a way that we can write

$$T = T_0 + \delta T, \tag{6.6}$$
$$U = U_0 + \delta U, \tag{6.7}$$
$$\bar{U} = \bar{U}_0 + \delta\bar{U}, \tag{6.8}$$
$$R = R_0 + \delta R, \tag{6.9}$$

where T is the trace of the energy-momentum tensor, X_0 terms are time-independent and δX terms oscillate in time. Both U and $\bar{U}$ depend on space and time, where the spatial dependence is restricted to U_0 and $\bar{U}_0$. R is the

Ricci scalar associated to (6.1), which reads

$$R = -6\ddot{\bar{U}} + 2\nabla^2(2\bar{U} - U), \tag{6.10}$$

where dot denotes derivative with respect to t.

Now let us explore Einstein's equations

$$R_{\mu\nu} - \frac{1}{2}Rg_{\mu\nu} = T_{\mu\nu}, \tag{6.11}$$

where $R_{\mu\nu}$ is the Ricci tensor, in order to relate some of these quantities. First, from the traceless part of the ij component we obtain

$$\bar{U}_0 = U_0. \tag{6.12}$$

Secondly, from the trace of the Einstein's equations, we have $-R = T$, which allows us to identify

$$R_0 = \rho. \tag{6.13}$$

On the other hand, from (6.10) we have the time-independent part of the Ricci scalar R_0 as a function of the gravitational potentials

$$R_0 = 2\nabla^2 U_0, \tag{6.14}$$

leading to the following Poisson equation

$$2\nabla^2 U_0 = \rho. \tag{6.15}$$

We can estimate the magnitude of U_0 by switching to Fourier space

$$U_0 \propto \frac{\rho}{k_a^2}, \tag{6.16}$$

where k_a is the wavenumber related to the ULA. Its value can be estimated from $k_a^2/m^2 = v^2$, where $v \simeq 10^{-3}$ is a typical velocity in our Galaxy.

The expression for the oscillating part $\delta\bar{U}$ is obtained from (6.10) by assuming $\delta\ddot{\bar{U}} \gg \nabla^2\delta\bar{U}$ and $\delta\ddot{\bar{U}} \gg \nabla^2\delta U$[1], which allows us to write [207]

$$\delta T = 6\delta\ddot{\bar{U}}. \tag{6.17}$$

By solving this equation we obtain

$$\delta\bar{U} = \frac{\rho}{8m^2}\cos(2mt). \tag{6.18}$$

In order to find δU we follow [204] and perform a change of frames, which retains the dependence on spatial derivatives of δU in the ij component of the

[1]This assumption is consistent with (6.2), where the spatial dependence of ϕ_0 was neglected [203].

Einstein's equations. Then we switch back to the halo frame by setting the relative velocity between the frames to zero, which leads to

$$\delta U = -\delta \bar{U}. \tag{6.19}$$

6.3 Gravitational Wave Resonance in the ULDM Halo

Let us now consider a gravitational wave around the space-time (6.1), which can be written as

$$h_{\mu\nu} = h\epsilon_{\mu\nu}, \tag{6.20}$$

where h is the amplitude and $\epsilon_{\mu\nu}$ is the polarization tensor. Since the latter is parallel transported along the geodesics, we can neglect its change due to the presence of the gravitational potentials U and $\bar{U}$ and write the equation of motion for the scalar amplitude h [208, 209]

$$\partial_\mu(\sqrt{-g}g^{\mu\nu}\partial_\nu h) = 0, \tag{6.21}$$

which leads to

$$\begin{aligned} &\ddot{h} - (1 + 2U + 2\bar{U})\nabla^2 h - \dot{U}\dot{h} - 3\dot{\bar{U}}\dot{h} + \\ &+\partial_i h \partial_i \bar{U} - \partial_i h \partial_i U = 0 \end{aligned} \tag{6.22}$$

up to linear order in U and $\bar{U}$. By substituting (6.18) and (6.19) in (6.22), we find, in Fourier space,

$$\begin{aligned} &\ddot{\bar{h}}_k + k^2 \bar{h}_k - 4\int d^3\vec{x} \exp(-i\vec{k}\cdot\vec{x}) U_0 \nabla^2 \bar{h} + \\ - \;& \frac{1}{2}\rho \cos(2mt)\bar{h}_k = 0, \end{aligned} \tag{6.23}$$

where $\bar{h} \equiv \exp(\delta U)h$. This field redefinition was performed in order to kill the friction terms present in (6.22). Defining $\tau \equiv mt$, we obtain

$$\begin{aligned} &\bar{h}_k'' + \frac{k^2}{m^2}\bar{h}_k - \frac{4}{m^2}\int d^3x \exp(-i\vec{k}\cdot\vec{x}) U_0 \nabla^2 \bar{h} + \\ - \;& \frac{1}{2}\frac{\rho}{m^2}\cos(2\tau)\bar{h}_k = 0, \end{aligned} \tag{6.24}$$

where prime denotes derivative with respect to τ. The remaining convolution is not trivial to perform, but it can be neglected if compared to the other kinetic term in the equation of motion. Because it is proportional to $(\rho/k_a^2)(k^2/m^2)\bar{h}_k$, it is very small compared to $(k^2/m^2)\bar{h}_k$, as $\rho/k_a^2 \ll 1$. For this reason, we

approximate

$$\begin{aligned} A\bar{h}_k &\equiv \frac{k^2}{m^2}\bar{h}_k - \frac{4}{m^2}\int d^3x \exp\left(-i\vec{k}\cdot\vec{x}\right)U_0\nabla^2\bar{h} \\ &\simeq \frac{k^2}{m^2}\bar{h}_k, \end{aligned} \tag{6.25}$$

which leads to

$$\bar{h}_k'' + A\bar{h}_k - 2q\cos\left(2\tau\right)\bar{h}_k = 0, \tag{6.26}$$

where $q \equiv \rho/m^2/4$. Although the remaining convolution is not negligible compared to the oscillating term, they play different roles in the Mathieu equation. The first, together with the other kinetic term, establishes where the resonance bands are centered, while the second is related to the amplification factor and to the band width. Therefore, equation (6.26) is a Mathieu equation, just like (5.1), in the first resonance band for $k^2 = m^2$. Solving it numerically we obtain Figure 6.1, which shows the amplification of the gravitational wave $\bar{h}_k$ in time τ for an illustrative high energy density.

According to the Floquet instability theory, the solution to (6.26) can be approximated as[2]

$$h_k \simeq \bar{h}_k \propto \exp\left(q\tau/2\right), \tag{6.27}$$

which allows us to estimate the time required for the amplification to become of $\mathcal{O}(1)$, i.e. $\tau \sim 1/q$. It is important to note that q, which contains the information about the ULA energy density ρ, depends on the fraction of ULAs as dark matter f, as

$$\rho = f\rho_{DM}, \tag{6.28}$$

where ρ_{DM} is the dark matter energy density.

6.3.1 Gravitational Wave Resonance Independently of Constraints on ULDM

Because the gravitational wave resonance could, in principle, be used to independently test ULAs, we first assume $f = 1$ for all masses, ignoring the constraints already imposed by other phenomena. In Section 6.3.2 we present the results considering these constraints.

Let us first consider the solar region, i.e. $\rho = 0.4\text{GeV/cm}^3$. In the most standard scenario, i.e. $m \simeq 10^{-22}\text{eV}$, one would wait for 3.9×10^{17} years to see an amplification of gravitational waves with frequency in the Pulsar Timing Array (PTA) range, which is larger than the age of the Universe. For ULAs of mass $m \simeq 10^{-27}\text{eV}$, the required time is 3.9×10^{12} years, still unfeasible for current tests.

[2]Due to the fact that $\exp\left(\delta U\right) \simeq 1$ we can approximate $h_k \simeq \bar{h}_k$.

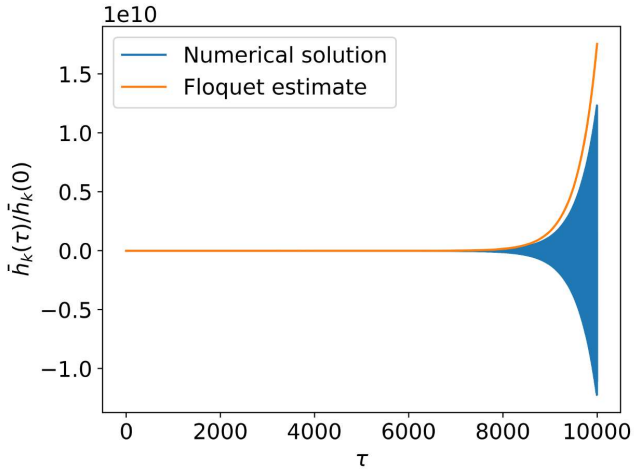

FIGURE 6.1: Gravitational wave resonance for $m = 10^{-22}$eV and $\rho = 10^{16} \times 0.4\text{GeV/cm}^3$, where the factor 10^{16} was introduced to speed up the resonance and reduce computational time. For the real value in the solar region, $\rho = 0.4\text{GeV/cm}^3$, assuming the ULA constitutes 100% of dark matter, the amplification becomes of $\mathcal{O}(1)$ around $\tau \sim 1/q \simeq 2.0 \times 10^{18}$, equivalent to 3.9×10^{17} years. The Floquet estimate corresponds to (6.27). The initial conditions used are $h_k(0) = 1$ and $h_k{}'(0) = 0$.

On the other hand, the prospects are largely improved if one considers very dense regions in the halos, although still satisfying $\rho/m^2 \ll 1$, which can arise, for instance, due to the existence of a black hole in the halo [210, 211, 212, 213]. For $\rho \simeq 1.4 \times 10^7\text{GeV/cm}^3$, the ULAs of mass 10^{-22}eV would take 1.1×10^{10} years to amplify gravitational waves, which is compatible with the time of formation of dark matter halos[3]. In this case, primordial gravitational waves in the PTA range could be amplified if they keep traveling through this region since the halo formation. Shorter, and therefore more realistic, time intervals are achieved in denser environments. Note that for this specific energy density, $\rho/m^2 \ll 1$ holds for $m \gtrsim 10^{-26}$.

[3]This corresponds to the most conservative assumption and a bigger gravitational wave amplification is obtained if one considers scenarios where dark matter halos formed earlier in the Universe history [214, 215, 216].

Figure 6.2 depicts the amplification, represented by the argument of the exponential function in (6.27), as a function of time and ULA masses. It is important to note that the formalism used here would break down when the condition $h \ll 1$ is not anymore satisfied, which sets an upper bound on the amplifications depending on the initial gravitational wave amplitude. The most interesting gravitational wave frequencies lie in the PTA range and correspond to $10^{-23}\text{eV} \lesssim m \lesssim 10^{-22}\text{eV}$, resulting in large time intervals for $\mathcal{O}(1)$ amplification, although still compatible with halo formation time. On the other hand, shorter time intervals are achieved by lighter ULAs, namely $10^{-26}\text{eV} \lesssim m \lesssim 10^{-24}\text{eV}$, which correspond to gravitational wave frequencies from $2.4 \times 10^{-10}\text{Hz}$ to $2.4 \times 10^{-12}\text{Hz}$. Although not covered by ongoing gravitational wave detectors, these frequencies could be explored in the future [217, 218].

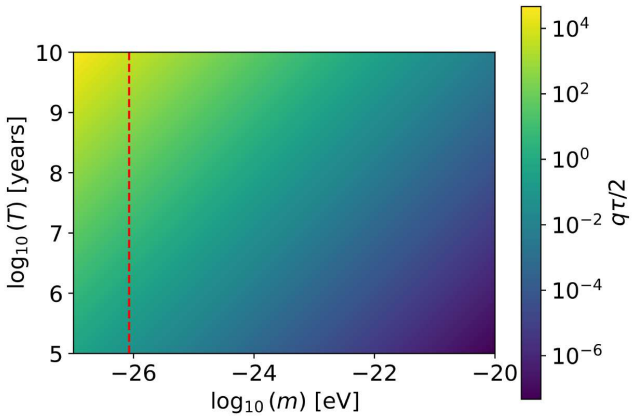

FIGURE 6.2: Argument of the amplification factor (6.27), $q\tau/2$, as a function of time and ULA masses assuming $f = 1$ for all masses in the very dense dark matter region, i.e. $1.4 \times 10^7\text{GeV/cm}^3$. The red line indicates when $\rho/m^2 \simeq 0.01$, representing a left bound to the region where $\rho/m^2 \ll 1$.

6.3.2 Gravitational Wave Resonance Considering Constraints on ULDM

Now let us consider constraints already imposed to the ULA fraction as dark matter f depending on the ULA mass m [219, 195], namely constraints from the Cosmic Microwave Backgrgouund (CMB) [197], the Baryon Oscillation Spectroscopic Survey (BOSS) [220], the Spitzer Photometry and Accurate Rotation Curves (SPARC) [221], Eridanus-II [222], Lyman-α forest [223] and galaxy weak lensing combined with Planck (+DES) [224]. Constraints from UV luminosity function and optical depth to reionization [225], as well as constraints from M87 black hole spin [226, 227, 228], are implicitly considered, as they do not further reduce the parameter space. Constraints from 21-cm cosmology were not taken into account, as the literature only presents results for $f = 1$. In [219] forecasts are obtained by relaxing the assumption on f, and it is expected that the Hydrogen Epoch of Reionization Array (HERA) [229] will be very sensitive to ULDM, comparable to the forecasts for the Cosmic Microwave Backgound Stage 4 (CMB-S4) [230]. Other constrains on ULAs can arise in specific scenarios, such as [231, 232]. Figure 6.3 presents the parameter space and the constraints explicitly considered in this chapter.

The Floquet estimates are then computed in the very dense dark matter region, i.e. $\rho_{DM} \simeq 1.4 \times 10^7 \mathrm{GeV/cm}^3$, assuming f from the constraints to determine ρ through (6.28). The results obtained for the gravitational wave resonance by considering all the constraints combined are shown in Figure 6.4. As expected, the constraints to f suppress q in the Mathieu equation, leading to reduced amplifications, although still significant for some ULA masses. Note that small values of f can be compensated by higher dark matter energy densities ρ_{DM}, as long as the latter can be justified in at least one physical regime and $\rho/m^2 \ll 1$.

6.4 Conclusions and Discussion

In this chapter we have shown gravitational waves are amplified due to parametric resonance with ULAs constituting the totality or part of a dark matter halo. All the ULA masses considered might only lead to significant amplifications nowadays in very dense dark matter regions, which could exist in different scenarios [210, 211].

Because the gravitational wave resonance could be, in principle, used to independently constrain ULDM (assuming the effect could be measured in a very dense dark matter environment), Section 6.3.1 presents the gravitational wave amplification for $f = 1$ for all masses, ignoring existing constraints. The results are depicted in Figure 6.2. On the other hand, in Section 6.3.2 the constraints summarized in Figure 6.3 are considered, leading to the gravitational wave amplifications depicted in Figure 6.4. Since smaller values of ρ

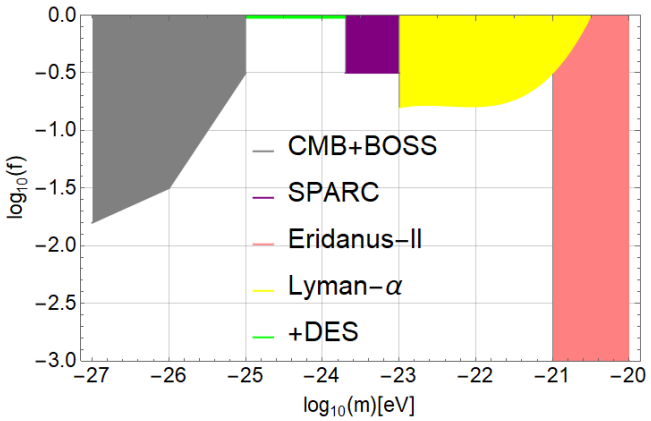

FIGURE 6.3: Constraints imposed to the ULA fraction as dark matter f depending on the ULA mass m for $10^{-27}\text{eV} \gtrsim m \gtrsim 10^{-20}\text{eV}$ [219], namely CMB+BOSS [197, 220], SPARC [221], Eridanus-II [222], Lyman-α forest [223] and galaxy weak lensing combined with Planck (+DES) [224].

suppress the parameter q in the Mathieu equation (6.26), the gravitational wave amplifications are also suppressed compared to $f = 1$. A reduced f can be compensated by a denser dark matter region, as long as it can be justified by at least one physical configuration, such as [210], and $\rho/m^2 \ll 1$.

Note that there exists an upper bound on the amplifications established by the condition $h \ll 1$, whose value depends on the initial amplitude of the gravitational wave considered. This results from the fact that the Mathieu equation (6.26) was obtained assuming perturbation theory.

Given that the parametric resonance occurs for $k = m$, the amplified gravitational waves lie in the range $\sim 10^{-8}$Hz to $\sim 10^{-13}$Hz, corresponding to 10^{-22}eV to 10^{-27}eV. Therefore, the possible gravitational wave sources are primordial perturbations and supermassive black hole binaries. Due to the large time scales for the resonance to become significant, the scenarios of interest should provide gravitational wave emission for a long time, which

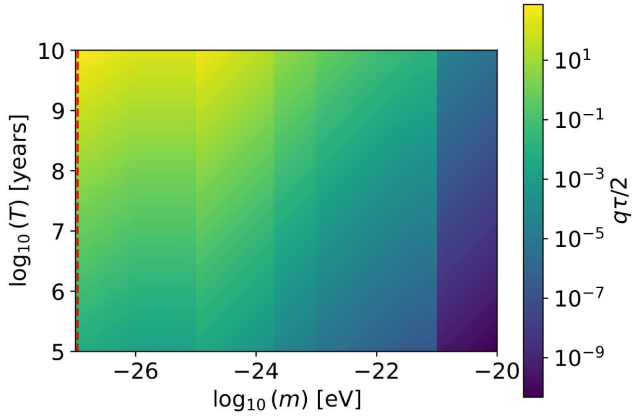

FIGURE 6.4: Argument of the amplification factor (6.27), $q\tau/2$, as a function of time and ULA masses, considering f according to the constraints in Figure 6.3, in the very dense dark matter region, i.e. $1.4 \times 10^7 \mathrm{GeV/cm^3}$. The red line indicates when $\rho/m^2 \simeq 0.01$, representing a left bound to the region where $\rho/m^2 \ll 1$.

does happen for the sources mentioned. In addition, note that, although supermassive black hole binaries suffer orbital decay, they present continuous gravitational wave emission long before merger, therefore consistent with the approach carried in this chapter. Finally, it is relevant to remember that the frequencies in the range 10^{-8} Hz to 10^{-9} Hz lie in the PTA range, with NANOGrav recently reporting the evidence for a gravitational wave background [233].

Throughout the whole chapter we have assumed GR and a minimal coupling to the ULAs. Different results could be obtained in modified scenarios such as [205], where gravitational wave resonance is obtained in the scope of dynamical Chern-Simons gravity.

Appart from ULAs, other phenomena can trigger the resonance, such as fast small oscillations in the Hubble parameter [234] or a varying gravitational

wave speed [173].

The consideration of a gravitational wave background might further enhance the resonance [176, 235, 39].

Chapter 7

Conclusions and Discussion

In this thesis we have explored different aspects and challenges of ΛCDM and motivated modified scenarios, mainly focusing on early Universe and gravitational wave physics. Our investigation included the proposal and analysis of a bouncing model that generates inflation naturally, the exclusion of bouncing models proposed to mitigate the CMB anomalies on large scales, the analysis of the effects of HDE during an inflationary phase, the conversion of gravitational waves to photons via parametric resonance and the resonant amplification of gravitational waves in ULDM halos. All these scenarios are motivated by different open questions in cosmology, such as the singularity problem, the generation of cosmological perturbations, the observed features that are anomalous within ΛCDM, the dark energy and the dark matter problem and, finally, the phenomena that might arise in gravitational wave dynamics.

Although we have provided the conclusions and discussion for each chapter separately, in this section we would like to reiterate the main points and deliberate the main implications of this thesis.

in Chapter 2 we have proposed a bouncing cosmology that addresses the initial singularity problem, generates inflation without an inflaton and leads to the usual radiation-dominated phase naturally [34]. All this rich phenomenology is generated by a very simple scale factor in function of conformal time $\bar{\eta}$, namely

$$a(\bar{\eta}) = a_b \left(y\bar{\eta} + \sqrt{1+y^2}\sqrt{1+\bar{\eta}^2} \right). \tag{7.1}$$

In our investigation, this scale factor was obtained due to quantum effects introduced by means of the Wheeler-DeWitt equation in the scope of the dBB quantum theory, but it is possible that other types of quantization might lead to similar asymmetric evolutions[1]. Regardless of its origin, this kind of scale

[1]We recall here that the term asymmetry in this context refers to the difference between the contracting and expanding phases. In this concrete scenario, the contraction is almost Minkowski, while the expansion presents an inflationary phase followed by the usual cosmic history.

factor presents a very interesting phenomenology, motivating the search for this kind of evolution in different theoretical approaches. In addition, other kinds of perfect fluids could be considered, where in this specific case the radiation fluid is the one that generates the qdS phase.

As we have shown, this scenario generates the observed amplitude of the scalar power spectrum, which is expected due to the existence of the naturally generated inflationary phase. However, this phase is closer to de Sitter than what observations indicate, leading to a spectral index too close to one (instead of the observed $n_s \simeq 0.96$). Additionally, the tensor-to-scalar ratio is incompatible with current cosmological constraints or, in other words, the amplitude of the tensor power spectrum is too high. This is caused by the similarity between the scalar and tensor Mukhanov-Sasaki equations, which differ only by the value of c_s. Therefore, given these incompatibilities, this scenario has to be supplemented with other ingredients, for example a curvaton field [100, 101, 102, 103]. The curvaton does not play a role in the background evolution, but it increases the amplitude of scalar perturbations with respect to the tensor ones, leading to a lower tensor-to-scalar-ratio. Additionally, the presence of the curvaton would generate a tiny deviation ϵ from radiation, $\omega = 1/3 + \epsilon$, which would then push the spectral index away from 1. Of course, the introduction of an extra field spoils one of the appealing features of this scenario, so another option would be to look for different asymmetric scale factors that generate a qdS phase with, for instance, matter as the perfect fluid. In this case, it has been shown that the amplitude of the generated primordial gravitational waves is sufficiently small [90].

In Chapter 3 we have investigated phenomenological bouncing models inspired by LQC that were proposed in order to mitigate the CMB anomalies on large scales. These scenarios had a very interesting phenomenological appeal, as they could fit CMB data on the power spectrum level even better than ΛCDM for some parameters. They simultaneously mitigated the power suppression and the dipolar and parity asymmetries, making these features more likely in a concrete realization of the temperature maps, and also alleviated the issue with the lensing parameter in the Planck analysis. These achievements were possible due to very large non-Gaussianities on very large scales, which decayed very quickly inside the horizon. Given this extremely fast decay, it was believed in the literature that experiments such as Planck could not impose constraints on the size of the non-Gaussianity due to cosmic variance.

We have explicitly computed the CMB reduced bispectrum [35], which is the quantity observed by Planck, and the corresponding SNR. Although the bispectrum decays indeed extremely fast, for very low multipoles the signal surpasses cosmic variance, leading to a cumulative SNR that is high enough to be detected. Since the overlap of this bispectrum with standard bispectrum shapes was low, we had to look for the signal in the actual Planck data [36]. What we obtained was an exclusion of all the scenarios that were able to mitigate the anomalies with high significances. Therefore, although

these bouncing scenarios seemed very promising from the phenomenological point of view, they cannot address the anomalies and they lose their most appealing advantages.

These results show the sensitivity of the Planck data beyond the pivot scale, rendering some features on very large scales testable despite cosmic variance. This can be explained by the fact that the CMB transfer functions relate each multipole to a rather broad band of wave numbers k, which can be seen from Figure 3.9. Additionally, these results are likely valid for other scenarios that make use of skewed statistics to alleviate the CMB anomalies.

In Chapter 4, we have considered the effective field theory of HDE, a dark energy candidate, and investigated its effect during a single-field slow-roll inflationary phase. We first analyzed its effects on the background level and concluded that the inflaton dominates the holographic and the dark radiation components, making HDE compatible with inflation. Then we computed the cosmological perturbations and the corresponding scalar and tensor power spectra, which contain corrections that decay very quickly in the first inflationary e-folds. Therefore, this scenario is compatible with current CMB constraints to the power spectra [38].

In Chapter 5 we have shown that gravitational waves can be damped due to parametric resonance with photons. The most efficient conversion happens when the electromagnetic field propagates in a medium with speed smaller than 1 in natural units (this is required in order to promote the resonance to the first band) [39].

Although our analysis has been performed in a Minkowski space-time, the generalization to an expanding background is possible. In the case of a scalar field, for instance, the equation of motion has a Hubble friction term, which can be removed by a field redefinition that takes the expansion into account. In a radiation-dominated Universe, a Mathieu equation is obtained in terms of conformal time, leading to the amplification of the redefined scalar. Therefore, although the field redshifts in the expanding background, the conversion still occurs.

The main challenges behind this conversion mechanism in the context of cosmology and astrophysics are the sufficiently high refractive index and time intervals required for the instability to develop. As an example, if one considers a black hole binary, one would have the resonance spoiled by the orbital decay (in addition to a very small refractive index in the accretion disk). Nevertheless, interesting directions to explore based on this conversion mechanism are the possibility of B-mode suppression in the CMB and indirect gravitational wave detection, i.e. detection of the amplified electromagnetic field amplified due to resonance with a gravitational wave.

Finally, in Chapter 6 we have investigated the amplification of gravitational waves due to parametric resonance in ULDM halos. Such dark matter candidates have some interesting phenomenological imprints, such as suppression

of structure formation on small scales, therefore solving the incompatibility between CDM simulations and observations [192]. Additionally, this kind of dark matter introduces a time oscillation in the gravitational potentials of the halo due to the oscillatory character of the ULA pressure. By using this property and recalling that "gravity bends gravity", we obtained a Mathieu equation for the gravitational wave. The first resonance band is achieved when the gravitational wave frequency is equal to the axion mass, interestingly encompassing the PTA frequency range.

We investigated the current amplification of a gravitational wave in this context and found that significant results can only be achieved in dense regions within the halo, which could arise for instance due to the presence of a black hole. The possible gravitational wave sources are primordial perturbations and supermassive black hole binaries, given the frequencies that are amplified for axion masses between 10^{-22}eV and 10^{-27}eV.

These results were obtained in GR minimally coupled to the ULAs. An interesting possibility for future work in this direction would be to consider a modified gravity theory where the oscillating mass term of the gravitational wave equation of motion becomes larger (therefore increasing the amplification). Moreover, the inclusion of a gravitational wave background might boost the resonance, which is worth exploring.

In summary, we have delved into various facets and complexities of ΛCDM and modified cosmologies, with a particular emphasis on early Universe dynamics and gravitational wave phenomena. With the findings discussed above, we have shed light on fundamental aspects and challenges and delineated potential avenues for further research, contributing to the ongoing discourse in theoretical and phenomenological cosmology.

Bibliography

[1] A.A. Starobinsky. "Relict gravitation radiation spectrum and initial state of the universe". In: *JETP Lett.* 30 (1979), p. 682.

[2] A. Guth. "Inflationary universe: A possible solution to the horizon and flatness problems". In: *Phys. Rev. D* 23 (1981), p. 347. DOI: 10.1103/PhysRevD.23.347.

[3] A. Linde. "A new inflationary universe scenario: A possible solution of the horizon, flatness, homogeneity, isotropy and primordial monopole problems". In: *Phys. Lett. B* 108 (1982), p. 389. DOI: 10.1016/0370-2693(82)91219-9.

[4] V. Mukhanov and G. Chibisov. "Quantum fluctuations and a nonsingular universe". In: *JETP Lett.* 33 (1981), p. 532.

[5] N. Aghanim et al. "Planck 2018 results. VI. Cosmological parameters". In: *Astron. Astrophys.* 641 (2020), A6. DOI: 10.1051/0004-6361/201833910. arXiv: 1807.06209 [astro-ph.CO].

[6] Arno Penzias and Robert Wilson. "A Measurement of Excess Antenna Temperature at 4080 Mc/s". In: *The Astrophysical Journal* 142.1 (1965), pp. 419–421.

[7] G. F. Smoot et al. "COBE Differential Microwave Radiometers Observations of the Cosmic Microwave Background Anisotropy". In: *The Astrophysical Journal* 396.1 (1992), pp. L1–L5.

[8] C. L. Bennett et al. "First-Year Wilkinson Microwave Anisotropy Probe (WMAP) Observations: Preliminary Maps and Basic Results". In: *The Astrophysical Journal Supplement Series* 148.1 (2003), pp. 1–27.

[9] Planck Collaboration. "A&A". In: 571 (2014), A16.

[10] Planck Collaboration. "A&A". In: 594 (2016), A13.

[11] Planck Collaboration. "A&A". In: 641 (2020), A6.

[12] B. P. Abbott, others (LIGO Scientific Collaboration, and Virgo Collaboration). "Observation of Gravitational Waves from a Binary Black Hole Merger". In: *Physical Review Letters* 116 (6 2016), p. 061102. DOI: 10.1103/PhysRevLett.116.061102.

[13] B. P. Abbott and others (LIGO Scientific Collaboration). "LIGO: The Laser Interferometer Gravitational-Wave Observatory". In: *Reports on Progress in Physics* 72 (7 2009), p. 076901. DOI: 10.1088/0034-4885/72/7/076901.

[14] B. Caron and others (Virgo Collaboration). "The Virgo Collaboration". In: *Classical and Quantum Gravity* 32 (2 2015), p. 024001. DOI: 10.1088/0264-9381/32/2/024001.

[15] The NANOGrav Collaboration et al. "The NANOGrav 15 yr Data Set: Evidence for a Gravitational-wave Background". In: *The Astrophysical Journal Letters* 951.1 (June 2023), p. L8. DOI: 10.3847/2041-8213/acdac6. URL: https://dx.doi.org/10.3847/2041-8213/acdac6.

[16] E. Aprile and others (XENON100 Collaboration). "Dark Matter Results from 225 Live Days of XENON100 Data". In: *Physical Review Letters* 109 (18 2012), p. 181301. DOI: 10.1103/PhysRevLett.109.181301.

[17] D.S. Akerib and others (LUX Collaboration). "Results from a Search for Dark Matter in the Complete LUX Exposure". In: *Physical Review Letters* 118 (2 2017), p. 021303. DOI: 10.1103/PhysRevLett.118.021303.

[18] P. Agnes and others (DarkSide Collaboration). "First Results from the DarkSide-50 Dark Matter Experiment at Laboratori Nazionali del Gran Sasso". In: *Physical Review Letters* 121 (8 2018), p. 081307. DOI: 10.1103/PhysRevLett.121.081307.

[19] A. G. Riess et al. "AJ". In: 116 (1998), p. 1009.

[20] S. Perlmutter et al. "ApJ". In: 517 (1999), p. 565.

[21] P. J. E. Peebles and B. Ratra. "Rev. Mod. Phys." In: 75 (2003), p. 559.

[22] V. Sahni and A.A. Starobinsky. "A Universal Equation of State for the Gravitational Fluid". In: *International Journal of Modern Physics D* 9 (4 2000), pp. 373–443. DOI: 10.1142/S0218271800000542.

[23] E.V. Linder. "The Cosmic Triangle: Revealing the State of the Universe". In: *Physical Review Letters* 90 (9 2003), p. 091301. DOI: 10.1103/PhysRevLett.90.091301.

[24] A.G. Riess et al. "A discrepancy between the Hubble constant inferred from cosmic microwave background radiation and from the distance ladder". In: *The Astrophysical Journal* 730 (2 2011), p. 119. DOI: 10.1088/0004-637X/730/2/119.

[25] M. Betoule et al. "Improved cosmological constraints from a joint analysis of the SDSS-II and SNLS supernova samples". In: *Astronomy & Astrophysics* 568 (2014), A22. DOI: 10.1051/0004-6361/201423413.

[26] T. Abbott et al. "Cosmological Results from the Dark Energy Survey Science Verification Year 1 Observations: Cosmological Constraints from Galaxy Clustering and Weak Lensing". In: *Monthly Notices of the Royal Astronomical Society* 481 (2 2018), pp. 2371–2395. DOI: 10.1093/mnras/sty1591.

[27] Elisabeth Krause et al. "The σ_8 tension: measurements, sources, and cosmological consequences". In: *Monthly Notices of the Royal Astronomical Society* 477 (4 2018), pp. 4915–4932. DOI: 10.1093/mnras/sty1009.

[28] A. Hajian et al. "Large-scale anomalies in the cosmic microwave background". In: *Physical Review D* 94 (8 2016), p. 083004. DOI: 10.1103/PhysRevD.94.083004.

[29] Ivan Agullo, Dimitrios Kranas, and V. Sreenath. "Large scale anomalies in the CMB and non-Gaussianity in bouncing cosmologies". In: *Class. Quant. Grav.* 38.6 (2021), p. 065010. DOI: 10.1088/1361-6382/abc521. arXiv: 2006.09605 [astro-ph.CO].

[30] A. Borde, A. H. Guth, and A. Vilenkin. "Inflationary Spacetimes Are Incomplete in Past Directions". In: *Phys. Rev. Lett.* 90 (2003), p. 151301. DOI: 10.1103/PhysRevLett.90.151301.

[31] Carlo Rovelli. "Quantum Gravity and the Wheeler-DeWitt Equation". In: *Physical Review D* 28 (10 1983), pp. 1920–1928. DOI: 10.1103/PhysRevD.28.1920.

[32] Paola C. M. Delgado. "Introdução à Cosmologia Quântica". In: (Aug. 2023). DOI: 10.47456/Cad.Astro.v4n2.41563. arXiv: 2308.07355 [gr-qc].

[33] Abhay Ashtekar, Tomasz Pawlowski, and Parampreet Singh. "Loop quantum cosmology: A brief review". In: *Physics Reports* 467 (1-3 2008), pp. 41–93. DOI: 10.1016/j.physrep.2008.09.001.

[34] Piero A. P. Molinari et al. "Radiation-dominated bouncing model with slow contraction and inflation". In: *Phys. Rev. D* 109.4 (2024), p. 043531. DOI: 10.1103/PhysRevD.109.043531. arXiv: 2310.16250 [gr-qc].

[35] Paola C. M. Delgado, Ruth Durrer, and Nelson Pinto-Neto. "The CMB bispectrum from bouncing cosmologies". In: *JCAP* 11 (2021), p. 024. DOI: 10.1088/1475-7516/2021/11/024. arXiv: 2108.06175 [astro-ph.CO].

[36] Bartjan van Tent, Paola C. M. Delgado, and Ruth Durrer. "Constraining the Bispectrum from Bouncing Cosmologies with Planck". In: *Phys. Rev. Lett.* 130.19 (2023), p. 191002. DOI: 10.1103/PhysRevLett.130.191002. arXiv: 2212.05977 [astro-ph.CO].

[37] C. Lin. "JCAP". In: 07 (2021), p. 003. eprint: arXiv:2101.08092[hep-th].

[38] Paola C. M. Delgado, Alexander Ganz, and Chunshan Lin. "Inflationary epoch in the presence of holographic dark energy". In: *JCAP* 08 (2022), p. 081. DOI: 10.1088/1475-7516/2022/08/081. arXiv: 2111.05760 [astro-ph.CO].

[39] Robert Brandenberger et al. "Graviton to photon conversion via parametric resonance". In: *Phys. Dark Univ.* 40 (2023), p. 101202. DOI: 10.1016/j.dark.2023.101202. arXiv: 2205.08767 [gr-qc].

[40] Paola C. M. Delgado. "Gravitational wave resonance in ultralight dark matter halos". In: *Phys. Rev. D* 108.12 (2023), p. 123539. DOI: 10.1103/PhysRevD.108.123539. arXiv: 2309.09946 [hep-ph].

[41] N. Aghanim and et al. "Planck 2018 results. I. Overview and the cosmological legacy of Planck". In: *Astron. Astrophys.* 642 (2020), A1. DOI: 10.1051/0004-6361/201833880. arXiv: 1807.06205 [astro-ph.CO].

[42] R.H. Cyburt et al. "Big bang nucleosynthesis: Present status". In: *Rev. Mod. Phys.* 88 (2016), p. 015004. DOI: 10.1103/RevModPhys.88.015004. arXiv: 1505.01076 [astro-ph.CO].

[43] T. Abbott and et al. "Dark Energy Survey Year 1 Results: Cosmological constraints from cluster abundances and weak lensing". In: *Phys. Rev. D* 102 (2020), p. 023509. DOI: 10.1103/PhysRevD.102.023509. arXiv: 2002.11124 [astro-ph.CO].

[44] B. Abolfathi and et al. "The Fourteenth Data Release of the Sloan Digital Sky Survey: First Spectroscopic Data from the Extended Baryon Oscillation Spectroscopic Survey and from the Second Phase of the Apache Point Observatory Galactic Evolution Experiment". In: *Astrophys. J. Suppl. Ser.* 235 (2018), p. 19. DOI: 10.3847/1538-4365/aa9e8a. arXiv: 1707.09322 [astro-ph.IM].

[45] Viatcheslav F. Mukhanov and G. V. Chibisov. "The Vacuum energy and large scale structure of the universe". In: *Sov. Phys. JETP* 56 (1982), pp. 258–265.

[46] R.C. Tolman. "On the theoretical requirements for a periodic behaviour of the universe". In: *Phys. Rev.* 38 (1931), p. 1758. DOI: 10.1103/PhysRev.38.1758.

[47] G. Murphy. "Big-bang model without singularities". In: *Phys. Rev.* 8 (1973), p. 4231. DOI: 10.1103/PhysRevD.8.4231.

[48] M. Novello and J.M. Salim. "Nonlinear photons in the universe". In: *Phys. Rev. D* 20 (1979), p. 377. DOI: 10.1103/PhysRevD.20.377.

[49] L.E. Allen and D. Wands. "Cosmological perturbations through a simple bounce". In: *Phys. Rev. D* 70 (2004), p. 063515. DOI: 10.1103/PhysRevD.70.063515. arXiv: astro-ph/0404441 [astro-ph.CO].

[50] J.C. Fabris et al. "Born-Infeld-like f(R) gravity". In: *Phys. Rev. D* 86 (2012), p. 103525. DOI: 10.1103/PhysRevD.86.103525. arXiv: 1205.3458 [astro-ph.CO].

[51] Y. Cai, D.A. Easson, and R. Brandenberger. "Towards a nonsingular bouncing cosmology". In: *J. Cosmol. Astropart. Phys.* 8 (2012), p. 020. DOI: 10.1088/1475-7516/2012/08/020. arXiv: 1206.2382 [astro-ph.CO].

[52] A. Ijjas and P.J. Steinhardt. "Classically stable nonsingular cosmological bounces". In: *Phys. Rev. Lett.* 117 (2016), p. 121304. DOI: 10.1103/PhysRevLett.117.121304. arXiv: 1606.08880 [gr-qc].

[53] A. Ilyas et al. "DHOST bounce". In: *J. Cosmol. Astropart. Phys.* 9 (2020), p. 002. DOI: 10.1088/1475-7516/2020/09/002. arXiv: 2002.08269 [astro-ph.CO].

[54] V. Melnikov and S. Orlov. "Nonsingular cosmology as a quantum vacuum effect". In: *Phys. Lett. A* 70 (1979), p. 263. DOI: 10.1016/0375-9601(79)90117-8.

[55] M.J. Gotay and J Demaret. "Quantum cosmological singularities". In: *Phys. Rev. D* 28 (1983), p. 2402. DOI: 10.1103/PhysRevD.28.2402.

[56] F.J. Tipler. "Interpreting the wave function of the universe". In: *Phys. Rep.* 137 (1986), p. 231. DOI: 10.1016/0370-1573(86)90011-6.

[57] J.A. de Barros, N. Pinto-Neto, and M.A Sagioro-Leal. "The causal interpretation of dust and radiation fluid non-singular quantum cosmologies". In: *Phys. Lett. A* 241 (1998), p. 229. DOI: 10.1016/S0375-9601(98)00169-8. arXiv: gr-qc/9710084.

[58] Jr. Colistete R., J.C. Fabris, and N. Pinto-Neto. "Gaussian superpositions in scalar-tensor quantum cosmological models". In: *Phys. Rev. D* 62 (2000), p. 083507. DOI: 10.1103/PhysRevD.62.083507. arXiv: gr-qc/0005013.

[59] M. Bojowald. "Absence of a singularity in loop quantum cosmology". In: *Phys. Rev. Lett.* 86 (2001), p. 5227. DOI: 10.1103/PhysRevLett.86.5227. arXiv: :gr-qc/0102069.

[60] J. Khoury et al. "Ekpyrotic universe: Colliding branes and the origin of the hot big bang". In: *Phys. Rev. D* 64 (2001), p. 123522. DOI: 10.1103/PhysRevD.64.123522. arXiv: hep-th/0103239.

[61] F.G. Alvarenga et al. "Quantum cosmological perfect fluid models". In: *Gen. Relat. Gravit.* 34 (2002), p. 651. DOI: 10.1023/A:1015986011295. arXiv: gr-qc/0106051.

[62] A. Ashtekar, T. Pawlowski, and P. Singh. "Quantum nature of the big bang". In: *Phys. Rev. Lett.* 14 (2006), p. 141301. DOI: 10.1103/PhysRevLett.96.141301. arXiv: gr-qc/0602086.

[63] P. Peter and N. Pinto-Neto. "Cosmology without inflation". In: *Phys. Rev. D* 78 (2008), p. 063506. DOI: 10.1103/PhysRevD.78.063506. arXiv: 0809.2022 [gr-qc].

[64] A. Ashtekar and P. Singh. "Loop quantum cosmology: A status report". In: *Class. Quant. Grav.* 28 (2011), p. 213001. DOI: 10.1088/0264-9381/28/21/213001. arXiv: 1108.0893 [gr-qc].

[65] S. Gielen and N. Turok. "Perfect quantum cosmological bounce". In: *Phys. Rev. Lett.* 117 (2016), p. 021301. DOI: 10.1103/PhysRevLett.117.021301. arXiv: 1510.00699 [hep-th].

[66] A. Ijjas and P.J. Steinhardt. "Implications of Planck2015 for inflationary, ekpyrotic and anamorphic bouncing cosmologies". In: *Class. Quantum Grav.* 33 (2016), p. 044001. DOI: 10.1088/0264-9381/33/4/044001/pdf. arXiv: 1512.09010 [astro-ph.CO].

[67] Y. Cai et al. "Searching for a matter bounce cosmology with low redshift observations". In: *Phys. Rev. D* 93 (2016), p. 043546. DOI: 10.1103/PhysRevD.93.043546. arXiv: 1512.08979 [astro-ph.CO].

[68] A.P. Bacalhau, N. Pinto-Neto, and S.D.P. Vitenti. "Consistent scalar and tensor perturbation power spectra in single fluid matter". In: *Phys. Rev. D* 97 (2018), p. 083517. DOI: 10.1103/PhysRevD.97.083517. arXiv: 1706.08830 [gr-qc].

[69] R.N. Raveendran and L. Sriramkumar. "Viable scalar spectral tilt and tensor-to-scalar ratio in near-matter bounces". In: *Phys. Rev. D* 100 (2019), p. 083523. DOI: 10.1103/PhysRevD.100.083523. arXiv: 1812.06803 [astro-ph.CO].

[70] I. Agullo, J. Olmedo, and V. Sreenath. "Predictions for the CMB from an anisotropic quantum bounce". In: *Phys. Rev. Lett.* 124 (2020), p. 251301. DOI: 10.1103/PhysRevLett.124.251301. arXiv: 2003.02304 [gr-qc].

[71] P. Singh, K. Vandersloot, and G.V. Vereshchagin. "Non-Singular Bouncing Universes in Loop Quantum Cosmology". In: *Phys. Rev. D* 74 (2006), p. 043510. DOI: 10.1103/PhysRevD.74.043510. arXiv: gr-qc/0606032.

[72] C. Kiefer. "Quantum geometrodynamics: whence, whither?" In: *Gen. Relativ. Gravit.* 41 (2009), p. 877. DOI: 10.1007/s10714-008-0750-1.

[73] D. Bohm. "A Suggested Interpretation of the Quantum Theory in Terms of "Hidden" Variables. I". In: *Phys. Rev.* 85 (1952), p. 166. DOI: 10.1103/PhysRev.85.166.

[74] D. Bohm. "A Suggested Interpretation of the Quantum Theory in Terms of "Hidden" Variables. II". In: *Phys. Rev.* 85 (1952), p. 180. DOI: 10.1103/PhysRev.85.180.

[75] C. Appignani and R. Casadio. "A radiation-like era before inflation". In: *JCAP* 10 (2008), p. 027. DOI: 10.1088/1475-7516/2008/10/027.

[76] A. Ijjas and P. J. Steinhardt. "Classically Stable Nonsingular Cosmological Bounces". In: *Phys. Rev. Lett.* 117 (2016), p. 121304. DOI: 10.1103/PhysRevLett.117.121304.

[77] W. G. Cook et al. "Supersmoothing through slow contraction". In: *Phys. Lett. B* 808 (2020), p. 135690. DOI: 10.1016/j.physletb.2020.135690.

[78] S. D. P. Vitenti and N. Pinto-Neto. "Large adiabatic scalar perturbations in a regular bouncing universe". In: *Phys. Rev. D* 85 (2012), p. 023524. DOI: 10.1103/PhysRevD.85.023524.

[79] R. Arnowitt, S. Deser, and C. W. Misner. "Dynamical Structure and Definition of Energy in General Relativity". In: *Phys. Rev.* 116 (1959), p. 1322. DOI: 10.1103/PhysRev.116.1322.

[80] P.A.M. Dirac. *Lectures on Quantum Mechanics*. Belfer Graduate School of Science. Monographs series. Belfer Graduate School of Science, Yeshiva University, 1964. URL: https://books.google.pl/books?id=oQNRAAAAMAAJ.

[81] Martin Bojowald. "Quantum cosmology: a review". In: *Reports on Progress in Physics* 78.2 (Jan. 2015), p. 023901. DOI: 10.1088/0034-4885/78/2/023901. URL: https://dx.doi.org/10.1088/0034-4885/78/2/023901.

[82] B. F. Schutz. "Perfect Fluids in General Relativity: Velocity Potentials and a Variational Principle". In: *Phys. Rev. D* 2 (1970), p. 2762. DOI: 10.1103/PhysRevD.2.2762.

[83] Nelson Pinto-Neto. "The de Broglie–Bohm Quantum Theory and Its Application to Quantum Cosmology". In: *Universe* 7.5 (2021). ISSN: 2218-1997. DOI: 10.3390/universe7050134. URL: https://www.mdpi.com/2218-1997/7/5/134.

[84] J. D. Brown and K. V. Kuchař. "Dust as a standard of space and time in canonical quantum gravity". In: *Phys. Rev. D* 51 (1995), p. 5600. DOI: 10.1103/PhysRevD.51.5600.

[85] V. Husain and T. Pawłowski. "Time and a Physical Hamiltonian for Quantum Gravity". In: *Phys. Rev. Lett.* 108 (2012), p. 141301. DOI: 10.1103/PhysRevLett.108.141301.

[86] M. de Cesare and V. Husain. "Physical Hamiltonian for mimetic gravity". In: *Phys. Rev. D* 102 (2020), p. 104052. DOI: 10.1103/PhysRevD.102.104052.

[87] N. Pinto-Neto. "Bouncing Quantum Cosmology". In: *Universe* 7 (2021), p. 110. DOI: 10.3390/universe7040110.

[88] N. Pinto-Neto and W. Struyve. "Bohmian quantum gravity and cosmology". In: (2018). eprint: arXiv:1801.03353.

[89] N. Pinto-Neto and J. C. Fabris. "Quantum cosmology from the de Broglie-Bohm perspective". In: *Class. Quant. Grav.* 30 (2013), p. 143001. DOI: 10.1088/0264-9381/30/14/143001.

[90] P. Peter and N. Pinto-Neto. "Cosmology without inflation". In: *Phys. Rev. D* 78 (2008), p. 063506. DOI: 10.1103/PhysRevD.78.063506.

[91] P. C. M. Delgado and N. Pinto-Neto. "Cosmological models with asymmetric quantum bounces". In: *Class. Quantum Grav.* 37 (2020), p. 125002. DOI: 10.1088/1361-6382/ab8bb8.

[92] E. J. C. Pinho and N. Pinto-Neto. "Scalar and vector perturbations in quantum cosmological backgrounds". In: *Phys. Rev. D* 76 (2007), p. 023506. DOI: 10.1103/PhysRevD.76.023506.

[93] J. B. Hartle. *Quantum Cosmology: Problems for the 21st Century*. 1997, p. 179.

[94] Y. Akrami et al. (Planck). "Planck 2018 results. X. Constraints on inflation". In: *Astron. Astrophys.* 641 (2020), A10. DOI: 10.1051/0004-6361/201833887.

[95] S. D. P. Vitenti, F. T. Falciano, and N. Pinto-Neto. "Quantum cosmological perturbations of generic fluids in quantum universes". In: *Phys. Rev. D* 87 (2013), p. 103503. DOI: 10.1103/PhysRevD.87.103503.

[96] D. J. H. Chung, A. Notari, and A. Riotto. "Minimal theoretical uncertainties in inflationary predictions". In: *JCAP* 10 (2003), p. 012. DOI: 10.1088/1475-7516/2003/10/012.

[97] D. C. F. Celani, N. Pinto-Neto, and S. D. P. Vitenti. "Particle creation in bouncing cosmologies". In: *Phys. Rev. D* 95 (2017), p. 023523. DOI: 10.1103/PhysRevD.95.023523.

[98] P. Peter, E. J. C. Pinho, and N. Pinto-Neto. "Tensor perturbations in quantum cosmological backgrounds". In: *JCAP* 07 (2005), p. 014. DOI: 10.1088/1475-7516/2005/07/014.

[99] I. Agullo, A. Wang, and E. Wilson-Ewing. "Loop Quantum Cosmology: Relation Between Theory and Observations". In: *Handbook of Quantum Gravity*. Ed. by C. Bambi, L. Modesto, and I. Shapiro. Springer, Singapore, 2023. DOI: 10.1007/978-981-19-3079-9_103-1.

[100] C. Gordon et al. "Adiabatic and entropy perturbations from inflation". In: *Phys. Rev. D* 63 (2000), p. 023506. DOI: 10.1103/PhysRevD.63.023506.

[101] J. Gong, N. Kitajima, and T. Terada. "Curvaton as dark matter with secondary inflation". In: *JCAP* 03 (2017), p. 053. DOI: 10.1088/1475-7516/2017/03/053.

[102] D. H. Lyth and D. Wands. "The CDM isocurvature perturbation in the curvaton scenario". In: *Phys. Rev. D* 68 (2003), p. 103516. DOI: 10.1103/PhysRevD.68.103516.

[103] Y. Cai, R. Brandenberger, and X. Zhang. "The matter bounce curvaton scenario". In: *JCAP* 03 (2011), p. 003. DOI: 10.1088/1475-7516/2011/03/003.

[104] A. Guth. "Inflationary universe: A possible solution to the horizon and flatness problems". In: *Phys. Rev. D* 23 (1981), p. 347. DOI: 10.1103/PhysRevD.23.347.

[105] V. F. Mukhanov and G. V. Chibisov. "Vacuum energy and large scale structure of the universe". In: *JETP Lett.* 56 (1982), p. 258.

[106] F. Bezrukov et al. "Higgs inflation: consistency and generalisations". In: *JHEP* 2011 (2011), p. 16. DOI: 10.1007/JHEP01(2011)016.

[107] M. Novello and J. M. Salim. "Nonlinear photons in the universe". In: *Phys. Rev. D* 20 (1979), p. 377. DOI: 10.1103/PhysRevD.20.377.

[108] V. Melnikov and S. Orlov. "Nonsingular cosmology as a quantum vacuum effect". In: *Phys. Lett. A* 70 (1979), p. 263. DOI: 10.1016/0375-9601(79)90117-8.

[109] Y. Cai, D. A. Easson, and R. Brandenberger. "Towards a nonsingular bouncing cosmology". In: *JCAP* 8 (2012), p. 020. DOI: 10.1088/1475-7516/2012/08/020.

[110] A. Ilyas et al. "DHOST bounce". In: *JCAP* 09 (2020), p. 002. DOI: 10.1088/1475-7516/2020/09/002.

[111] M. Zhu et al. "Scalar and tensor perturbations in DHOST bounce cosmology". In: *JCAP* 11 (2021), p. 045. DOI: 10.1088/1475-7516/2021/11/045.

[112] G. Barca, E. Giovannetti, and G. Montani. "An Overview on the Nature of the Bounce in LQC and PQM". In: *Universe* 7 (2021), p. 327. DOI: 10.3390/universe7090327.

[113] E. Battista. "Nonsingular bouncing cosmology in general relativity: physical analysis of the spacetime defect". In: *Class. Quantum Grav.* 38 (2021), p. 195007. DOI: 10.1088/1361-6382/ac1900.

[114] L. E. Allen and D. Wands. "Cosmological perturbations through a simple bounce". In: *Phys. Rev. D* 70 (2004), p. 063515. DOI: 10.1103/PhysRevD.70.063515.

[115] P. Peter, E. Pinho, and N. Pinto-Neto. "A non inflationary model with scale invariant cosmological perturbations". In: *Phys. Rev. D* 75 (2007), p. 023516. DOI: 10.1103/PhysRevD.75.023516.

[116] A. Ashtekar and P. Singh. "Loop quantum cosmology: A status report". In: *Class. Quantum Grav.* 28 (2011), p. 213001. DOI: 10.1088/0264-9381/28/21/213001.

[117] G. Montani et al. "Semiclassical and quantum analysis of the isotropic Universe in the polymer paradigm". In: *Phys. Rev. D* 99 (2019), p. 063534. DOI: 10.1103/physrevd.99.063534.

[118] E. Giovannetti and G. Montani. "The role of spatial curvature in constraining the Universe anisotropies across a Big Bounce". In: *Eur. Phys. J. C* 83 (2023), p. 752. DOI: 10.1140/epjc/s10052-023-11921-0.

[119] Ivan Agullo, Boris Bolliet, and V. Sreenath. "Non-Gaussianity in loop quantum cosmology". In: *Phys. Rev. D* 97.6 (2018), p. 066021. DOI: 10.1103/PhysRevD.97.066021. arXiv: 1712.08148 [gr-qc].

[120] D.J. Schwarz et al. "CMB Anomalies after Planck". In: *Class. Quant. Grav.* 33.18 (2016), p. 184001. DOI: 10.1088/0264-9381/33/18/184001/meta. arXiv: 1510.07929 [astro-ph.CO].

[121] Planck Collaboration: Y. Akrami and et al. "Planck 2018 results. IX. Constraints on primordial non-Gaussianity". In: *Astron. Astrophys.* 641 (2018), A9. DOI: 10.1051/0004-6361/201935891. arXiv: 1905.05697 [astro-ph.CO].

[122] N. Aghanim et al. "Planck 2018 results. I. Overview and the cosmological legacy of Planck". In: *Astron. Astrophys.* 641 (2020), A1. DOI: 10.1051/0004-6361/201833880. arXiv: 1807.06205 [astro-ph.CO].

[123] Jaiseung Kim and Pavel Naselsky. "Lack of angular correlation and odd-parity preference in CMB data". In: *Astrophys. J.* 739 (2011), p. 79. DOI: 10.1088/0004-637X/739/2/79. arXiv: 1011.0377 [astro-ph.CO].

[124] Ruth Durrer. *The Cosmic Microwave Background*. Cambridge: Cambridge University Press, 2008. ISBN: 978-0-511-81720-5. DOI: 10.1017/CBO9780511817205.

[125] Ivan Agullo, Dimitrios Kranas, and V. Sreenath. "Anomalies in the Cosmic Microwave Background and Their Non-Gaussian Origin in Loop Quantum Cosmology". In: *Front. Astron. Space Sci.* 8 (2021), p. 703845. DOI: 10.3389/fspas.2021.703845. arXiv: 2105.12993 [gr-qc].

[126] Y. Akrami et al. "Planck 2018 results. VII. Isotropy and Statistics of the CMB". In: *Astron. Astrophys.* 641 (2020), A7. DOI: 10.1051/0004-6361/201935201. arXiv: 1906.02552 [astro-ph.CO].

[127] Abhay Ashtekar and Parampreet Singh. "Loop Quantum Cosmology: A Status Report". In: *Class. Quant. Grav.* 28 (2011), p. 213001. DOI: 10.1088/0264-9381/28/21/213001. arXiv: 1108.0893 [gr-qc].

[128] P. A. R. Ade et al. "Planck 2015 results. XVII. Constraints on primordial non-Gaussianity". In: *Astronomy & Astrophysics* 594 (Sept. 2016), A17. ISSN: 1432-0746. DOI: 10.1051/0004-6361/201525836. URL: http://dx.doi.org/10.1051/0004-6361/201525836.

[129] Enea Di Dio et al. "The Full-Sky Angular Bispectrum in Redshift Space". In: *JCAP* 04 (2019), p. 053. DOI: 10.1088/1475-7516/2019/04/053. arXiv: 1812.09297 [astro-ph.CO].

[130] Julien Lesgourgues. "The Cosmic Linear Anisotropy Solving System (CLASS) I: Overview". In: (Apr. 2011). arXiv: 1104.2932 [astro-ph.IM].

[131] Diego Blas, Julien Lesgourgues, and Thomas Tram. "The Cosmic Linear Anisotropy Solving System (CLASS) II: Approximation schemes". In: *JCAP* 07 (2011), p. 034. DOI: 10.1088/1475-7516/2011/07/034. arXiv: 1104.2933 [astro-ph.CO].

[132] P. A. R. Ade et al. "Planck 2015 results. XV. Gravitational lensing". In: *Astron. Astrophys.* 594 (2016), A15. DOI: 10.1051/0004-6361/201525941. arXiv: 1502.01591 [astro-ph.CO].

[133] D. Nelson Limber. "The Analysis of Counts of the Extragalactic Nebulae in Terms of a Fluctuating Density Field." In: *Astrophys. J.* 117 (Jan. 1953), p. 134. DOI: 10.1086/145672.

[134] Eiichiro Komatsu and David N. Spergel. "Acoustic signatures in the primary microwave background bispectrum". In: *Phys. Rev. D* 63 (2001), p. 063002. DOI: 10.1103/PhysRevD.63.063002. arXiv: astro-ph/0005036.

[135] Wayne Hu and Takemi Okamoto. "Principal power of the CMB". In: *Phys. Rev. D* 69 (2004), p. 043004. DOI: 10.1103/PhysRevD.69.043004. arXiv: astro-ph/0308049.

[136] Martin Bucher, Bartjan Van Tent, and Carla Sofia Carvalho. "Detecting Bispectral Acoustic Oscillations from Inflation Using a New Flexible Estimator". In: *Mon. Not. Roy. Astron. Soc.* 407 (2010), p. 2193. DOI: 10.1111/j.1365-2966.2010.17089.x. arXiv: 0911.1642 [astro-ph.CO].

[137] Martin Bucher, Benjamin Racine, and Bartjan van Tent. "The binned bispectrum estimator: template-based and non-parametric CMB non-Gaussianity searches". In: *JCAP* 05 (2016), p. 055. DOI: 10.1088/1475-7516/2016/05/055. arXiv: 1509.08107 [astro-ph.CO].

[138] P. A. R. Ade et al. "Planck 2013 Results. XXIV. Constraints on primordial non-Gaussianity". In: *Astron. Astrophys.* 571 (2014), A24. DOI: 10.1051/0004-6361/201321554. arXiv: 1303.5084 [astro-ph.CO].

[139] Y. Akrami et al. "Planck 2018 results. IV. Diffuse component separation". In: *Astron. Astrophys.* 641 (2020), A4. DOI: 10.1051/0004-6361/201833881. arXiv: 1807.06208 [astro-ph.CO].

[140] Gabriel Jung, Benjamin Racine, and Bartjan van Tent. "The bispectra of galactic CMB foregrounds and their impact on primordial non-Gaussianity estimation". In: *JCAP* 11 (2018), p. 047. DOI: 10.1088/1475-7516/2018/11/047. arXiv: 1810.01727 [astro-ph.CO].

[141] G. Hinshaw et al. "ApJS". In: 208 (2013), p. 19.

[142] David Parkinson et al. "Phys. Rev. D". In: 86 (2012), p. 103518.

[143] S. Ho et al. "Phys. Rev. D". In: 78 (2008), p. 043519.

[144] T. Giannantonio et al. "Phys. Rev. D". In: 77 (2008), p. 123520.

[145] C. Ma and T. Zhang. "ApJ". In: 730 (2011), p. 74.

[146] T. M. C. Abbott et al. "Phys. Rev. D". In: 102 (2020), p. 023509.

[147] T. M. C. Abbott et al. "arXiv:2105.13549 [astro-ph.CO]". In: (2021).

[148] G. 't Hooft. "arXiv:gr-qc/9310026". In: (1993).

[149] L. Susskind. "Journal of Mathematical Physics". In: 36 (1995), p. 6377.

[150] A. G. Cohen, D. B. Kaplan, and A. E. Nelson. "Phys. Rev. Lett." In: 82 (1999), pp. 4971–4974. eprint: hep-th/9803132.

[151] S. Weinberg. "Rev. Mod. Phys." In: 61 (1989), pp. 1–23.

[152] M. Li. "Phys. Lett. B". In: 603 (2004), pp. 1–5.

[153] S. Wang, Y. Wang, and M. Li. "Physics Reports". In: 696 (2017), pp. 1–57.

[154] A. Ganz and C. Lin. "arXiv:2109.07420 [gr-qc]". In: (2021).

[155] A. H. Guth. "Phys. Rev. D". In: 23 (1981), p. 347.

[156] A. Albrecht and P. J. Steinhardt. "Phys. Rev. Lett." In: 48 (1982), p. 1220.

[157] A. D. Linde. "Phys. Lett. B". In: 129 (1983), pp. 177–181.

[158] A. A. Starobinskiĭ. "Soviet Journal of Experimental and Theoretical Physics Letters". In: 30 (1979), p. 682.

[159] B. Chen, M. Li, and Y. Wang. "Nuclear Physics B". In: 774 (2007), pp. 1–3.

[160] S. Nojiri, S. D. Odintsov, and E. N. Saridakis. "Phys. Lett. B". In: 797 (2019), p. 134829.

[161] M. Li et al. "Phys. Rev. D". In: 88 (2013), p. 023503.

[162] M. Li and R. Miao. "arXiv:1210.0966[hep-th]". In: (2012).

[163] Jennie H. Traschen and Robert H. Brandenberger. "Particle Production During Out-of-equilibrium Phase Transitions". In: *Phys. Rev. D* 42 (1990), pp. 2491–2504. DOI: 10.1103/PhysRevD.42.2491.

[164] A. D. Dolgov and D. P. Kirilova. "ON PARTICLE CREATION BY A TIME DEPENDENT SCALAR FIELD". In: *Sov. J. Nucl. Phys.* 51 (1990), pp. 172–177.

[165] Rouzbeh Allahverdi et al. "Reheating in Inflationary Cosmology: Theory and Applications". In: *Ann. Rev. Nucl. Part. Sci.* 60 (2010), pp. 27–51. DOI: 10.1146/annurev.nucl.012809.104511. arXiv: 1001.2600 [hep-th].

[166] Mustafa A. Amin et al. "Nonperturbative Dynamics Of Reheating After Inflation: A Review". In: *Int. J. Mod. Phys. D* 24 (2014), p. 1530003. DOI: 10.1142/S0218271815300037. arXiv: 1410.3808 [hep-ph].

[167] Lev Kofman, Andrei D. Linde, and Alexei A. Starobinsky. "Reheating after inflation". In: *Phys. Rev. Lett.* 73 (1994), pp. 3195–3198. DOI: 10.1103/PhysRevLett.73.3195. arXiv: hep-th/9405187.

[168] Y. Shtanov, Jennie H. Traschen, and Robert H. Brandenberger. "Universe reheating after inflation". In: *Phys. Rev. D* 51 (1995), pp. 5438–5455. DOI: 10.1103/PhysRevD.51.5438. arXiv: hep-ph/9407247.

[169] Lev Kofman, Andrei D. Linde, and Alexei A. Starobinsky. "Towards the theory of reheating after inflation". In: *Phys. Rev. D* 56 (1997), pp. 3258–3295. DOI: 10.1103/PhysRevD.56.3258. arXiv: hep-ph/9704452.

[170] Patrick B. Greene and Lev Kofman. "Preheating of fermions". In: *Phys. Lett. B* 448 (1999), pp. 6–12. DOI: 10.1016/S0370-2693(99)00020-9. arXiv: hep-ph/9807339.

[171] Mustafa A. Amin et al. "Nonperturbative Dynamics Of Reheating After Inflation: A Review". In: *Int. J. Mod. Phys. D* 24 (2014), p. 1530003. DOI: 10.1142/S0218271815300037. arXiv: 1410.3808 [hep-ph].

[172] Yi-Fu Cai et al. "Primordial Black Holes from Sound Speed Resonance during Inflation". In: *Phys. Rev. Lett.* 121.8 (2018), p. 081306. DOI: 10.1103/PhysRevLett.121.081306. arXiv: 1805.03639 [astro-ph.CO].

[173] Yi-Fu Cai et al. "Sound speed resonance of the stochastic gravitational wave background". In: *Phys. Rev. Lett.* 126.7 (2021), p. 071303. DOI: 10.1103/PhysRevLett.126.071303. arXiv: 2009.09833 [gr-qc].

[174] V. Zanchin et al. "Reheating in the presence of inhomogeneous noise". In: *Phys. Rev. D* 60 (2 June 1999), p. 023505. DOI: 10.1103/PhysRevD.60.023505. URL: https://link.aps.org/doi/10.1103/PhysRevD.60.023505.

[175] R. Carmona and J. Lacroix. *Spectral Theory of Random Schroedinger Operators*. Boston: Birkhaeuser, 1990.

[176] V. Zanchin et al. "Reheating in the presence of noise". In: *Phys. Rev. D* 57 (8 Apr. 1998), pp. 4651–4662. DOI: 10.1103/PhysRevD.57.4651. URL: https://link.aps.org/doi/10.1103/PhysRevD.57.4651.

[177] R. Brandenberger and W. Craig. "Towards a New Proof of Anderson Localization". In: *Eur. Phys. J. C* 72 (2012), p. 1881. DOI: 10.1140/epjc/s10052-012-1881-9. eprint: 0805.4217.

[178] P. Creminelli et al. "Resonant Decay of Gravitational Waves into Dark Energy". In: *JCAP* 10 (2019), p. 072. DOI: 10.1088/1475-7516/2019/10/072. eprint: 1906.07015.

[179] Z. Zhou et al. "Primordial Black Holes and Gravitational Waves from Resonant Amplification during Inflation". In: *Phys. Rev. D* 102.10 (2020), p. 103527. DOI: 10.1103/PhysRevD.102.103527. eprint: 2010.03537.

[180] M. Alsarraj and R. Brandenberger. "Title of the Paper". In: *J. Phys.: Conf. Ser.* 1051 (2018), p. 012001. DOI: 10.1088/1742-6596/1051/1/012001.

[181] P. Chen. "Resonant Photon-Graviton Conversion and Cosmic Microwave Background Fluctuations". In: *Phys. Rev. Lett.* 74 (1995), pp. 634–637. DOI: 10.1103/PhysRevLett.74.634.

[182] G. Brodin and M. Marklund. "Parametric Excitation of Plasma Waves by Gravitational Radiation". In: *Phys. Rev. Lett.* 82 (1999), pp. 3012–3015. DOI: 10.1103/PhysRevLett.82.3012. eprint: astro-ph/9810128.

[183] M. Servin et al. "Parametric Excitation of Alfven Waves by Gravitational Radiation". In: *Phys. Rev. E* 62 (2000). DOI: 10.1103/PhysRevE.62.8493. eprint: physics/9910029v2.

[184] M. Forsberg et al. "Nonlinear Interactions between Gravitational Radiation and Modified Alfven Modes in Astrophysical Dusty Plasmas". In: *Phys. Rev. D* 74 (2006), p. 064014. DOI: 10.1103/PhysRevD.74.064014. eprint: gr-qc/0606072.

[185] G. Brodin et al. "Interaction between Gravitational Waves and Plasma Waves in the Vlasov Description". In: *J. Plasma Phys.* 76 (2010), p. 345. DOI: 10.1017/S0022377809990535. eprint: 0911.2190.

[186] S. Vagnozzi and A. Loeb. "The Challenge of Ruling Out Inflation via the Primordial Graviton Background". In: *Astrophys. J. Lett.* 939.2 (2022), p. L22. DOI: 10.3847/2041-8213/ac9b0e. eprint: 2208.14088.

[187] V. S. Gorelik et al. "Title of the Paper". In: *J. Phys.: Conf. Ser.* 1051 (2018), p. 012001. DOI: 10.1088/1742-6596/1051/1/012001.

[188] V. I. Pustovoit et al. "Title of the Paper". In: *J. Phys.: Conf. Ser.* 1348 (2019), p. 012008. DOI: 10.1088/1742-6596/1348/1/012008.

[189] A. Arbey and F. Mahmoudi. "Dark matter and the early Universe: A review". In: *Progress in Particle and Nuclear Physics* 119 (2021), p. 103865. ISSN: 0146-6410. DOI: https://doi.org/10.1016/j.ppnp.2021.103865. URL: https://www.sciencedirect.com/science/article/pii/S0146641021000193.

[190] Lars Bergström. "Dark matter candidates". In: *New Journal of Physics* 11.10 (Oct. 2009), p. 105006. DOI: 10.1088/1367-2630/11/10/105006. URL: https://dx.doi.org/10.1088/1367-2630/11/10/105006.

[191] Bernard Carr and Florian Kuhnel. "Primordial black holes as dark matter candidates". In: *SciPost Phys. Lect. Notes* (2022), p. 48. DOI: 10.21468/SciPostPhysLectNotes.48. URL: https://scipost.org/10.21468/SciPostPhysLectNotes.48.

[192] Joel R. Primack. "Cosmology: small scale issues revisited". In: *New J. Phys.* 11 (2009), p. 105029. DOI: 10.1088/1367-2630/11/10/105029. arXiv: 0909.2247 [astro-ph.CO].

[193] Wayne Hu, Rennan Barkana, and Andrei Gruzinov. "Cold and fuzzy dark matter". In: *Phys. Rev. Lett.* 85 (2000), pp. 1158–1161. DOI: 10.1103/PhysRevLett.85.1158. arXiv: astro-ph/0003365.

[194] Jae-Weon Lee. "Characteristic size and mass of galaxies in the Bose–Einstein condensate dark matter model". In: *Physics Letters B* 756 (2016), pp. 166–169. ISSN: 0370-2693. DOI: https://doi.org/10.1016/j.physletb.2016.03.016. URL: https://www.sciencedirect.com/science/article/pii/S0370269316001878.

[195] Elisa G. M. Ferreira. "Ultra-light dark matter". In: *Astron. Astrophys. Rev.* 29.1 (2021), p. 7. DOI: 10.1007/s00159-021-00135-6. arXiv: 2005.03254 [astro-ph.CO].

[196] Asimina Arvanitaki et al. "String axiverse". In: *Phys. Rev. D* 81 (12 June 2010), p. 123530. DOI: 10.1103/PhysRevD.81.123530. URL: https://link.aps.org/doi/10.1103/PhysRevD.81.123530.

[197] Renée Hlozek et al. "A search for ultralight axions using precision cosmological data". In: *Phys. Rev. D* 91.10 (2015), p. 103512. DOI: 10.1103/PhysRevD.91.103512. arXiv: 1410.2896 [astro-ph.CO].

[198] F Siddhartha Guzmán and Tonatiuh Matos. "Scalar fields as dark matter in spiral galaxies". In: *Classical and Quantum Gravity* 17.1 (Jan. 2000), p. L9. DOI: 10.1088/0264-9381/17/1/102. URL: https://dx.doi.org/10.1088/0264-9381/17/1/102.

[199] Bartosz Fornal, Kassandra Garcia, and Erika Pierre. "Testing Unification and Dark Matter with Gravitational Waves". In: (May 2023). arXiv: 2305.12566 [hep-ph].

[200] Markus R. Mosbech et al. "Gravitational-wave event rates as a new probe for dark matter microphysics". In: *Phys. Rev. D* 108.4 (2023), p. 043512. DOI: 10.1103/PhysRevD.108.043512. arXiv: 2207.14126 [astro-ph.CO].

[201] Rome Samanta and Federico R. Urban. "Testing super heavy dark matter from primordial black holes with gravitational waves". In: *JCAP* 06.06 (2022), p. 017. DOI: 10.1088/1475-7516/2022/06/017. arXiv: 2112.04836 [hep-ph].

[202] Anish Ghoshal and Alessandro Strumia. "Probing the Dark Matter density with gravitational waves from super-massive binary black holes". In: (June 2023). arXiv: 2306.17158 [astro-ph.CO].

[203] Andrei Khmelnitsky and Valery Rubakov. "Pulsar timing signal from ultralight scalar dark matter". In: *JCAP* 02 (2014), p. 019. DOI: 10.1088/1475-7516/2014/02/019. arXiv: 1309.5888 [astro-ph.CO].

[204] Arata Aoki and Jiro Soda. "Detecting ultralight axion dark matter wind with laser interferometers". In: *Int. J. Mod. Phys. D* 26.07 (2016), p. 1750063. DOI: 10.1142/S0218271817500638. arXiv: 1608.05933 [astro-ph.CO].

[205] Tomohiro Fujita et al. "Resonant gravitational waves in dynamical Chern-Simons-axion gravity". In: *Class. Quant. Grav.* 38.4 (2021), p. 045010. DOI: 10.1088/1361-6382/abce49. arXiv: 2008.02764 [gr-qc].

[206] Mohammad Aghaie et al. "Bounds on Ultralight Dark Matter from NANOGrav". In: (Aug. 2023). arXiv: 2308.04590 [astro-ph.CO].

[207] Arata Aoki and Jiro Soda. "Nonlinear resonant oscillation of gravitational potential induced by ultralight axion in $f(R)$ gravity". In: *Phys. Rev. D* 96.2 (2017), p. 023534. DOI: 10.1103/PhysRevD.96.023534. arXiv: 1703.03589 [astro-ph.CO].

[208] P. C. Peters. "Index of refraction for scalar, electromagnetic, and gravitational waves in weak gravitational fields". In: *Phys. Rev. D* 9 (1974), pp. 2207–2218. DOI: 10.1103/PhysRevD.9.2207.

[209] Margherita Grespan and Marek Biesiada. "Strong Gravitational Lensing of Gravitational Waves: A Review". In: *Universe* 9.5 (2023), p. 200. DOI: 10.3390/universe9050200.

[210] Man Ho Chan and Chak Man Lee. "Indirect Evidence for Dark Matter Density Spikes around Stellar-mass Black Holes". In: *Astrophys. J. Lett.* 943.2 (2023), p. L11. DOI: 10.3847/2041-8213/acaafa. arXiv: 2212.05664 [astro-ph.HE].

[211] Sourabh Nampalliwar et al. "Modeling the Sgr A* Black Hole Immersed in a Dark Matter Spike". In: *Astrophys. J.* 916.2 (2021), p. 116. DOI: 10.3847/1538-4357/ac05cc. arXiv: 2103.12439 [astro-ph.HE].

[212] Abhishek Banerjee et al. "Relaxion Stars and their detection via Atomic Physics". In: *Commun. Phys.* 3 (2020), p. 1. DOI: 10.1038/s42005-019-0260-3. arXiv: 1902.08212 [hep-ph].

[213] Dmitry Budker et al. "A Generic Formation Mechanism of Ultralight Dark Matter Solar Halos". In: (June 2023). arXiv: 2306.12477 [hep-ph].

[214] Stefano Savastano et al. "Primordial dark matter halos from fifth forces". In: *Phys. Rev. D* 100.8 (2019), p. 083518. DOI: 10.1103/PhysRevD.100.083518. arXiv: 1906.05300 [astro-ph.CO].

[215] C. J. Hogan and M. J. Rees. "AXION MINICLUSTERS". In: *Phys. Lett. B* 205 (1988), pp. 228–230. DOI: 10.1016/0370-2693(88)91655-3.

[216] Malcolm Fairbairn et al. "Structure formation and microlensing with axion miniclusters". In: *Phys. Rev. D* 97.8 (2018), p. 083502. DOI: 10.1103/PhysRevD.97.083502. arXiv: 1707.03310 [astro-ph.CO].

[217] Shinnosuke Hisano et al. "Detailed study of detection method for ultralow frequency gravitational waves with pulsar spin-down rate statistics". In: *Mon. Not. Roy. Astron. Soc.* 487.1 (2019), pp. 97–103. DOI: 10.1093/mnras/stz1285. arXiv: 1902.04787 [astro-ph.HE].

[218] William DeRocco and Jeff A. Dror. "Using Pulsar Parameter Drifts to Detect Sub-Nanohertz Gravitational Waves". In: (Dec. 2022). arXiv: 2212.09751 [astro-ph.HE].

[219] Jordan Flitter and Ely D. Kovetz. "Closing the window on fuzzy dark matter with the 21-cm signal". In: *Phys. Rev. D* 106.6 (2022), p. 063504. DOI: 10.1103/PhysRevD.106.063504. arXiv: 2207.05083 [astro-ph.CO].

[220] Alex Laguë et al. "Constraining ultralight axions with galaxy surveys". In: *JCAP* 01.01 (2022), p. 049. DOI: 10.1088/1475-7516/2022/01/049. arXiv: 2104.07802 [astro-ph.CO].

[221] Nitsan Bar, Kfir Blum, and Chen Sun. "Galactic rotation curves versus ultralight dark matter: A systematic comparison with SPARC data". In: *Phys. Rev. D* 105.8 (2022), p. 083015. DOI: 10.1103/PhysRevD.105.083015. arXiv: 2111.03070 [hep-ph].

[222] David J. E. Marsh and Jens C. Niemeyer. "Strong Constraints on Fuzzy Dark Matter from Ultrafaint Dwarf Galaxy Eridanus II". In: *Phys. Rev. Lett.* 123.5 (2019), p. 051103. DOI: 10.1103/PhysRevLett.123.051103. arXiv: 1810.08543 [astro-ph.CO].

[223] Takeshi Kobayashi et al. "Lyman-α constraints on ultralight scalar dark matter: Implications for the early and late universe". In: *Phys. Rev. D* 96.12 (2017), p. 123514. DOI: 10.1103/PhysRevD.96.123514. arXiv: 1708.00015 [astro-ph.CO].

[224] Mona Dentler et al. "Fuzzy dark matter and the Dark Energy Survey Year 1 data". In: *Mon. Not. Roy. Astron. Soc.* 515.4 (2022), pp. 5646–5664. DOI: 10.1093/mnras/stac1946. arXiv: 2111.01199 [astro-ph.CO].

[225] Brandon Bozek et al. "Galaxy UV-luminosity function and reionization constraints on axion dark matter". In: *Mon. Not. Roy. Astron. Soc.* 450.1 (2015), pp. 209–222. DOI: 10.1093/mnras/stv624. arXiv: 1409.3544 [astro-ph.CO].

[226] Fabrizio Tamburini, Bo Thidé, and Massimo Della Valle. "Measurement of the spin of the M87 black hole from its observed twisted light". In: *Mon. Not. Roy. Astron. Soc.* 492.1 (2020), pp. L22–L27. DOI: 10.1093/mnrasl/slz176. arXiv: 1904.07923 [astro-ph.HE].

[227] Hooman Davoudiasl and Peter B Denton. "Ultralight Boson Dark Matter and Event Horizon Telescope Observations of M87*". In: *Phys. Rev. Lett.* 123.2 (2019), p. 021102. DOI: 10.1103/PhysRevLett.123.021102. arXiv: 1904.09242 [astro-ph.CO].

[228] Caner Ünal, Fabio Pacucci, and Abraham Loeb. "Properties of ultralight bosons from heavy quasar spins via superradiance". In: *JCAP* 05 (2021), p. 007. DOI: 10.1088/1475-7516/2021/05/007. arXiv: 2012.12790 [hep-ph].

[229] David R. DeBoer et al. "Hydrogen Epoch of Reionization Array (HERA)". In: *Publ. Astron. Soc. Pac.* 129.974 (2017), p. 045001. DOI: 10.1088/1538-3873/129/974/045001. arXiv: 1606.07473 [astro-ph.IM].

[230] Renée Hložek et al. "Future CMB tests of dark matter: Ultralight axions and massive neutrinos". In: *Phys. Rev. D* 95.12 (2017), p. 123511. DOI: 10.1103/PhysRevD.95.123511. arXiv: 1607.08208 [astro-ph.CO].

[231] Vid Iršič, Huangyu Xiao, and Matthew McQuinn. "Early structure formation constraints on the ultralight axion in the postinflation scenario". In: *Phys. Rev. D* 101.12 (2020), p. 123518. DOI: 10.1103/PhysRevD.101.123518. arXiv: 1911.11150 [astro-ph.CO].

[232] Patrick J. Fox, Neal Weiner, and Huangyu Xiao. "Recurrent Axinovae and their Cosmological Constraints". In: (Feb. 2023). arXiv: 2302.00685 [hep-ph].

[233] Gabriella Agazie et al. "The NANOGrav 15 yr Data Set: Evidence for a Gravitational-wave Background". In: *Astrophys. J. Lett.* 951.1 (2023), p. L8. DOI: 10.3847/2041-8213/acdac6. arXiv: 2306.16213 [astro-ph.HE].

[234] Gen Ye and Alessandra Silvestri. "Can the gravitational wave background feel wiggles in spacetime?" In: (July 2023). arXiv: 2307.05455 [astro-ph.CO].

[235] V. Zanchin et al. "Reheating in the presence of inhomogeneous noise". In: *Phys. Rev. D* 60 (1999), p. 023505. DOI: 10.1103/PhysRevD.60.023505. arXiv: hep-ph/9901207.